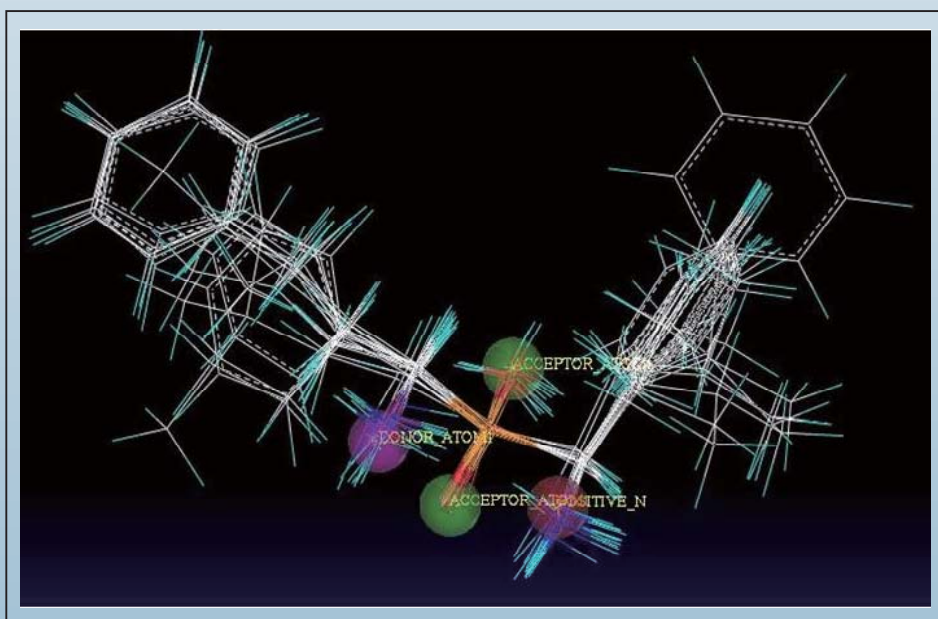


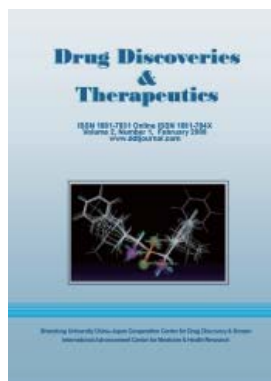
Drug Discoveries & Therapeutics

ISSN 1881-7831 Online ISSN 1881-784X
Volume 2, Number 1, February 2008
www.ddtjournal.com



Shandong University China-Japan Cooperation Center for Drug Discovery & Screen
International Advancement Center for Medicine & Health Research

Drug Discoveries & Therapeutics



Editor-in-Chief:

Kazuhisa SEKIMIZU
(The University of Tokyo, Tokyo, Japan)

Associate Editor:

Norihiro KOKUDO
(The University of Tokyo, Tokyo, Japan)

Drug Discoveries & Therapeutics is a peer-reviewed international journal published bimonthly by *Shandong University China-Japan Cooperation Center for Drug Discovery & Screen* (SDU-DDSC) and *International Advancement Center for Medicine & Health Research Co., Ltd.* (IACMHR Co., Ltd.).

Drug Discoveries & Therapeutics mainly publishes articles related to basic and clinical pharmaceutical research such as pharmaceutical and therapeutical chemistry, pharmacology, pharmacy, pharmacokinetics, industrial pharmacy, pharmaceutical manufacturing, pharmaceutical technology, drug delivery, toxicology, and traditional herb medicine. Studies on drug-related fields such as biology, biochemistry, physiology, microbiology, and immunology are also within the scope of this journal.

Subject Coverage: Basic and clinical pharmaceutical research including Pharmaceutical and therapeutical chemistry, Pharmacology, Pharmacy, Pharmacokinetics, Industrial pharmacy, Pharmaceutical manufacturing, Pharmaceutical technology, Drug delivery, Toxicology, and Traditional herb medicine.

Language: English

Issues/Year: 6

Published by: IACMHR and SDU-DDSC

ISSN: 1881-7831 (Online ISSN 1881-784X)

Editorial and Head Office

Wei TANG, MD PhD
Secretary-in-General

TSUIN-IKIZAKA 410
2-17-5 Hongo, Bunkyo-ku
Tokyo 113-0033, Japan
Tel: 03-5840-9697
Fax: 03-5840-9698

E-mail: office@ddtjournal.com

URL: www.ddtjournal.com



Drug Discoveries & Therapeutics

Editorial Board

Editor-in-Chief:

Kazuhisa SEKIMIZU (*The University of Tokyo, Tokyo, Japan*)

Associate Editor:

Norihiro KOKUDO (*The University of Tokyo, Tokyo, Japan*)

Secretary-in-General:

Wei TANG (*The University of Tokyo, Tokyo, Japan*)

Office Manager:

Munehiro NAKATA (*Tokai University, Kanagawa, Japan*)

Web Editor:

Yu CHEN (*The University of Tokyo, Tokyo, Japan*)

English Editor:

Curtis BENTLEY (*Roswell, GA, USA*)

China Office:

Wenfang XU (*Shandong University, Shandong, China*)

Editors:

Yoshihiro ARAKAWA (*Tokyo, Japan*)

Fen Er CHEN (*Shanghai, China*)

Chandradhar DWIVEDI (*Brookings, SD, USA*)

Mohamed F. EL-MILIGI (*Cairo, Egypt*)

Hiroshi HAMAMOTO (*Tokyo, Japan*)

Langchong HE (*Xi'an, China*)

David A. HORNE (*Duarte, CA, USA*)

Wei HUANG (*Shanghai, China*)

Toshiaki KATADA (*Tokyo, Japan*)

Hiromichi KIMURA (*Tokyo, Japan*)

Kam Ming KO (*Hong Kong, China*)

Toshiro KONISHI (*Tokyo, Japan*)

Chun Guang LI (*Victoria, Australia*)

Ji-Kai LIU (*Kunming, China*)

Ken-ichi MAFUNE (*Tokyo, Japan*)

Tohru MIZUSHIMA (*Kumamoto, Japan*)

Masahiro MURAKAMI (*Osaka, Japan*)

Yutaka ORIHARA (*Tokyo, Japan*)

Wei-San PAN (*Shenyang, China*)

Abdel Aziz M. SALEH (*Cairo, Egypt*)

Yasufumi SAWADA (*Tokyo, Japan*)

Brahma N. SINGH (*Commack, NY, USA*)

Benny K. H. TAN (*Singapore, Singapore*)

Murat TURKOGLU (*Istanbul, Turkey*)

Takako YOKOZAWA (*Toyama, Japan*)

Jian-Ping ZUO (*Shanghai, China*)

Santad CHANPRAPAPH (*Bangkok, Thailand*)

Guanhua DU (*Beijing, China*)

Harald HAMACHER (*Tuebingen, Germany*)

Xiao-Jiang HAO (*Kunming, China*)

Yongzhou HU (*Hangzhou, China*)

Hans E. JUNGINGER (*Phitsanulok, Thailand*)

Ibrahim S. KHATTAB (*Safat, Kuwait*)

Shiroh KISHIOKA (*Wakayama, Japan*)

Nobuyuki KOBAYASHI (*Nagasaki, Japan*)

Masahiro KUROYANAGI (*Hiroshima, Japan*)

Hongmin LIU (*Zhengzhou, China*)

Hongxiang LOU (*Jinan, China*)

Norio MATSUKI (*Tokyo, Japan*)

Abdulla M. MOLOKHIA (*Alexandria, Egypt*)

Yoshinobu NAKANISHI (*Ishikawa, Japan*)

Xiao-Ming OU (*Jackson, MS, USA*)

Adel SAKR (*Cincinnati, OH, USA*)

Tomofumi SANTA (*Tokyo, Japan*)

Hongbin SUN (*Nanjing, China*)

Ren-Xiang TAN (*Nanjing, China*)

Stephen G. WARD (*Bath, UK*)

Liangren ZHANG (*Beijing, China*)

News

- 1** **Tes, a potential Mena-related cancer therapy target.**

Xun Li

Policy Forums

- 2-4** **Dynamic of modernizing traditional Chinese medicine and the standards system for its development.**

Ruoyan Gai, Huanli Xu, Xianjun Qu, Fengshan Wang, Hongxiang Lou, Jinxiang Han, Munehiro Nakata, Norihiro Kokudo, Yasuhiko Sugawara, Chushi Kuroiwa, Wei Tang

- 5-6** **Three decades of GMP implementation in Thailand: Hardships and success.**

Santad Chanprapaph

Brief Reports

- 7-9** **Establishment of a new cell line for performing sensitive screening of nuclear export inhibitors.**

Ken Watanabe, Saiko Noda, Nobuyuki Kobayashi

- 10-13** **Localization of glucagon-like peptide-2 receptor mRNA expression at different sites in the small intestine of rats.**

Kenji Ikeda, Michiaki Myotoku, Nobuo Kurokawa, Yoshihiko Hirotani

Reviews

- 14-23** **Sensing and reacting to dangers by caspases: Caspase activation via inflammasomes.**

Asuka Takeishi, Erina Kuranaga, Masayuki Miura

Original Articles

- 24-34** **Pharmacologic action of oseltamivir on the nervous system.**
Kenichi Ishii, Hiroshi Hamamoto, Takuya Sasaki, Yuji Ikegaya, Kenzo Yamatsugu, Motomu Kanai, Masakatsu Shibasaki, Kazuhisa Sekimizu
- 35-44** **Immunosuppressive effect of ER-38925, a retinoic acid receptor subtype α -selective agonist, in mouse models of human graft-vs-host disease.**
Takayuki Hida, Kohdoh Shikata, Naoki Tokuhara, Akira Ishibashi, Mitsuo Nagai, Toshihiko Yamauchi, Seiichi Kobayashi
- 45-51** **A new method of preparing TRH derivative-loaded poly(dl-lactide-co-glycolide) microspheres based on a solid solution system.**
Akihiro Matsumoto, Yasuhisa Matsukawa, Yukiko Nishioka, Masanobu Harada, Yuji Horikiri, Hiroshi Yamahara
- 52-57** **3D-QSAR study with pharmacophore-based molecular alignment of hydroxamic acid-related phosphinates that are aminopeptidase N inhibitors.**
Huawei Zhu, Hao Fang, Luyao Wang, Wenxiang Hu, Wenfang Xu

Guide for Authors

Copyright

Tes, a potential Mena-related cancer therapy target

Xun Li

Keywords: Tes, Mena, Cancer target

Cancer remains one of the world's most prominent causes of human morbidity and mortality, particularly in developing countries. According to 2005 statistics from the WHO, approximately 7.6 million people died of cancer out of 58 million deaths worldwide, with 9 million people estimated to die from cancer in 2015 and 11.4 million to die in 2030 (<http://www.who.int/mediacentre/factsheets/fs297/en/index.html>).

The principal and internationally recognized methods of cancer treatment are surgery, radiotherapy, chemotherapy, or multimodality therapy. With the recent development of cancer biology, more and more tumor-related targets have been identified, ushering in a new era for target therapy.

Every possible step that causes cellular cancer, such as signal transduction pathways, oncogenes and anti-oncogenes, cytokines and receptors, anti-angiogenesis, suicide genes, and telomerase (*Shay JW, Keith WN. Br J Cancer 2008*), that is biologically relevant, reproducibly measurable, and definably correlated with clinical benefit represents a target for target therapies like targeting gene-virotherapy and monoclonal antibody-directed therapy. These therapies can specifically inhibit the growth of tumor cells at the molecular level and even kill them.

Generally speaking, cancer-related targets should be crucial to the tumor's malignant phenotype, easily measurable in readily obtained clinical samples, and yield a significant clinical response. Since tumorigenesis is a very complex process involving the interaction of multiple factors and pathways, target treatment offers hopes to maximize efficacy while minimizing toxicity and specificity. More importantly, treatment should have little or no toxicity on normal

cells, thus representing the most promising aspect of cancer research (*Friday BB, Adjei AA. Clin Cancer Res 2008; 14:342-346*).

A recent cancer study has provided exciting information. According to *Xinhua News* from London, Michael Way and fellow researchers from Cancer Research UK, have found a specific tumor-related protein, "Tes," that can prevent the diffusion of cancer cells through a Mena-dependent mechanism (http://news.xinhuanet.com/newscenter/2007-12/29/content_7337328.htm, available as of December 28, 2007).

Research has found that a large amount of "Mena" protein is expressed in tumor tissues, helping cancer cells to diffuse throughout the body. Nevertheless, the protein "Tes" adheres to Mena, preventing it from reacting with another specific substance and rendering it ineffective, thus stopping Mena from helping cancer cells to diffuse somewhere else. However, there are large amounts of Mena in a tumor, so Tes is usually unable to stop the diffusion of cancer cells.

In light of other research, Way explained that new study results will open the door to new directions in cancer therapy research. Way also noted that if drugs containing large amounts of the protein Tes are developed in the future, they could stop Mena's action in the body, and thus prevent the massive diffusion of cancer cells.

Results of the study by Way and colleagues have been published in a recent issue of the journal *Molecular Cell* (*Boëda B, Briggs DC, Higgins T, et al. Mol Cell 2007; 28:1071-1082*).

(Xun Li, Shandong University, Ji'nan, China)

Dynamic of modernizing traditional Chinese medicine and the standards system for its development

Ruoyan Gai^{1,2}, Huanli Xu^{2,3}, Xianjun Qu², Fengshan Wang², Hongxiang Lou²,
Jinxiang Han⁴, Munehiro Nakata^{2,5}, Norihiro Kokudo³, Yasuhiko Sugawara^{3,4},
Chushi Kuroiwa^{1,2}, Wei Tang^{2,3,4,*}

The "Japan-China Joint Team for Medical Research and Cooperation":

¹ Department of Health Policy and Planning, The University of Tokyo, Tokyo, Japan;

² China-Japan Cooperation Center for Drug Discovery & Screen, Shandong University, Jinan, China;

³ Hepato-Biliary-Pancreatic Surgery Division, Department of Surgery, Graduate School of Medicine, The University of Tokyo, Tokyo, Japan;

⁴ Shandong Academy of Medical Sciences, Jinan, China;

⁵ Department of Applied Biochemistry, Tokai University, Kanagawa, Japan.

ABSTRACT: This article reviewed the process of Traditional Chinese Medicine's modernization on a global scale. This process is motivated by the potential need for traditional medicine as a result of health transitions and increasing drug R&D based on know-how from TCM. The established standards system for modern medicine serves as a basic model yet has limitations in terms of comprehensively evaluating TCM. Spurred by policy commitments, research to provide supplements suited to TCM's features and principles is underway. Advanced and interdisciplinary technology and methodology is expected to play an essential role in TCM development.

Keywords: Traditional Chinese Medicine, Standards system, Drug development

Traditional Chinese medicine (TCM) has assembled both empirical and theoretical know-how over its long history in China. An essential component of the health care system, TCM accounts for around 40% of all health care provided in China. Modernizing TCM has been a long-term national effort since 1997, when TCM modernization was an essential goal of the Resolution of Health Sector Reform and Development issued by the State Council (1).

This effort by the Chinese government is prompted by two recent trends in global society. One is the

*Correspondence to: Dr. Wei Tang, HBP Surgery Division, Department of Surgery, Graduate School of Medicine, The University of Tokyo, 7-3-1 Hongo, Bunkyo-ku, Tokyo 113-8655, Japan;
e-mail: tang-sur@h.u-tokyo.ac.jp

potential need for traditional medicine accompanying health transitions. Epidemiological and demographic changes have created an opportunity to integrate traditional medicine into the health system (2). Recent studies have indicated a dramatic shift in the distribution of global mortality and the disease burden from infectious, maternal, perinatal, and nutritional causes to chronic, lifestyle-related, and debilitating diseases causes (3,4). Meanwhile, social and economic development results in most developing countries still shouldering "double burdens," namely, both non-infectious diseases and emerging and re-emerging infectious diseases such as HIV/AIDS and malaria. Moreover, the manner of medical practice has changed from disease treatment alone to integrated approaches including prevention, health care, treatment, and rehabilitation (5). The World Health Organization (WHO) emphasizes that traditional medicine can play an important role in achieving the goal of "Health for All" and is dedicated to facilitating the integration of traditional medicine with Western medicine worldwide (6). Thus, traditional medicine such as TCM has received greater attention worldwide as an alternative to established modern medicine and its legitimization has joined policymakers' agenda in order to solve complicated issues resulting from health transitions.

Another is increasing drug development from herbal remedies. Due to relatively high costs and long periods for development of new chemical drugs, enterprises have recently focused on herbal remedies to identify active ingredients and to isolate one or several bioactive compounds for drug development. An epoch-making successful case dates back to the 1970s, when Chinese scientists isolated artemisinin from Qinghao (*Artemisia annua*). On a global scale, many bioactive compounds, such as atropine, reserpinum, digoxin,

ergometrine, levodopa, ephedrinum, and camptothecin, are isolated from herbal remedies. The abundant know-how assembled over the long history of TCM provides a clue to discovery: there are 12,807 kinds of crude remedies and numerous prescriptions described in the voluminous literature on TCM (7). Policymakers believe TCM's rich know-how and biodiversity would benefit its development in China.

Thus, TCM modernization has been regarded as a crucial strategy for Chinese pharmaceutical industry development, helping to fuel China's economic growth. Paralleling Western practices, the Chinese government has over the past ten years formulated and implemented a series of standards to regulate the pharmaceutical industry, such as Regulations for New Drug Approval, Good Laboratory Practice (GLP), Good Clinical Practice (GCP), Good Manufacture Practice (GMP) (8), Good Supply Practice (GSP), and Good Agricultural Practice for crude herbal and animal remedies (GAP) (Table 1). Currently, TCM development is also following the standards system. Moreover, large Chinese pharmaceutical companies with innovative natural drugs, such as Zhejiang Kanglaite Pharmaceutical Co., Ltd. (Zhejiang, China), have opted to submit to regulatory systems in Western countries and have had some success (9,10).

On the other hand, there are limitations to the established Western standards system for TCM development (10). In most cases of TCM, the prescription is usually complex involves a mixture of various bioactive compounds that have diverse mechanisms of action and synergistic/combinational effects. Moreover, the diagnostic principles of TCM emphasize the overall condition of the individual patient and a holistic approach rather than a particular disease process and allopathic approaches. Additionally, the active ingredients of TCM are affected by environmental conditions and are too unstable to be precisely measured. All of these factors have contributed to the controversy on whether TCM remedies can be approved as "drugs." In fact, some professionals in China are skeptical and critical of TCM; they are concerned that it has been based on inaccurate and mysterious interpretations and experientialism rather than scientific evidence such as definite pharmacokinetic analysis, toxicity testing, and double-blinded clinical trials (11). Therefore, Chinese policymakers now emphasize a comprehensive approach to develop methodologies to test traditional features and principles of TCM in addition to earlier attempts to screen and isolate active ingredients from herbal remedies (12).

In 2007, a new plan was issued to expedite innovation in TCM with a comprehensive approach (13). It aims to establish scientific standards specially tailored to TCM, in terms of interpretation of the following technicalities of TCM in multiple languages:

Table 1. China's current standards for the pharmaceutical industry paralleling international practices

Years implemented	A series of standards
1999	Regulations for New Drug Approval
1999	Good Clinical Practice
1999	Good Laboratory Practice
2000	Good Supply Practice
2001	Good Manufacture Practice
2002	Good Agriculture Practice

TCM clinical practice guidelines, evaluation of the efficacy and safety of TCM, management and quality control in plantation, conservation, preparation and manufacture, and drug approval. Through the new plan, the government set a course towards TCM modernization (13). With this policy commitment, huge investment has flowed into related research programs such as the Herbalome Project (11), which is expected to provide the scientific evidence for establishment of a standards system for TCM.

Advanced experimental technologies and methodologies in molecular biotechnology, pharmacokinetics, and bioinformatics, such as chromatography, fingerprint analysis, genomics, proteomics, metabonomics, and computer pattern interpretation, have been used to trace herbal remedies and to identify active ingredients (14). This progress favors a recent attempt to treat bio-active compounds in several herbal remedies as one target for pharmacological tests and consequently identify various compounds and interactions, opening the door for TCM development (15).

In conclusion, TCM modernization represents increasing medical pluralism with health transitions and economic incentives for potential expansion of the global pharmaceutical market. There is an urgent need for systematic scientific standards to objectively evaluate the safety and efficacy of TCM and to strictly control its quality, which are key aspects of international criteria for drug approval and should be central to the ongoing standards system for TCM. The established standards system for modern medicine can clearly serve as a basic model, but further research is definitely needed to provide supplements suited to TCM's features and principles. This long-term challenge is now in its initial stages. Advanced and interdisciplinary technology and methodology is expected to play an essential role in TCM development.

Acknowledgements

This study was supported by Grants-in-Aid from the Ministry of Education, Science, Sports and Culture of Japan, Yuasa International Education and Academic Exchange Fund, and Japan-China Medicine Association.

References

1. The resolution of health sector reform and development. The document available at: <http://www.moh.gov.cn/newshtml/8478.htm> (in Chinese, accessed January 16, 2008)
2. Janes CR. The health transition, global modernity and the crisis of traditional medicine: the Tibetan case. *Soc Sci Med* 1999; 48:1803-1820.
3. Lopez AD, Mathers CD, Ezzati M, Jamison DT, Murray CJ. Global and regional burden of disease and risk factors, 2001: systematic analysis of population health data. *Lancet* 2006; 367:1747-1757.
4. Mathers CD, Loncar D. Projections of global mortality and burden of disease from 2002 to 2030. *PLoS Med* 2006; 3:2011-2030.
5. Li W, Jiang J, Chen J. Chinese medicine and its modernization demands. *Arch Med Res* 2008; 39: 246-251.
6. The World Health Organization. WHO Traditional Medicine Strategy 2002-2005. The document available at http://whqlibdoc.who.int/hq/2002/WHO_EDM_TRM_2002.1.pdf (accessed August 19, 2007).
7. The data available at <http://www.satcm.gov.cn/lanmu/keyan/index.htm> (in Chinese, accessed August 19, 2007)
8. Gai RY, Qu XJ, Lou H, Han J, Cui SX, Nakata M, Kokudo N, Sugawara Y, Kuroiwa C, Tang W. GMP implementation in China: A double-edged sword for the pharmaceutical industry. *Drug Discov Ther* 2007; 1:12-13.
9. Hardy J, Singleton A, Gwinn-Hardy K. The new face of traditional Chinese medicine. *Science* 2003; 299:188-191.
10. Basu P. Trading on traditional medicines. *Nat Biotechnol* 2004; 22:263-265.
11. Stone R. Lifting the veil on traditional Chinese medicine. *Science* 2008; 319:709-710.
12. Qiu J. China plans to modernize traditional medicine. *Nature* 2007; 446:590-591.
13. The traditional Chinese medicine innovation development plan (2006-2020). The document available at: <http://www.moh.gov.cn/newshtml/18247.htm> (in Chinese, accessed August 19, 2007).
14. Tarasawa K. How to accomplish the universality of Japanese-Oriental (Kampo) medicine: looking for harmonization between the eastern and western paradigms. *Nippon Yakurigaku Zasshi* 2006; 128: 389-394. (in Japanese)
15. Chen X, Du G. Target validation: a door to drug discovery. *Drug Discov Ther* 2007; 1:23-29.

(Received November 11, 2007; Revised February 16, 2008; Accepted February 21, 2008)

Three decades of GMP implementation in Thailand: Hardships and success

Santad Chanprapaph*

Department of Pharmacology, Faculty of Pharmaceutical Sciences, Chulalongkorn University, Bangkok, Thailand.

ABSTRACT: Thailand has implemented GMP for almost three decades. GMP Guidelines from the World Health Organization (WHO) were adopted starting in 1978. A few years later, those guidelines were revised twice in 1992 according to ASEAN's version and the WHO's version of GMP, respectively. In 2003, GMP was enforced by law after 25 years of voluntary compliance. In 2007, 153 out of 163 of modern pharmaceutical manufacturers have complied with GMP (93.87%). The rest are closing buildings and facilities for renovation in order to meet GMP requirements.

Keywords: GMP, FDA, Thailand

Pharmaceutical industries in Thailand have existed for more than 40 years. In the beginning, there were only two types of pharmaceutical industries. The first was midstream industry producing raw materials for both active ingredients and inert substances such as paracetamol, aluminium hydroxide compressed gel, magnesium hydroxide compressed gel, sorbitol, sodium chloride, and dextrose monohydrate. The second was downstream industry producing pharmaceutical products in formulations. Thailand never had upstream industry requiring massive investment for new drug development. Before the GMP system was implemented, the country was facing numerous problems including unexpected contamination of products, insufficient or excess active ingredient, and incorrect labels on containers. The Thai FDA took a caution approach to this crisis. The sole solution put forth at that time was the GMP system (1). Therefore, GMP Guidelines from World Health Organization (WHO) were adopted as the first Guidelines for Thailand's GMP in 1978 to ensure that products are

consistently produced and controlled according to quality standards (2).

Since GMP compliance was voluntary and not compulsory in the beginning, compliance by pharmaceutical manufacturers was lacking, especially among local companies, though not among multinational companies. This was because of large investments to improve the standard of manufacturing and quality control. The big question was "Is it really worth spending our money to do this?" In response to this very challenging question, the Thai FDA then arranged many more training programs and provided more information and documents about GMP for both officials responsible for GMP implementation and pharmaceutical companies. Furthermore, the Thai FDA also worked closely with those manufacturers by setting up the Quality Improvement Team (QIT) to work as a board of consultants for companies in all matters relating to GMP. In 1987, Thailand, as a member of ASEAN, revised the aforementioned guidelines according to ASEAN's GMP, and these new guidelines became the second version of GMP Guidelines for Thailand. Later, in 1993, these GMP guidelines were revised again in order to comply with the WHO's 1992 version of GMP, and these become the current GMP guidelines for Thailand. At this stage, GMP compliance was still voluntary for pharmaceutical manufacturers.

Within the first 2 decades of GMP implementation, only 126 out of 175 modern pharmaceutical manufacturers (72%) complied with GMP. However, the Thai FDA consistently worked to further promote compliance with GMP among those pharmaceutical manufacturers. The average number of pharmaceutical companies obtaining GMP certificates gradually increased each year (Table 1). Eventually, in the year 2003 the GMP system was enforced by law after 25 years of voluntary compliance. The year 2007 marks almost three decades of GMP implementation in Thailand, and 153 out of 163 modern pharmaceutical manufacturers have complied with the GMP (93.87%). The rest are closing buildings and facilities for renovation in order to meet the GMP requirements (3).

In addition, Thailand has sought membership in the Pharmaceutical Inspection Convention/Pharmaceutical

*Correspondence to: Dr. Santad Chanprapaph, Department of Pharmacology, Faculty of Pharmaceutical Sciences, Chulalongkorn University, Bangkok 10330, Thailand;
e-mail: schanprapaph@yahoo.com

Table 1. Total number of modern pharmaceutical manufacturers that have obtained a GMP certificate^a

Year	Total number of modern pharmaceutical manufacturers ^b	Total number of modern pharmaceutical manufacturers that have obtained a GMP certificate ^c
1978	188	0
1979	189	0
1980	189	0
1981	188	0
1982	187	0
1983	188	0
1984	189	0
1985	188	0
1986	187	0
1986	188	0
1987	189	0
1988	188	0
1989	188	59 (31.38%)
1990	188	79 (40.03%)
1991	184	95 (51.63%)
1992	180	105 (58.33%)
1993	180	112 (62.22%)
1994	178	117 (65.73%)
1995	180	122 (67.77%)
1996	175	122 (69.71%)
1997	175	126 (72.00%)
1998	176	130 (73.86%)
1999	176	130 (73.86%)
2000	174	127 (72.99%)
2001	172	131 (76.16%)
2002	174	134 (77.01%)
2003	174	133 (76.43%)
2004	171	141 (82.46%)
2005	166	151 (90.96%)
2006	162	153 (94.44%)
2007	163	153 (93.87%)

^aSource: Thai FDA Annual Report and Thai FDA's Website (http://wwwapp1.fda.moph.go.th/drug/zone_search/files/sea001_008.asp)

^bModern pharmaceutical manufacturers: pharmaceutical manufacturers that produce drugs intended for use in the practice of modern medicine or treatment of animal diseases.

^cThe Thai FDA started issuing a GMP certificate in 1989.

Inspection Cooperation Scheme (PIC/S) since 2006 and its application is under consideration (4). In the meantime, more critical and harder steps are planned. The Thai FDA is adopting the current PIC/S GMP Guide as a mandatory requirement for manufacturers, and this process will be accomplished within the year 2008. Implementation is expected to be completed within one year afterwards.

Acknowledgements

The author wishes to thank Thai FDA officials for their kind assistance in providing detailed information on Thailand's GMP.

References

1. <http://elib.fda.moph.go.th/library/fulltext1/private/picture.asp?temp=3347> (accessed as of February 12, 2007)
2. WHO. "GMP questions and answers," http://www.who.int/medicines/areas/quality_safety/quality_assurance/gmp/en/ (accessed as of February 12, 2007)
3. http://wwwapp1.fda.moph.go.th/drug/zone_search/files/sea001_008.asp (accessed as of February 12, 2007)
4. PIC/S Annual Report 2006. This document is available at: <http://www.picscheme.org/index.php?p=report> (accessed as of February 12, 2007)

(Received December 20, 2007; Revised February 12, 2008; Accepted February 15, 2008)

Brief Report

Establishment of a new cell line for performing sensitive screening of nuclear export inhibitors

Ken Watanabe¹, Saiko Noda¹, Nobuyuki Kobayashi^{1, 2,*}

¹Laboratory of Molecular Biology of Infectious Agents, Graduate School of Biomedical Sciences, Nagasaki University, Nagasaki, Japan;

²Central Research Center, AVSS Corporation, Nagasaki, Japan.

ABSTRACT: Cell nuclear import and export of proteins are among the most important processes for cellular homeostasis. Viruses, including influenza virus and HIV-1 also utilize nuclear export machinery for their propagation. Therefore, the specific inhibition of nuclear export can be a good target for the development of antiviral drugs. This report documents the establishment of Madin-Darby Canine Kidney (MDCK) cells stably expressing GFP-NES fusion protein for the sensitive screening of novel nuclear export inhibitors. Leptomycin B (LMB), an inhibitor for the interaction between substrate nuclear export signal (NES) and cellular export factor, CRM1, was used for evaluating the screening system. The low concentration (30 pg/mL) and short time treatment (~10 min) of LMB resulted in the nuclear accumulation of GFP fluorescence.

Keywords: Nuclear export, Screening, Antiviral drug

Introduction

The transport of proteins through nuclear pore complexes (NPCs) is mediated by importins and exportins (1). CRM1/exportin1 is the most characterized exportin. The formation of exportin-substrate molecule complexes is regulated by Ran. The export substrates of CRM1 possess a leucine-rich nuclear export signal (NES). The NES was identified in Heat shock cognate protein 70 (Hsc70), influenza virus NS2, HIV-1 Rev (2), protein kinase A inhibitor (3) (Figure 1) and other proteins.

A virus is a unique pathogen which is incapable of replicating without a host cell. It utilizes the host cell

environment and cellular factors for its propagation (for a review, see *Ref. 4*). Nuclear export of proteins from the nucleus seems to be an attractive target for antiviral therapy because viruses such as human immunodeficiency virus (HIV) and influenza virus utilize this environment. Development of antiviral drugs is one of the most important strategies, however, some viruses, especially RNA viruses, easily resist drugs designed for virus gene products. It is well recognized that influenza virus, which is resistant to amantadine (the inhibition of viral M2 protein), are already spreading all over the world. The same problems are serious in HIV treatment, and a recent protocol, termed HAART therapy, a multi drug combination therapy, is essential to treat patients with HIV. To make such antiviral therapy more effective, further development of novel drugs which target cellular proteins is essential. Therefore, inhibitors which control or inhibit the nuclear export system could be good candidates. However, only leptomycin A (LMA) and leptomycin B (LMB) are available for research use as inhibitors of CRM1-mediated nuclear export.

Recently, Hsc70 was identified to be a mediator for nuclear export of influenza viral ribonucleoprotein complex (RNP). Hsc70 has been found to possess NES (5) and involve nuclear export of importin and transportin (6). These findings also suggest that the inhibition of nuclear export of influenza viral RNP by LMB is effective for reducing influenza virus production (7). Although LMB is effective *in vitro*, it can also damage the cellular activity.

Recently a new cell line expressing GFP fused HIV-1 protease was established for screening anti-HIV protease activity (8). This report describes the establishment of a stable cell line which expresses the GFP - nuclear export signal (NES) fusion protein. The established cells (GES5) were sensitive to LMB. This cell line can be utilized to develop a new, high-throughput screening system for nuclear export inhibitors without using free virus.

Materials and Methods

*Correspondence to: Dr. Nobuyuki Kobayashi, Laboratory of Molecular Biology of Infectious Agents, Graduate School of Biomedical Sciences, Nagasaki University, 1-14 Bunkyo-machi, Nagasaki 852-8521, Japan; e-mail: nobnob@nagasaki-u.ac.jp

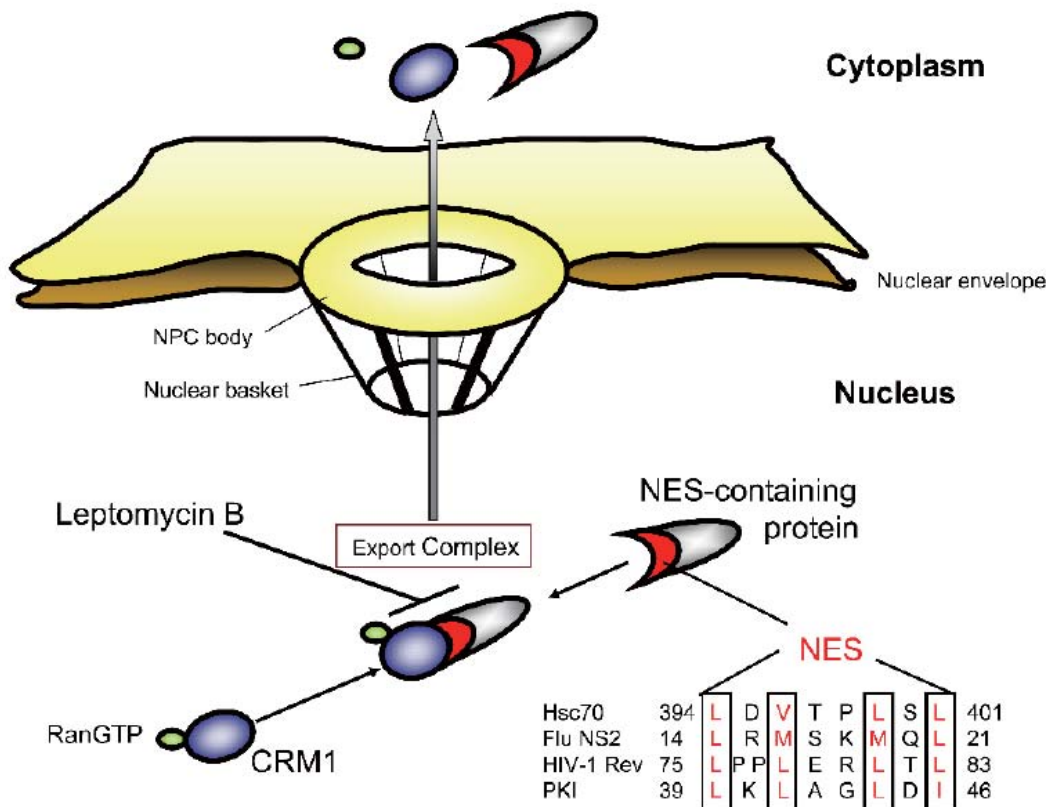


Figure 1. The general mechanism of nuclear export and representative NES-containing proteins. NES-containing protein binds to CRM1. Leptomycin B inhibits NES-CRM1 interaction. CRM1 is an Importin-beta family protein and binds to Ran-GTP. The complex is exported from the nucleus to cytoplasm through NPC. The dissociation of NES containing protein-CRM1-Ran-GTP complex is triggered by conversion of Ran-GTP to Ran-GDP. The representative leucine-rich NES are also shown.

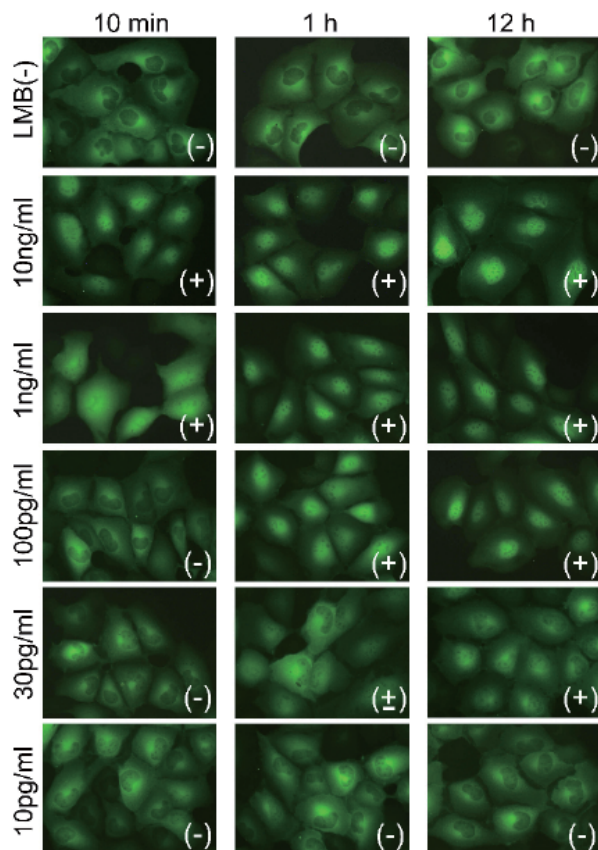


Figure 2. LMB sensitivity of GES5 cells. GES5 cells were treated with LMB as indicated. GFP fluorescence accumulates at 10 min after addition of 10 ng/mL or 1 ng/mL of LMB and is retained in the nucleus up to 12 h, whereas very low concentration of LMB treatment (100 pg/mL or 30 pg/mL) requires 1 h for nuclear accumulation of GFP fluorescence. The nuclear accumulation of GFP fluorescence is shown as (-), (±) and (+).

Cells, chemicals and plasmids

Madin-Darby canine kidney (MDCK) cells were maintained in MEM supplemented with 5% FBS. LMB was purchased from LC Laboratories, Inc. (Woburn, MA, USA) and dissolved in 70% ethanol to a final concentration of 10 µg/mL and stored at -20°C. A plasmid for expressing GFP-NES fusion protein (pEGFP-NES) was kindly supplied by Dr. Shoko Saitoh (Tsukuba University, Japan) (9). For the establishment of cell lines, ~90% confluent MDCK cells were transfected in a 24 well plate with 2 µg of pEGFP-NES in the presence of 6 µL of lipofectamine 2000 (Invitrogen). The cells were incubated for 5 h with the DNA-lipofectamine 2000 complex, and then were washed once with MEM, and replaced with MEM containing 5% FBS. Twenty-one hours later, the cells were trypsinized and seeded into 90 mm dishes. G418 sulfate (Nacalai, Kyoto Japan) was added to a final concentration of 600 µg/mL. The cell lines expressing high intensity fluorescence were selected under fluorescence microscopy (Axiovert25, Carl Zeiss).

Nuclear translocation assays using Leptomycin B (LMB)

GES5 cells were grown on coverslips, and LMB was added at the final concentrations indicated in Figure 2. The accumulation of fluorescence into the nucleus was observed under fluorescence microscopy (Axiophot, Carl Zeiss).

Results and Discussion

Establishment of a cell line which expresses GFP-NES fusion protein

To establish cell lines stably expressing GFP-NES fusion protein, MDCK cells were transfected with pEGFP-NES and colonies were selected in the presence of G418 sulfate. A cell line, designated MDCK-GFP-NES#5 (GES5) was selected, and tested for LMB sensitivity (Figure 2). Fluorescence of GFP was diffusely distributed in both the nucleus and cytoplasm (data not shown), whereas that of GFP-NES clearly distributed in cytoplasm (Figure 2). When LMB was added, CRM1-dependent nuclear export was inhibited, thus resulting in nuclear accumulation of GFP-NES protein. This effect was observed at 10 min after addition of LMB.

This cell line system is sensitive to LMB and it is safe, because there is no need to use live HIV-1 or influenza virus. The newly established cell line, GES5, was easily maintained with conventional medium and serum. The addition of nuclear export inhibitors such as LMB rapidly results in nuclear accumulation of GFP fluorescence. Indeed, when the MDCK cell line expressing GFP-Hsc70 and GFP-Hsc54 (5) were tested

for LMB sensitivity, accumulation of fluorescence in nucleus requires 24 h and 6 h, respectively (data not shown). Moreover, LMB is generally used at a concentration of 5-10 ng/mL as reported previously (5,9,10). In this system, nuclear accumulation of GFP fluorescence is observed with a 30 pg/mL treatment (Figure 2). Therefore, the GES5 cell line is thus considered to be useful for a sensitive and high-throughput screening system.

Acknowledgements

We thank Dr S. Saitoh (Tsukuba University, Japan) for providing the GFP-NES expression vector. This work was supported in part by a Grant-in-Aid for Ministry of Education, Culture, Sports, Science and Technology and by a Grant-in-Aid for Scientific Research from Nagasaki University, Japan (K.W.).

References

1. Fornerod M, Ohno M, Yoshida M, Mattaj IW. CRM1 is an export receptor for leucine-rich nuclear export signals. *Cell* 1997; 90:1051-1060.
2. Fischer U, Huber J, Boelens WC, Mattaj IW, Luhrmann R. The HIV-1 Rev activation domain is a nuclear export signal that accesses an export pathway used by specific cellular RNAs. *Cell* 1995; 82:475-483.
3. Wen W, Meinkoth JL, Tsien RY, Taylor SS. Identification of a signal for rapid export of proteins from the nucleus. *Cell* 1995; 82:463-473.
4. Kitazato K, Wang Y, Kobayashi N. Viral infectious disease and natural products with antiviral activity. *Drug Discov Ther* 2007; 1:14-22.
5. Tsukahara F, Maru Y. Identification of novel nuclear export and nuclear localization-related signals in human heat shock cognate protein 70. *J Biol Chem* 2004; 279:8867-8872.
6. Kose S, Furuta M, Koike M, Yoneda Y, Imamoto N. The 70-kD heat shock cognate protein (hsc70) facilitates the nuclear export of the import receptors. *J Cell Biol* 2005; 171:19-25.
7. Watanabe K, Fuse T, Asano I, Tsukahara F, Maru Y, Nagata K, Kitazato K, Kobayashi N. Identification of Hsc70 as an influenza virus matrix protein (M1) binding factor involved in the virus life cycle. *FEBS Lett* 2006; 580:5785-5790.
8. Fuse T, Watanabe K, Kitazato K, Kobayashi N. Establishment of a new cell line inducibly expressing HIV-1 protease for performing safe and highly sensitive screening of HIV protease inhibitors. *Microbes Infect* 2006; 8:1783-1789.
9. Saito S, Miyaji-Yamaguchi M, Nagata K. Aberrant intracellular localization of SET-CAN fusion protein, associated with a leukemia, disorganizes nuclear export. *Int J Cancer* 2004; 111:501-507.
10. Watanabe K, Takizawa N, Katoh M, Hoshida K, Kobayashi N, Nagata K. Inhibition of nuclear export of ribonucleoprotein complexes of influenza virus by leptomycin B. *Virus Res* 2001; 77:31-42.

(Received November 5, 2007; Accepted November 6, 2007)

Brief Report

Localization of glucagon-like peptide-2 receptor mRNA expression at different sites in the small intestine of rats

Kenji Ikeda^{1,*}, Michiaki Myotoku¹, Nobuo Kurokawa², Yoshihiko Hirotsu¹

¹Laboratory of Clinical Pharmaceutics, Faculty of Pharmacy, Osaka Ohtani University, Tondabayashi, Osaka, Japan;

²Department of Pharmacy, Osaka University Hospital, Suita, Osaka, Japan.

ABSTRACT: Preproglucagon is known to be processed into glucagon-like peptide (GLP)-1, GLP-2, and glicentin in the L cells of the intestinal tract. GLP-2 has been shown to possess intestinotrophic activity in rodents. However, the ligand-binding mechanisms of GLP-2 receptor (GLP-2R) have not been extensively investigated. The present study sought to determine the localization of GLP-2R in the small intestine by analyzing GLP-2R mRNA expression using the reverse transcriptase-polymerase chain reaction (RT-PCR) method. GLP-2R mRNA expression was detected at all sites in the small intestine; its expression levels were particularly high in the jejunum. Moreover, GLP-2R mRNA expression was detected in both non-mucosal intestinal tissues and intestinal mucosa. These findings suggest that in addition to the intestinal mucosa, the functional sites of GLP-2 may be present in the non-mucosal tissues. These results imply that GLP-2 peptide acts as an intestinotrophic factor that may affect the intestines from outside the mucosa. The intestinotrophic effect of GLP-2 from outside the mucosa may be a function of the enteric neurons transmitting several growth signals to mucosal cells.

Keywords: GLP-2, GLP-2 receptor, Small intestine, Localization, Mucosa

Introduction

Preproglucagon, a precursor of enteroglucagon, is known to be processed into glucagon-like peptide (GLP)-1, GLP-2, and glicentin in the L cells of in the intestinal tract (1). GLP-1 regulates blood glucose via the stimulation of glucose-dependent insulin secretion, inhibition of gastric emptying, and inhibition of

secretion of glucagons. Research has shown that GLP-2 has an intestinotrophic effect in rodents (2). Myojo *et al.* (1) demonstrated that glicentin has a direct trophic effect on rat small intestinal mucosa and on the IEC-6 rat small intestinal cell line, and they suggested that this peptide forms the active site of enteroglucagon. Moreover, the current authors reported that methionyl-rat glicentin has a growth-enhancing effect on the mucosa during an intestinal adaptive response following 70% resection of the rat small intestine (3). In the residual intestine of rats with 70% of the distal small intestine resected, furthermore, the jejunum mucosal weight increased as a result of GLP-2 treatment (4) and small intestinal injury following methotrexate administration (5).

The distribution of receptors to these peptides suggests that GLP-2, like glucagon and GLP-1, acts through a distinct and specific novel receptor expressed in its principal target tissue—the gastro intestinal tract (6). The novel expression sites (*e.g.*, jejunum) for both glucagon and GLP-1 receptor gene in the mouse have previously been identified (7).

GLP-2 is known to be an intestine-derived peptide with intestinotrophic properties that may be therapeutically useful in treating diseases characterized by intestinal damage or insufficiency (8). Nian *et al.* provided evidence demonstrating the divergence in the mechanisms of tissue-specific regulation of proglucagon genes in humans and rodents (9). Moreover, the structural changes and the ligand-binding mechanisms of GLP-2 receptor (GLP-2R) have previously been investigated (10-13). The present study sought to determine the localization of GLP-2R in the intestines by analyzing the GLP-2R mRNA expression of rat intestinal sites (*i.e.*, the duodenum, jejunum, ileum, and each mucosal site) by using a reverse transcriptase-polymerase chain reaction (RT-PCR) method.

Materials and Methods

Preparation of intestinal samples

All experimental procedures were conducted in

*Correspondence to: Dr Kenji Ikeda, Laboratory of Clinical Pharmaceutics, Faculty of Pharmacy, Osaka Ohtani University, 3-11-1 Nishikiori-kita, Tondabayashi, Osaka 584-8540, Japan;
e-mail: ikedak@osaka-ohtani.ac.jp

accordance with Osaka University Medical School guidelines for the care and use of laboratory animals.

The experiments were carried out using male Wistar rats (180-200 g) (Clea Japan, Inc., Tokyo, Japan). The small intestines of the rats were removed 24 h after fasting. Each portion of intestinal tissue was divided into the following 3 sites: the duodenum (D), jejunum (J), and ileum (I). The mucosal tissue (M) at each site was then harvested and collected. Further, each site of non-mucosal tissue (NM) was divided into proximal (1), middle (2), and distal (3) sites. These 12 sites of the rat small intestine were used for the experiment described below. On preparation, these samples were immediately stored in liquid nitrogen until assay.

Semi-quantitative RT-PCR

Total RNA was isolated from rat intestinal tissues using an RNeasy[®] Mini Kit (Qiagen K.K., Tokyo, Japan) and identified by ultraviolet (UV) spectrophotometry. For the generation of first strand cDNA templates for RT-PCR, 3 µg of DNase I-treated total RNA from the rat intestines were reverse transcribed at 42°C for 50 min using the SuperScript[™] First-Strand Synthesis System (Invitrogen Japan K.K., Tokyo, Japan). An aliquot of the first-strand reaction solution (volume, 1/20) was used as a template for PCR with KOD-plus DNA polymerase (Toyobo Co., Ltd., Osaka, Japan). PCR was performed over a range of cycles spanning the exponential phase of amplification kinetics, and linearity was shown for relative cDNA input across 2 orders of magnitude. Primer pairs selected for PCR were as follows: rat GLP-2R, 5'-GCTGGCCTCATTCTTATCC-3' and 5'-AACAAAGAAGAGTGTAAGAGCC-3'; and rat β-actin (encoded by the *ACTB* gene), 5'-ATCATGTTT GAGACCTTCAACAC-3' and 5'-TCTGCGCAAGTT AGGTTTTGTC-3'. Samples for GLP-2R analysis were denatured at 94°C for 2 min and subjected to 34 cycles of PCR (94°C for 15 sec, 56°C for 30 sec, and 68°C for 1 min) with an additional extension at 72°C for 8 min; this resulted in the generation of a 291-base-pair (bp) product spanning the entire GLP-2R open reading frame. *ACTB* cDNA amplification was performed at an annealing temperature of 60°C for 24 cycles, resulting in the generation of an 825-bp product. *ACTB* cDNA amplification was used as an internal control to monitor the efficiency of first-strand cDNA synthesis. PCR products were separated by gel electrophoresis on a 1% agarose gel, stained with ethidium bromide, and imaged under UV light. The expression ratios of GLP-2R were normalized to that of the housekeeping gene *ACTB*.

Statistical analysis

Student's *t*-test was performed in order to calculate the statistical significance of differences among the means of mRNA expression levels normalized to that

of *ACTB*. Data presented in the figures denote mean ± SD values of the results collected from at least 2 independent experiments.

Results and Discussion

In order to isolate an equal amount of total RNA from each site, the wet weights of the divided tissues were determined. The wet weight of jejunum was found to be the highest. The values of M and NM were 10.0 mg/cm and 63.8 mg/cm, respectively. However, the NM/M wet weight ratio of the duodenum and that of the jejunum were equal (*i.e.*, 6.4). Among the 3 intestinal sites, the NM/M wet weight ratio (7.3) of the ileum was the highest (Table 1). These results demonstrated that the rat ileum contains a smaller amount of mucosal tissue than the jejunum and duodenum. Further, these values of NM/M wet weight ratio were used to calculate the total expression at each site per length based on GLP-2R mRNA expression values.

Following the measurement of wet weight, amplification curves of rat GLP-2R and *ACTB* mRNA expression in RT-PCR were investigated using the total RNA from the jejunum in order to establish suitable conditions for semiquantitative detection. A linear relationship between PCR products and cycle numbers was obtained: 32-36 and 24-32 cycles of PCR for GLP-2R and *ACTB*, respectively. Accordingly, the conditions selected for the semiquantitative detection of GLP-2R and *ACTB* were 34 and 24 cycles of PCR, respectively.

Having determined the appropriate PCR conditions, the expression ratio of GLP-2R mRNA to *ACTB* mRNA at the 3 aforementioned sites was investigated. Each NM site of D, J, and I was measured after they were divided into proximal (1), middle (2) and distal (3) sites. GLP-2R mRNA expression was observed at all of the sites. Among these sites, however, GLP-2R mRNA expression was the highest in the jejunum NM site (Figure 1A). Additionally, among the rat intestinal tissues, the expression ratio of GLP-2R mRNA to *ACTB* mRNA was highest at the J-1 site and relatively lower at the ileum site (Figure 1B). The J-1 site was located in the initial 1-2 cm of the proximal jejunum. At the J-2 and J-3 sites, which were near the beginning of the ileum, the level of GLP-2R expression was lower.

Table 1. The wet weight and GLP-2R mRNA expression ratio of mucosal and non-mucosal tissues

Intestinal site	Wet weight			NM/M ratio of GLP-2R mRNA expression (mean ± SD, n = 3)
	Mucosal (M) (mg/cm)	Non-mucosal (NM) (mg/cm)	NM/M ratio	
Duodenum	8.7	55.3	6.4	1.29 ± 0.27
Jejunum	10.0	63.8	6.4	2.06 ± 1.00
Ileum	8.1	59.4	7.3	1.03 ± 0.05

NM/M ratio of GLP-2R mRNA expression represents the ratio of the GLP-2R mRNA expression normalized to *ACTB* mRNA.

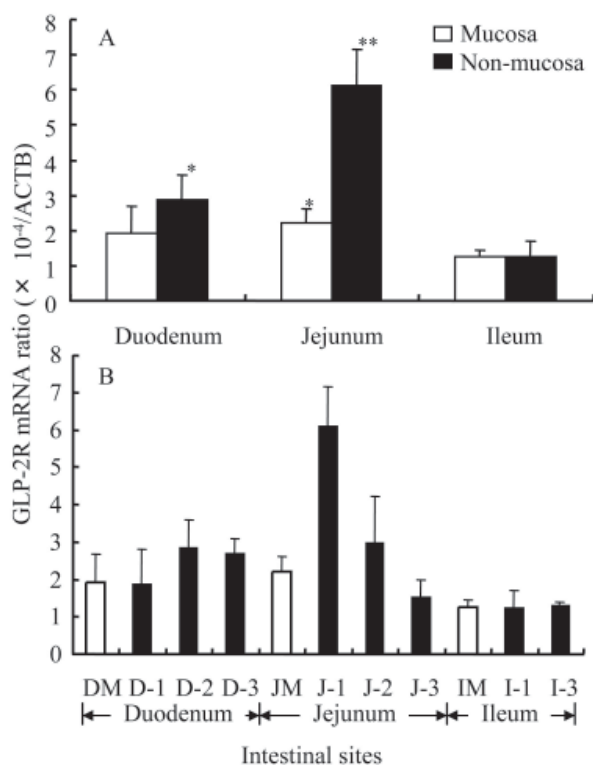


Figure 1. A: The differences in the expression ratios of GLP-2R mRNA to ACTB mRNA at intestinal sites and between mucosal (M) and non-mucosal (NM) tissues. Values are expressed as mean \pm SD ($n = 3$). * $p < 0.05$, ** $p < 0.01$ vs. the ileum. B: The differences in the expression ratios of GLP-2R mRNA to ACTB mRNA among all the divided intestinal sites. Values are expressed as mean \pm SD ($n = 3$). DM, duodenal mucosa; D-1, proximal duodenum; D-2, middle duodenum; D-3, distal duodenum; JM, jejunal mucosa; J-1, proximal jejunum; J-2, middle jejunum; J-3, distal jejunum; IM, ileal mucosa; I-1, proximal ileum; and I-3, distal ileum. GLP-2R mRNA expression was not detected in I-2, which represented the middle of the ileum.

These results suggest that GLP-2 peptide may transmit several signals to response cells at the J-1 site.

At each of the duodenum, jejunum, and ileum sites, the ratio of GLP-2R mRNA expression at the non-mucosal site to that at the mucosal site was greater than 1; this ratio was highest at the jejunum (greater than 2) (Table 1). The result indicated in Table 1 implies that at all sites the expression was not limited to the mucosa. However, these expression ratios were normalized to ACTB and the total expression levels at each site were estimated based on the wet weight of each site. This estimation indicated that total GLP-2R expression at the non-mucosal proximal jejunum site may be more than 10-fold of the level at mucosal proximal jejunum site.

GLP-2 has an intestinotrophic effect through a specific receptor expressed in its principal target tissue—the gastrointestinal tract (14,15). However, the cellular localization of the GLP-2 receptor and the nature of its signaling network in the gut remain poorly defined. Reports have indicated that the antiapoptotic effects of GLP-2 on intestinal crypt cells may be useful for the attenuation of chemotherapy-induced intestinal mucositis (13,16).

Identifying the functional site of GLP-2 peptide in the small intestine should prove beneficial to

providing pharmacotherapy for several small intestinal injuries. The present study compared GLP-2R mRNA expression levels at different sites in the intestinal tract. The GLP-2R mRNA expression levels were highest in the jejunum. Further, the mRNA expression level in the jejunum, particularly in the proximal jejunum, was markedly higher at the non-mucosal site than at the mucosal site. These findings suggest that the jejunum may be the main site of GLP-2 binding and that, in addition to the intestinal mucosa, functional sites of GLP-2 may be present in the non-mucosal tissues. Additionally, GLP-2 peptide may affect the intestines as an intestinotrophic factor from outside the mucosa. Bjerknes *et al.* reported that the nervous system is a key component of a feedback loop that regulates epithelial growth and repair (17). The current data implicates GLP-2 as a potentially crucial neurotransmitter involved in the regulation of food intake and body weight. The intestinotrophic effect of GLP-2 from outside the mucosa may be a function of the enteric neurons, which transmit several signals to mucosal cells.

References

1. Myojo S, Tsujikawa T, Sasaki M, Fujiyama Y, Bamba T. Trophic effects of glicentin on rat small-intestinal mucosa *in vivo* and *in vitro*. *J Gastroenterol* 1997; 32:300-305.
2. Drucker DJ. Glucagon-like peptides. *Diabetes* 1998; 47:159-169.
3. Hirotani Y, Taki M, Kataoka K, Kurokawa N, Satoh T, Sasaki K, Yanaihara C, Luo WQ, Yanaihara N. Effect of rat glicentin on intestinal adaptation in small intestine-resected rats. *Ann N Y Acad Sci* 1998; 865:601-605.
4. Hirotani Y, Yamamoto K, Yanaihara C, Balaspiri L, Yanaihara N, Kurokawa N. Distinctive effects of glicentin, GLP-1 and GLP-2 on adaptive response to massive distal small intestine resection in rats. *Ann N Y Acad Sci* 2000; 921:460-463.
5. Hirotani Y, Yamamoto K, Ikeda K, Arakawa Y, Li J, Kitamura K, Kurokawa N, Tanaka K. Correlation between plasma glucagon-like peptide 2 levels and proliferative makers in small intestinal injury in rats induced by methotrexate administration. *Biol Pharm Bull* 2006; 29:2327-2330.
6. Munroe DG, Gupta AK, Kooshesh F, Vyas TB, Rizkalla G, Wang H, Demchyshyn L, Yang ZJ, Kamboj RK, Chen H, McCallum K, Sumner-Smith M, Drucker DJ, Crivici A. Prototypic G protein-coupled receptor for the intestinotrophic factor glucagon-like peptide 2. *Proc Natl Acad Sci USA* 1999; 96:1569-1573.
7. Campos RV, Lee YC, Drucker DJ. Divergent tissue-specific and developmental expression of receptors for glucagon and glucagon-like peptide-1 in the mouse. *Endocrinology* 1994; 134:2156-2164.
8. Drucker DJ, Boushey RP, Wang F, Hill ME, Brubaker PL, Yusta B. Biologic properties and therapeutic potential of glucagon-like peptide-2. *JPEN J Parenter Enteral Nutr* 1999; 23:S98-S100.
9. Nian M, Drucker DJ, Irwin D. Divergent regulation of human and rat proglucagon gene promoters *in vivo*. *Am*

- J Physiol 1999; 277:G829-G837.
10. Yusta B, Somwar R, Wang F, Munroe D, Grinstein S, Klip A, Drucker DJ. Identification of glucagon-like peptide-2 (GLP-2)-activated signaling pathways in baby hamster kidney fibroblasts expressing the rat GLP-2 receptor. *J Biol Chem* 1999; 274:30459-30467.
 11. DaCambre MP, Yusta B, Sumner-Smith M, Crivici A, Drucker DJ, Brubaker PL. Structural determinants for activity of glucagon-like peptide-2. *Biochemistry* 2000; 39:8888-8894.
 12. Walsh NA, Yusta B, DaCambre MP, Anini Y, Drucker DJ, Brubaker PL. Glucagon-like peptide-2 receptor activation in the rat intestinal mucosa. *Endocrinology* 2003; 144:4385-4392.
 13. Rocha FG, Shen KR, Jasleen J, Tavakkolizadeh A, Zinner MJ, Whang EE, Ashley SW. Glucagon-like peptide-2: divergent signaling pathways. *J Surg Res* 2004; 121:5-12.
 14. Yusta B, Huang L, Munroe D, Wolff G, Fantaske R, Sharma S, Demchyshyn L, Asa SL, Drucker DJ. Enteroendocrine localization of GLP-2 receptor expression in humans and rodents. *Gastroenterology* 2000; 119:744-755.
 15. Petersen YM, Elnif J, Schmidt M, Sangild PT. Glucagon-like peptide 2 enhances maltase-glucoamylase and sucrase-isomaltase gene expression and activity in parenterally fed premature neonatal piglets. *Pediatr Res* 2002; 52:498-503.
 16. Boushey RP, Yusta B, Drucker DJ. Glucagon-like peptide (GLP)-2 reduces chemotherapy-associated mortality and enhances cell survival in cells expressing a transfected GLP-2 receptor. *Cancer Res* 2001; 61:687-693.
 17. Bjerknes M, Cheng H. Modulation of specific intestinal epithelial progenitors by enteric neurons. *Proc Natl Acad Sci USA* 2001; 98:12497-12502.

(Received December 21, 2007; Revised December 25, 2007; Accepted December 26, 2007)

Review**Sensing and reacting to dangers by caspases: Caspase activation via inflammasomes**Asuka Takeishi¹, Erina Kuranaga^{1,2}, Masayuki Miura^{1,2,*}¹Department of Genetics, Graduate School of Pharmaceutical Sciences, The University of Tokyo, Tokyo, Japan;²CREST, JST.

ABSTRACT: Caspases are well known as mediators of programmed cell death, or apoptosis, in which their functions are highly conserved throughout evolution. In addition to inducing apoptosis, caspases have important roles in immune reactions. As part of a cell's response to pathogens or alarm (cellular danger) signals from damaged cells, caspase-1 is activated by forming an inflammatory complex with apoptosis-associated speck like protein containing a caspase recruitment domain (ASC) and nucleotide-binding oligomerization domain like receptor (NLR) family proteins. The activated caspase-1 then cleaves and promotes the maturation of cytokines, such as IL-1 β , IL-18, and IL-33. Although it has long been unclear how hosts recognize diverse stresses, including injury and pathogen infection, and react appropriately, recent analyses have revealed many details about the sensing mechanisms provided by NLRs. Members of the NLR family are activated and yield different outcomes depending on the stimulus. For example, the NLR member cryopyrin/NALP3 induces cytokine secretion and lipid synthesis in response to viral dsRNA and K⁺ efflux, while another NLR, IPAF, induces IL-1 β in response to the virulence protein, flagellin. Cryopyrin/NALP3-mediated caspase-1 activation is involved not only in the immune response to pathogens but also in the stress response to UV irradiation in human skin. In this review, we focus on the stress responses that particularly involve inflammatory caspases. Since host reactions to stresses have been studied in invertebrates as well as in mammals, we also review the caspase-mediated immune responses that have been identified in the fruit fly *Drosophila melanogaster*, and suggest that the contribution of caspases to general stress responses is evolutionally conserved.

*Correspondence to: Dr. Masayuki Miura, Department of Genetics, Graduate School of Pharmaceutical Sciences, The University of Tokyo, 7-3-1 Hongo, Bunkyo-ku, Tokyo 113-0033, Japan; e-mail: miura@mol.f.u-tokyo.ac.jp

Keywords: Caspase, Inflammasome, Stress response, Danger signal, *Drosophila*

Introduction

Caspases are a family of cysteine proteases that are highly conserved in multicellular organisms. They are known as the central regulators of apoptosis. A cell death-executing caspase was first identified as Ced-3 in *Caenorhabditis elegans*, and since then, the regulatory functions of caspases following apoptotic stimulation have been studied in detail (1,2). On the other hand, recent studies have also indicated various non-apoptotic functions of caspases (3). In mammals, the first Ced-3 homolog reported was caspase-1 (interleukin-1 β -converting enzyme, ICE), a cysteine protease responsible for the processing of prointerleukin 1 β (proIL-1 β) and the secretion of mature IL-1 β (4-6). Thus, the first-described function of the mammalian Ced-3 homolog was in the immune response. Not only caspase-1, but also caspase-5 and caspase-11 have been reported as inflammatory caspases (7,8).

Caspase-1 is synthesized as an inactive procaspase-1. When activated, the enzyme is cleaved into subunits p20 and p10, which form a heterotetramer (8,9). In macrophages, caspase-1 activation promotes the secretion of IL-1 β in response to pathogen associated molecular patterns (PAMPs), which include bacterial compounds and viral infections, or to endogenous molecules released from damaged cells (10). Caspase-1 also processes IL-18 and IL-33, and thus is responsible for both inflammatory and innate immune responses (11). However, many questions about the mechanism remain: How do cells sense various PAMPs and endogenous alarms, and distinguish them from the cell itself? Does each "danger signal" activate caspase-1 differently? And how does caspase-1 respond to each signal? Here, we review some of the pathways in various stress responses that occur through caspase-1.

Inflammasomes

The caspase-1-activating complex is called the "inflammasome" (9,12). It is composed of caspase-1 and apoptosis-associated speck-like protein containing a caspase-recruitment domain (CARD) (ASC/ PYCARD/ CARD5/ TMS1ASC) in addition to apoptotic protease activating factor-1 (Apaf-1)-like inflammasome components such as NALP1 (Defcap/ Nac/ CARD7), cryopyrin (NALP3/ Cias1/ Pypaf1), and ICE protease activating factor (IPAF/ CARD12), which can sense different bacteria, toxins, or endogenous danger signals released from damaged cells (13-16) (Figure 1).

In the case of microbial pathogens, host cells recognize them by germ-line encoded pattern recognition receptors (PRRs), which contain leucine-rich repeats (LRRs). The best known of these signaling systems are triggered by the LRR-containing Toll-like receptors (TLRs) on the surface of the cells. For instance, TLR4 senses lipopolysaccharide (LPS), TLR5 senses flagellin, TLR7 and 8 recognize toxins and antiviral imidazoquinoline R837 and R848, and TLR9 recognizes bacterial and viral nucleic-acid motifs (17-21). TLR activation induces the synthesis of proIL-1 β which assembles into an inflammasome with caspase-1 and constitutively expresses ASC. TLR activation also leads to the induction of IL-16 and tumor necrosis factor (TNF) production (22).

In addition to TLRs, nucleotide-binding

oligomerization domain (NOD)-like receptors (NLRs/ CATERPILLER proteins) also sense pathogens. NLRs are cytosolic proteins that recognize microbial pathogens within the compromised cells, which means they function as intracellular PRRs (23,24). Both extracellular and intracellular PRRs trigger intracellular immune responses, such as assembly of the inflammasome, activation of caspase-1, and secretion of cytokines including IL-1 β , IL-18, and IL-33 (11) (Figure 2).

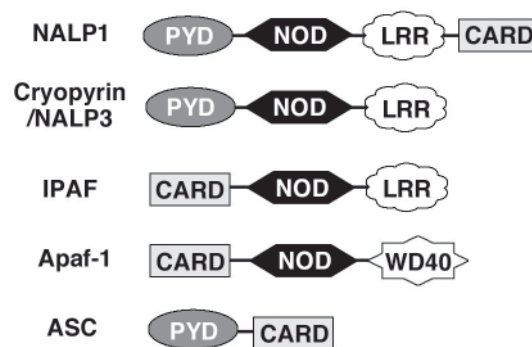


Figure 1. NLR family proteins and ASC. Members of the nucleotide-binding oligomerization domain (NOD)-like receptor (NLR) family contain common domains such as the Pyrin domain (PYD), caspase recruitment domain (CARD), NOD, leucine-rich repeat (LRR), or WD40, which contribute to the NLR's ability to sense and react to various stresses. The apoptosis-associated speck like protein containing a CARD (ASC) structure is also illustrated.

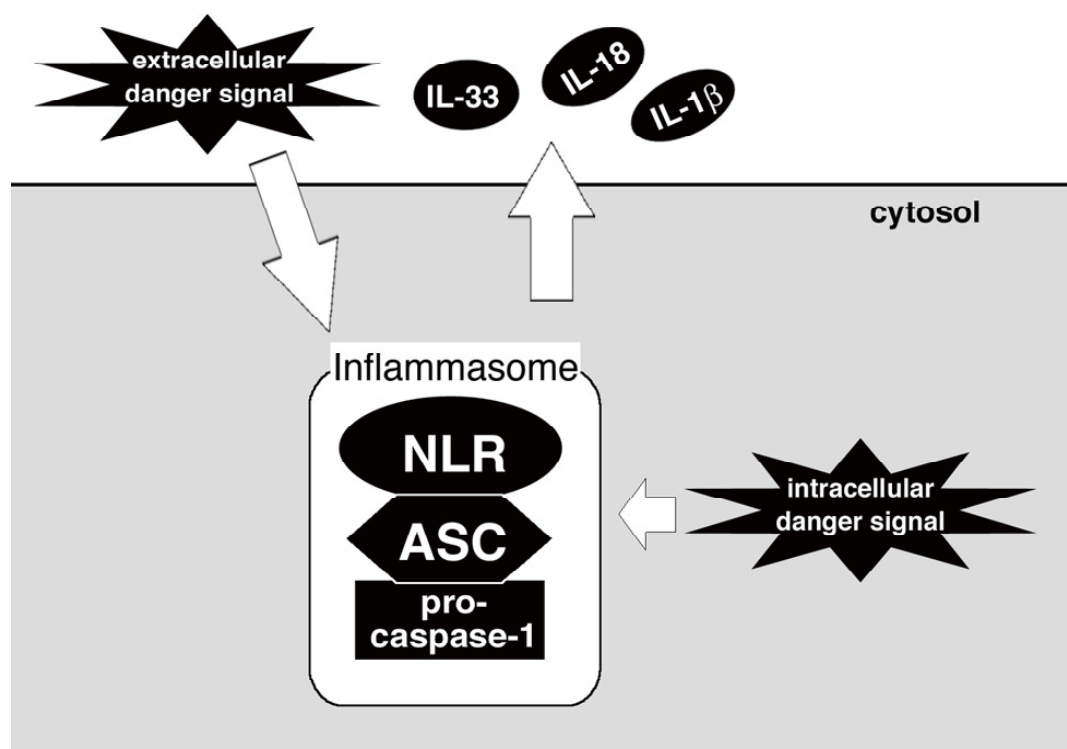


Figure 2. Mechanism for the intracellular and extracellular stress response. Both intracellular and extracellular danger signals induce the assembly of the inflammasome, which is generally composed of NLR, ASC, and procaspase-1. Activated caspase-1 then functions to process and promote the secretion of cytokines such as IL-1 β , IL-18, and IL-33.

Cryopyrin/NALP3 inflammasome

In the case of viral infection, viral DNA, single stranded RNA (ssRNA), and double stranded RNA (dsRNA) are produced during viral replication. After viruses are endocytosed into mammalian cells, DNA, ssRNA, and dsRNA are detected by TLRs in the endosomes, and the TLRs then activate NF- κ B and mitogen-activated protein kinase (MAPK) pathways, which lead to IL-6 and TNF α secretion (22). IL-1 β and IL-18 are not secreted *via* TLRs, but *via* the cryopyrin/NALP3-dependent pathway. Cryopyrin/NALP3 is a product of the cold-induced autoinflammatory syndrome 1 (CIAS1) gene and a member of the NLR family. It has some functional structures, such as CARD domains and carboxyl-terminal LRRs, that detect specific pathogens by the presence of monosodium urate (MSU), calcium pyrophosphate dehydrate crystals (CPPD), or PAMPs, including bacterial RNA and synthetic antiviral purine analogs (14,23,25,26). Cryopyrin/NALP3 forms an inflammasome with ASC and caspase-1, but its specificity for sensing pathogens was unclear until recently.

It was recently reported that the ligand-recognition function of cryopyrin/NALP3 is highly specific for dsRNA (27) (Figure 3). When macrophages are infected

with a virus, neither ssRNA nor dsDNA, but dsRNA is essential for the cryopyrin/NALP3-dependent induction of caspase-1 activation. Cryopyrin/NALP3 is necessary to induce IL-1 β and IL-18 secretion, but is dispensable for interferon α (IFN α), TNF α , or IL-6 production. This sensing ability of cryopyrin/NALP3 that distinguishes dsRNA from ssRNA may have an important role in discriminating viral RNA from endogenous host RNA to avoid harmful activation of the inflammasome (27).

On the other hand, another report shows that cryopyrin/NALP3 activates caspase-1 in response to specific factors that induce an intracellular K⁺ efflux (15) (Figure 3). When macrophages are infected by Gram-positive bacteria such as *Staphylococcus aureus* and *Listeria monocytogenes*, ATP stimulates the P2X₇ receptor, which opens a channel for cytosolic K⁺ efflux. This decrease in cytosolic K⁺ level is a signal for formation of the inflammasome, and it triggers the caspase-1-dependent cleavage and secretion of IL-1 β (28,29). In this pathway, TLR signaling still seems to be required for the expression of proteins other than cryopyrin/NALP3, including proIL-1 β . In addition to these components, live bacteria may be necessary to trigger this pathway, since heat-killed *L. monocytogenes* decreases the IL-1 β induction (15).

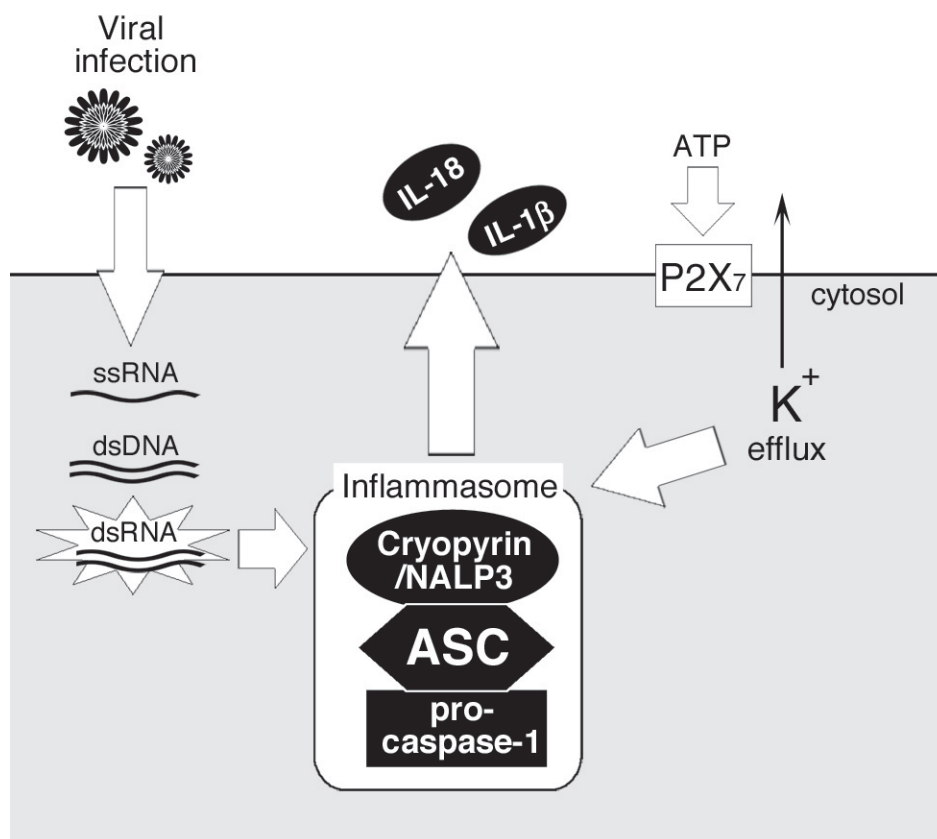


Figure 3. Cryopyrin/NALP3 inflammasome. Cryopyrin/NALP3, ASC, and procaspase-1 form the inflammasome in response to K⁺ efflux and viral dsRNA produced during viral replication, to activate caspase-1, leading to cytokine secretion.

IPAF inflammasome

Intracellular Gram-negative bacteria *Salmonella typhimurium* translocate effector virulence proteins, including flagellin, to the cytosol of the host cell (Figure 4). Extracellular flagellin is sensed by TLR5, and stimulated TLR5 induces the activation of NF- κ B and MAPK, leading to the secretion of IL-6 and a chemokine, monocyte chemoattractant protein-1 (MCP-1) (30). TLR5 also mediates the transcription and translocation of proIL-1 β . However, the intracellular mechanism by which flagellin activates caspase-1 to lead to IL-1 β secretion has remained poorly defined. Although the cytosolic invasion mechanism of the *S. typhimurium* flagellin is still unclear, it was recently shown that flagellin protein is essential for both caspase-1 activation and IL-1 β secretion in *S. typhimurium*-infected macrophages. Macrophages in which *S. typhimurium* replicate, respond to the bacteria via IPAF, a NOD-LRR protein that was first identified as a human CED4/Apaf-1 family member (31,32). As IPAF-deficient macrophages cannot activate caspase-1 or secrete IL-1 β , IPAF seems to be indispensable for

the caspase-1 activation and IL-1 β processing (13,33). Unlike cryopyrin/NALP3, ASC modulates but is not essential for the IPAF-dependent caspase-1 activation, since ASC-deficient cells show only a partial defect in their response to cytoplasmic flagellin (34). IPAF contains a CARD domain, and it may interact with the CARD of caspase-1 or ASC. Whether flagellin activates host cytosolic IPAF directly remains to be determined. This signaling pathway is independent of TLR5, given that extracellular flagellin stimulates neither caspase-1 nor IL-1 β activation in macrophages. Moreover, the lack of caspase-1 activation in stimulated IPAF-deficient macrophages is not due to a decreased expression level of procaspase-1 (34,35). In addition, *S. typhimurium* induces apoptosis in cells via IPAF and caspase-1 activation (13,36). IPAF is necessary to control the caspase-1 activation in response to *S. typhimurium* infection, but it is dispensable for responses to heat-killed *S. typhimurium*, *F. tularensis*, LPS, and ATP (35). Thus, the function of IPAF in the innate immune response might be more restricted than those of cryopyrin/NALP3.

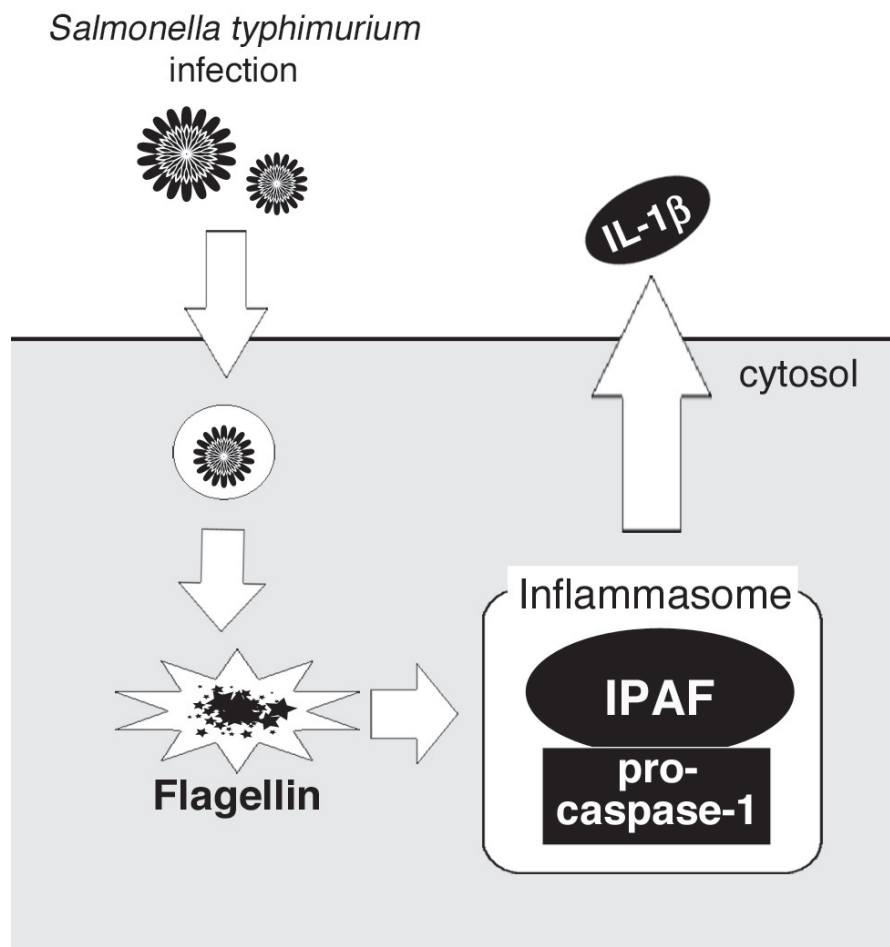


Figure 4. IPAF inflammasome. IPAF and procaspase-1 form an inflammasome without ASC in response to flagellin, a virulence protein produced by certain bacteria such as *Salmonella typhimurium*.

Caspase-1 mediates the SREBP pathway

There are many microorganisms and bacteria that produce pore-forming toxins to invade target cells. The infected cells respond to the toxin in various ways, such as by undergoing apoptosis or necrosis or by surviving, depending on the toxin, the target cells, and the size of the pores (37,38). These cellular mechanisms are still unclear, but one survival mechanism of such infected cells was recently reported (39). One of the pore-forming toxins, aerolysin, which is secreted by *Aeromonas hydrophila*, binds to glycosylphosphatidylinositol (GPI)-anchored proteins at the surface of target cells. Aerolysin then exposes its hydrophobic domain to the cell membrane like a circular ring. These pores are not permeable for proteins but for ions, and lead to K^+ efflux (40). Some unique cellular reactions to *A. hydrophila* infection are reported, such as the release of calcium from the endoplasmic reticulum (ER), vacuolation of the ER, and the production of proinflammatory molecules including $TNF\alpha$, IL- 1β , IL-6, and prostaglandin E2 (41,42). Among these various responses, the K^+ efflux acts to trigger the assembly of the inflammasome to activate caspase-1.

Activated caspase-1 stimulates the sterol regulatory element binding protein (SREBP) pathway in addition to IL- 1β , -18, and -33 secretion (39) (Figure 5).

SREBPs promote lipid metabolism, which functions predominantly in cholesterol and fatty acid biosynthesis. Although SREBPs initially reside in the ER, their activation requires proteolytic cleavage in the Golgi, which means that SREBPs require transport from the ER to the Golgi (43), and cleaved SREBPs translocate to the nucleus to activate genes involved in lipid metabolism. SREBPs are regulated principally by cellular cholesterol levels, but they are also activated by phagocytosis, the depletion of ER Ca^{2+} stores, or the exposure of cells to hypotonic media (44,45). In the case of *A. hydrophila* infection, K^+ efflux-induced caspase-1 activation is required for the transportation and activation of SREBPs, and this signaling is independent of Ca^{2+} entry (39). Furthermore, this ionic perturbation is sensed not only by the cryopyrin/NALP3, but also by the IPAF inflammasome. Whether IPAF and cryopyrin/NALP3 sense the toxin-induced K^+ decrease directly *via* their LRR domains is not yet known. The caspase-1-dependent SREBP activation pathway promotes cell survival in response to pore

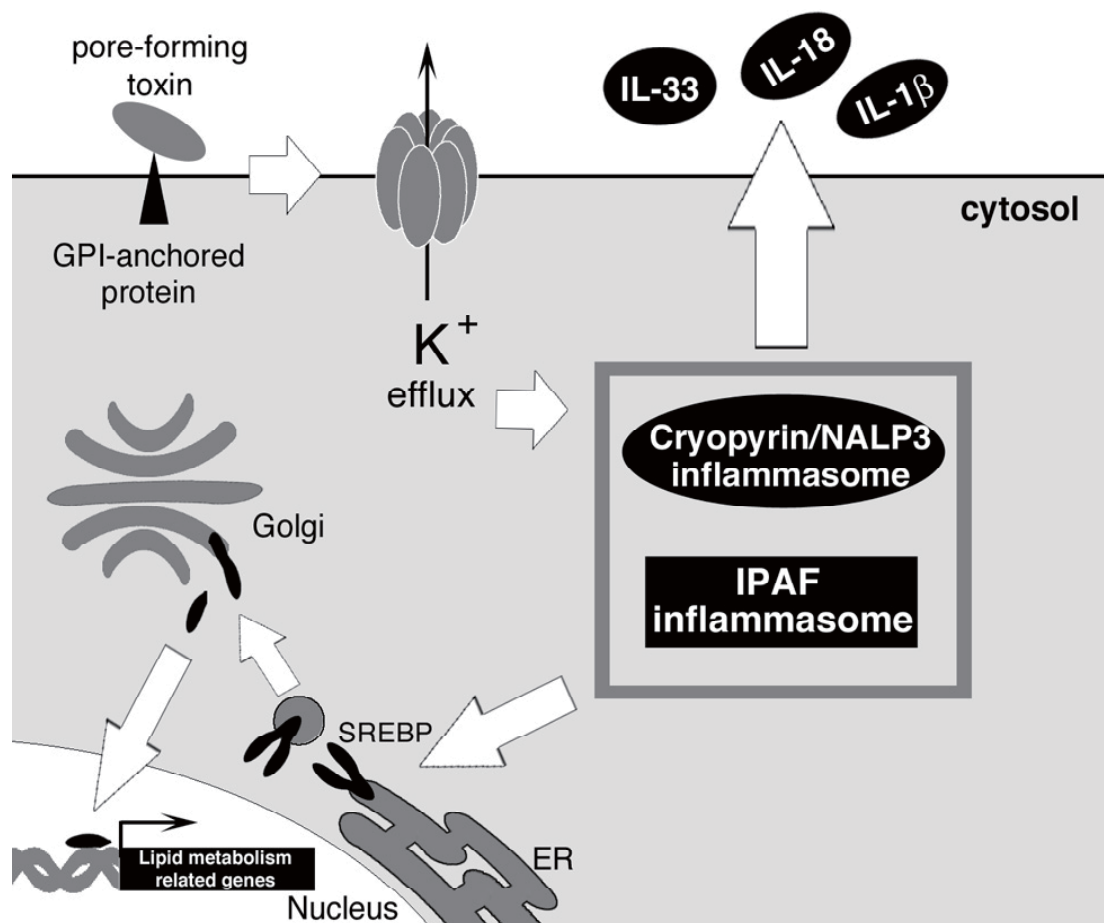


Figure 5. Host response to pore-forming toxins. Pore-forming toxin binds to glycosylphosphatidylinositol (GPI)-anchored protein and produces a pore in the host membrane. Both cryopyrin/NALP3 and the IPAF inflammasome recognize K^+ efflux through the pore and activate caspase-1, which induces cytokine secretion and lipid synthesis *via* the sterol regulatory element binding protein (SREBP) pathway.

formation, perhaps by facilitating membrane repair (39). On the other hand, caspase-2 is reported to be a transcriptional target of SREBPs and has been suggested to participate in lipid homeostasis under both physiological and pathogenic conditions (46).

Inflammasomes in nonprofessional immune cells

Inflammasomes are present even in the keratinocytes of human skin. Inflammasome proteins including NALP1, cryopyrin/NALP3, and IPAF are constitutively expressed in human skin. Likewise, although proIL-1 α , -1 β , and -18 exist constitutively, their secretion from keratinocytes is not detected under normal conditions. However, UVB irradiation induces caspase-1 activation and the secretion of IL-1 β in human primary keratinocytes (47). The UVB-irradiated skin of caspase-1 knockout mice shows a defect in neutrophil infiltration, indicating that caspase-1 is indispensable for UVB-induced skin inflammation. Caspase-1 activation is also important in the response of human skin to irradiation, and similar to the case of pathogen infection, caspase-1 is activated by an intracellular response to UVB irradiation. An inflammasome containing cryopyrin/NALP3, ASC, and caspase-1 is necessary, but IPAF is dispensable for the IL-1 β secretion by irradiated human keratinocytes. Since the

binding of caspase-1 to ASC is detected only outside the cells, the activation of caspase-1 and the secretion may be coupled, or the secretion may occur just after activation (Figure 6). In Chinese hamster ovary (CHO) or HeLa cells, pore-forming toxin induced K⁺ efflux triggers assembly of the inflammasome without requiring an increase in Ca²⁺, and LPS stimulated macrophages require both Ca²⁺ increase and K⁺ efflux (39,48). On the other hand, the triggering of inflammasome activation in irradiated keratinocytes is dependent only on the increase in cytoplasmic Ca²⁺ through its release from intracellular stores (49).

In addition, the estrogen-responsive B box protein (EBBP/TRIM16) pathway is reported to be involved in the IL-1 β secretion in keratinocytes. Under UV irradiated condition, endogenous EBBP colocalizes with IL-1 β at the cell membrane in the perinuclear region of keratinocytes and macrophages. EBBP does not interact with ASC but binds to procaspase-1, NALP1, and proIL-1 β via its ret finger protein (RFP) domain. The coexpression of EBBP with proIL-1 β , procaspase-1, and NALP1 enhances the IL-1 β secretion (50), although the detailed mechanisms and functions of EBBP are still unknown. These findings together support the idea that the caspase-1 dependent inflammasome exists even in nonprofessional immune cells.

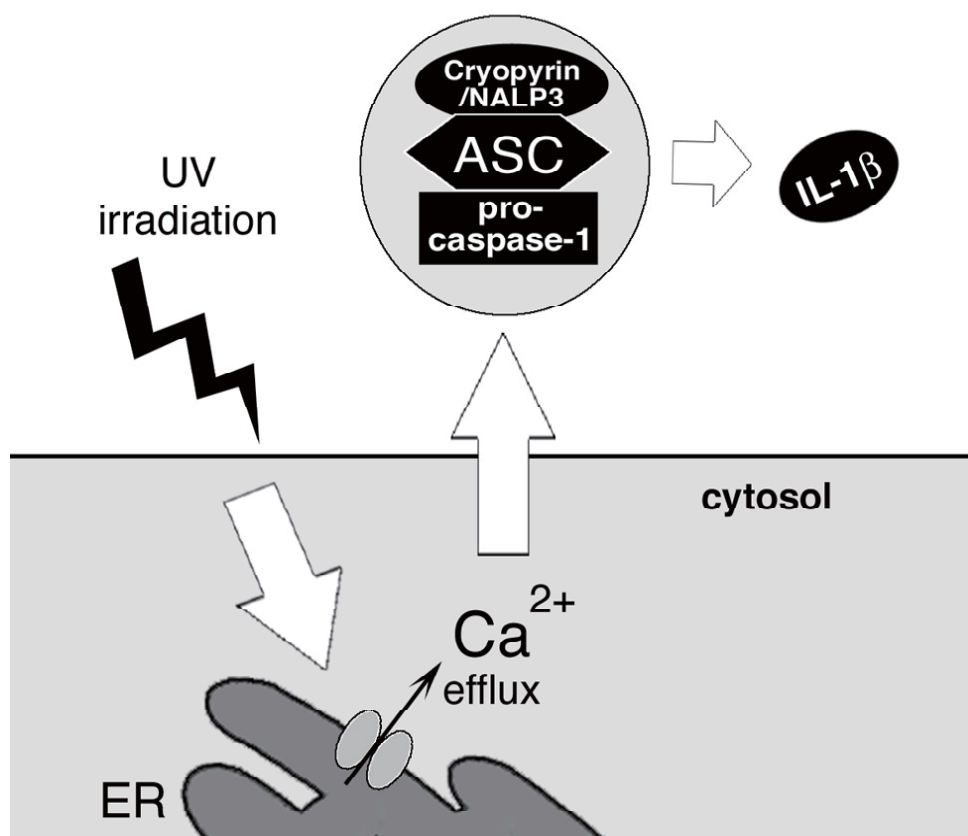


Figure 6. Inflammatory response in keratinocytes. The cryopyrin/NALP3-dependent inflammasome activates caspase-1 to induce cytokine secretion in response to Ca²⁺ efflux from the endoplasmic reticulum (ER), which is caused by UV irradiation.

Endogenous danger signals

Caspases are essential not only in the immune reaction to PAMPs, the invaders, but also, recent findings indicate that caspases mediate a greater range of immune responses, including those to endogenous danger signals. For example, in a course frequently leading to death, sepsis occurs after infection or injury and leads to the organs becoming dysfunctional. Caspases are thought to be involved in the mechanisms causing this disease, since apoptotic lymphocytes accumulate at the organs during sepsis, and the organ damage is reduced by blocking apoptosis with caspase inhibitors (51-53). Caspase-1 knockout mice are resistant and show less apoptosis in the splenocyte and macrophages during septic shock induced by bacteria than wild-type mice, although IL-1 β knockout or double-knockout mice of IL-1 β and IL-18 are not protected (54). On the other hand, high mobility group box 1 (HMGB1) is known to accumulate and mediate organ damage in sepsis (55,56). HMGB1 release occurs by the exposure of macrophages to necrotic cell debris, or to both apoptotic T cells and apoptotic macrophages. Although apoptotic cells have the ability to release HMGB1 from macrophages, and the inhibition of HMGB1 reduces sepsis, the inhibition of HMGB1 showed no significant decrease in the development of sepsis-induced apoptosis. These results indicate that at least part of the HMGB1 function is downstream of caspases (57).

In the case of gout and pseudogout, which are common joint diseases, aberrant activation of the cryopyrin/NALP3 inflammasome induces IL-1 β constitutively. The known symptom of gout is the deposition of MSU or CPPD crystals at the joints and periarticular tissues (58). These unique pathogenic agents, MSU and CPPD, activate caspase-1 to secrete IL-1 β in an ASC- and cryopyrin/NALP3-dependent manner. This notion is supported by the observation that caspase-1- or ASC-deficient mice show reduced neutrophil influx when MSU or CPPD is injected (14). Moreover, macrophages from Muckle-Wells syndrome patients spontaneously secrete active IL-1 β in a caspase-1-dependent manner, even without stimulation (59). Because many of these patients have a mutation in the cryopyrin/NALP3 gene, Muckle-Wells syndrome is thought to be caused by the increased processing and secretion of IL-1 β via caspase-1 and the mutated cryopyrin/NALP3 (60). Therefore, caspases also play important roles in the reaction to various endogenous danger signals.

Invertebrate immune system

To date, *Drosophila melanogaster* has contributed to the study of numerous apoptotic and non-apoptotic functions of caspases. Is the immune system in

invertebrates completely different from that in mammals? To overcome PAMPs, flies have several immune mechanisms such as the humoral immune response, melanization, and the cellular immune response. Among these, the most well-characterized is probably the humoral immune response, which is composed of two major pathways, immune deficiency (IMD) and Toll. These pathways independently regulate distinct classes of NF- κ B proteins. The IMD pathway is activated by Gram-negative bacteria and induces Relish activation. The Toll pathway is triggered by fungi or Gram-positive bacteria and leads to Dorsal and Dif activation (61). Genetic screening experiments designed to dissect the IMD pathway identified *dredd*, a *Drosophila* ortholog of caspase-8. A loss-of-function mutant of *dredd* is viable and fertile, but highly susceptible to Gram-negative bacteria, and it is defective in the production of antibacterial peptides, such as dipterin and attacin. In addition, *dredd* has been shown physically interact with the NF- κ B homolog, Relish, in *Drosophila* mbn-2 (hemocyte-like) cells. *Dredd* mutant flies fail to process Relish, which contains Rel-homology domains at the N-terminus and I κ B-like domains at the C-terminus. These observations suggest that *dredd* is involved in NF- κ B activation (3,62).

Another report indicates that *eiger*, the only fly homolog of TNF (63,64), is involved in the fly's immune machinery. Microarray analysis showed that *eiger* is up-regulated after LPS exposure to mbn-2 cells (65). *Eiger* acts to protect the cells against extracellular pathogens independently from Toll and IMD signals. *Eiger* mutant flies show decreased phagocytosis, which functions to exclude pathogens, indicating that *eiger* has a role in limiting the growth of pathogens via phagocytosis. These mutants are also unable to suppress pathogens that have phagocyte-defeating activity (67). However, induced *eiger* can be harmful for flies if there is no proper target for it (66,67). Mammals as well as flies die as a result of too much TNF secretion (68). Thus, the immune responses of the fly have similarities to those of mammals in terms of cytokine secretion mechanisms and autoinflammatory diseases.

In the nematode *C. elegans*, caspase is involved in the immune responses, and the *ced-3* mutant is sensitive to some pathogens, including *S. typhimurium* infection (69). *Drosophila* has just one NOD-like protein, *dark/dapaf-1/HAC-1*, which forms the apoptosome. In addition to the domains required to trigger caspase activation, *dark* also contains a WD40 region, which may be functionally equivalent to the LRR that recognizes some pathogens or danger signals because cytochrome c released from mitochondria can be considered as an intracellular alert signal in stressed cells. Therefore, we expect *dark* to sense dangers and trigger caspase activation in response to stresses even in *Drosophila*, perhaps by forming an inflammasome-like

complex.

Although each organism seems to have diverse machinery for eliciting stress responses, the major mediators might be represented by caspase. Inflammatory caspases function to get rid of exogenous and endogenous dangers, and apoptotic caspases function to remove the organism's own cells that are dangerous. Since these systems for eliminating harmful cells are indispensable for all species to develop normally and survive in this stressful world, the substantial roles of caspase in stress responses, not only in the apoptosome but also in the inflammasome, may have been conserved evolutionally in both vertebrates and invertebrates.

Acknowledgments

We apologize to colleagues whose work could not be cited owing to space limitations. This work was supported in part by grants from the Naito Foundation, the Uehara Memorial Foundation, the Takeda Science Foundation and Research Aid of Inoue Foundation for Science to E. K. This work was also supported in part by grants from the Japanese Ministry of Education, Science, Sports, Culture and Technology to E. K. and M. M. In addition, this work was supported in part by a RIKEN Bioarchitect Research Grant, the TORAY Science Foundation, The Cell Science Research Foundation, Naito Foundation and the Astellas Foundation for Research on Metabolic Disorders to M. M.

References

- Ellis HM, Horvitz HR. Genetic control of programmed cell death in the nematode *C. elegans*. *Cell* 1986; 6:817-829.
- Yuan J, Shaham S, Ledoux S, Ellis HM, Horvitz HR. The *C. elegans* cell death gene *ced-3* encodes a protein similar to mammalian interleukin-1 β -converting enzyme. *Cell* 1993; 4:641-652.
- Kuranaga E, Miura M. Nonapoptotic functions of caspases: caspases as regulatory molecules for immunity and cell-fate determination. *Trends Cell Biol* 2007; 3:135-144.
- Thornberry NA, Bull HG, Calaycay JR, *et al.* A novel heterodimeric cysteine protease is required for interleukin-1 β processing in monocytes. *Nature* 1992; 357:768-774.
- Cerretti DP, Kozlosky CJ, Mosley B, *et al.* Molecular cloning of the interleukin-1 β converting enzyme. *Science* 1992; 255:97-100.
- Miura M, Zhu H, Rotello R, Hartwig EA, Yuan J. Induction of apoptosis in fibroblasts by IL-1 β -converting enzyme, a mammalian homolog of the *C. elegans* cell death gene *ced-3*. *Cell* 1993; 4:653-660.
- Lin XY, Choi MS, Porter AG. Expression analysis of the human caspase-1 subfamily reveals specific regulation of the CASP5 gene by lipopolysaccharide and interferon- γ . *J Biol Chem* 2000; 275:39920-39926.
- Wang S, Miura M, Jung YK, Zhu H, Li E, Yuan J. Murine caspase-11, an ICE-interacting protease, is essential for the activation of ICE. *Cell* 1998; 94:501-509.
- Martinon F, Burns K, Tschopp J. The inflammasome: a molecular platform triggering activation of inflammatory caspases and processing of proIL-1 β . *Mol Cell* 2002; 10:417-426.
- Bianchi ME. DAMPs, PAMPs and alarmins: all we need to know about danger. *J Leukoc Biol* 2007; 81:1-5.
- Schmitz J, Owyang A, Oldham E, Song Y, Murphy E, McClanahan TK, Zurawski G, Moshrefi M, Qin J, Li X, Gorman DM, Bazan JF, Kastelein RA. IL-33, an interleukin-1-like cytokine that signals via the IL-1 receptor-related protein ST2 and induces T helper type 2-associated cytokines. *Immunity* 2005; 22:479-490.
- Nadiri A, Wolinski MK, Saleh M. The inflammatory caspases: key players in the host response to pathogenic invasion and sepsis. *J Immunol* 2006; 177:4239-4245.
- Mariathasan S, Newton K, Monack DM, Vucic D, French DM, Lee WP, Roose-Girma M, Erickson S, Dixit VM. Differential activation of the inflammasome by caspase-1 adaptors ASC and Ipaf. *Nature* 2004; 431:213-218.
- Martinon F, Petrilli V, Mayor A, Tardivel A, Tschopp J. Gout-associated uric acid crystals activate the NALP3 inflammasome. *Nature* 2006; 440:237-241.
- Mariathasan S, Weiss DS, Newton K, McBride J, O'Rourke K, Roose-Girma M, Lee WP, Weinrauch Y, Monack DM, Dixit VM. Cryopyrin activates the inflammasome in response to toxins and ATP. *Nature* 2006; 440:228-232.
- Sutterwala FS, Ogura Y, Szczepanik M, Lara-Tejero M, Lichtenberger GS, Grant EP, Bertin J, Coyle AJ, Galan JE, Askenase PW, Flavell RA. Critical role for NALP3/CIAS1/Cryopyrin in innate and adaptive immunity through its regulation of caspase-1. *Immunity* 2006; 24:317-327.
- Akira S, Takeda K. Toll-like receptor signalling. *Nat Rev Immunol* 2004; 4:499-511.
- Strober W, Murray PJ, Kitani A, Watanabe T. Signalling pathways and molecular interactions of NOD1 and NOD2. *Nat Rev Immunol* 2006; 6:9-20.
- Hemmi H, Kaisho T, Takeuchi O, Sato S, Sanjo H, Hoshino K, Horiuchi T, Tomizawa H, Takeda K, Akira S. Small anti-viral compounds activate immune cells via the TLR7 MyD88-dependent signaling pathway. *Nat Immunol* 2002; 3:196-200.
- Jurk M, Heil F, Vollmer J, Schetter C, Krieg AM, Wagner H, Lipford G, Bauer S. Human TLR7 or TLR8 independently confer responsiveness to the antiviral compound R-848. *Nat Immunol* 2002; 3:499.
- Ting JP, Kastner DL, Hoffman HM. CATERPILLERS, pyrin and hereditary immunological disorders. *Nat Rev Immunol* 2006; 6:183-195.
- Alexopoulou L, Holt AC, Medzhitov R, Flavell RA. Recognition of double-stranded RNA and activation of NF- κ B by Toll-like receptor 3. *Nature* 2001; 413:732-738.
- Inohara, Chamaillard, McDonald C, Nunez G. NOD-LRR proteins: role in host-microbial interactions and inflammatory disease. *Annu Rev Biochem* 2005; 74:355-383.
- Philpott DJ, Girardin SE. The role of Toll-like receptors

- and Nod proteins in bacterial infection. *Mol Immunol* 2004; 11:1099-1108.
25. Athman R, Philpott D. Innate immunity *via* Toll-like receptors and Nod proteins. *Curr Opin Microbiol* 2004; 1:25-32.
 26. Kanneganti TD, Ozoren N, Body-Malapel M, *et al.* Bacterial RNA and small antiviral compounds activate caspase-1 through cryopyrin/Nalp3. *Nature* 2006; 7081:233-236.
 27. Kanneganti TD, Body-Malapel M, Amer A, Park JH, Whitfield J, Franchi L, Taraporewala ZF, Miller D, Patton JT, Inohara N, Nunez G. Critical role for Cryopyrin/Nalp3 in activation of caspase-1 in response to viral infection and double-stranded RNA. *J Biol Chem* 2006; 48:36560-36568.
 28. Perregaux D, Gabel CA. Interleukin-1 β maturation and release in response to ATP and nigericin. Evidence that potassium depletion mediated by these agents is a necessary and common feature of their activity. *J Biol Chem* 1994; 21:15195-15203.
 29. Solle M, Labasi J, Perregaux DG, Stam E, Petrushova N, Koller BH, Griffiths RJ, Gabel CA. Altered cytokine production in mice lacking P2X(7) receptors. *J Biol Chem* 2001; 1:125-132.
 30. Hayashi F, Smith KD, Ozinsky A, Hawn TR, Yi EC, Goodlett DR, Eng JK, Akira S, Underhill DM, Aderem A. The innate immune response to bacterial flagellin is mediated by Toll-like receptor 5. *Nature* 2001; 6832:1099-1103.
 31. Poyet JL, Srinivasula SM, Tnani M, Razmara M, Fernandes-Alnemri T, Alnemri ES. Identification of Ipaf, a human caspase-1-activating protein related to Apaf-1. *J Biol Chem* 2001; 30:28309-28313.
 32. Damiano JS, Stehlik C, Pio F, Godzik A, Reed JC. CLAN, a novel human CED-4-like gene. *Genomics* 2001; 1-3:77-83.
 33. Damiano JS, Newman RM, Reed JC. Multiple roles of CLAN (caspase-associated recruitment domain, leucine-rich repeat, and NAIP CIIA HET-E, and TP1-containing protein) in the mammalian innate immune response. *J Immunol* 2004; 10:6338-6345.
 34. Miao EA, Alpuche-Aranda CM, Dors M, Clark AE, Bader MW, Miller SI, Aderem A. Cytoplasmic flagellin activates caspase-1 and secretion of interleukin 1 β *via* Ipaf. *Nat Immunol* 2006; 6:569-575.
 35. Franchi L, Amer A, Body-Malapel M, Kanneganti TD, Ozoren N, Jagirdar R, Inohara N, Vandenabeele P, Bertin J, Coyle A, Grant EP, Nunez G. Cytosolic flagellin requires Ipaf for activation of caspase-1 and interleukin 1 β in salmonella-infected macrophages. *Nat Immunol* 2006; 6:576-582.
 36. Hersh D, Monack DM, Smith MR, Ghori N, Falkow S, Zychlinsky A. The *Salmonella* invasin SipB induces macrophage apoptosis by binding to caspase-1. *Proc Natl Acad Sci USA* 1999; 5:2396-2401.
 37. Ratner AJ, Hippe KR, Aguilar JL, Bender MH, Nelson AL, Weiser JN. Epithelial cells are sensitive detectors of bacterial pore-forming toxins. *J Biol Chem* 2006; 18:12994-12998.
 38. Alouf JE. Pore-forming bacterial protein toxins: an overview. *Curr Top Microbiol Immunol* 2001; 1-14.
 39. Gurcel L, Abrami L, Girardin S, Tschopp J, van der Goot FG. Caspase-1 activation of lipid metabolic pathways in response to bacterial pore-forming toxins promotes cell survival. *Cell* 2006; 6:1135-1145.
 40. Iacovache I, Paumard P, Scheib H, Lesieur C, Sakai N, Matile S, Parker MW, van der Goot FG. A rivet model for channel formation by aerolysin-like pore-forming toxins. *Embo J* 2006; 3:457-466.
 41. Abrami L, Fivaz M, van der Goot FG. Adventures of a pore-forming toxin at the target cell surface. *Trends Microbiol* 2000; 4:168-172.
 42. Abrami L, Fivaz M, van der Goot FG. Surface dynamics of aerolysin on the plasma membrane of living cells. *Int J Med Microbiol* 2000; 4-5:363-367.
 43. Goldstein JL, DeBose-Boyd RA, Brown MS. Protein sensors for membrane sterols. *Cell* 2006; 1:35-46.
 44. Castoreno AB, Wang Y, Stockinger W, Jarzylo LA, Du H, Pagnon JC, Shieh EC, Nohturfft A. Transcriptional regulation of phagocytosis-induced membrane biogenesis by sterol regulatory element binding proteins. *Proc Natl Acad Sci USA* 2005; 37:13129-13134.
 45. Lee JN, Ye J. Proteolytic activation of sterol regulatory element-binding protein induced by cellular stress through depletion of Insig-1. *J Biol Chem* 2004; 43:45257-45265.
 46. Logette E, Le Jossic-Corcoc C, Masson D, Solier S, Sequeira-Legrand A, Dugail I, Lemaire-Ewing S, Desoche L, Solary E, Corcos L. Caspase-2, a novel lipid sensor under the control of sterol regulatory element binding protein 2. *Mol Cell Biol* 2005; 21:9621-9631.
 47. Kondo S, Sauder DN, Kono T, Galley KA, McKenzie RC. Differential modulation of interleukin-1 alpha (IL-1 α) and interleukin-1 β (IL-1 β) in human epidermal keratinocytes by UVB. *Exp Dermatol* 1994; 1:29-39.
 48. Andrei C, Margiocco P, Poggi A, Lotti LV, Torrisi MR, Rubartelli A. Phospholipases C and A2 control lysosome-mediated IL-1 β secretion: Implications for inflammatory processes. *Proc Natl Acad Sci USA* 2004; 26:9745-9750.
 49. Feldmeyer L, Keller M, Niklaus G, Hohl D, Werner S, Beer HD. The inflammasome mediates UVB-induced activation and secretion of interleukin-1 β by keratinocytes. *Curr Biol* 2007; 13:1140-1145.
 50. Munding C, Keller M, Niklaus G, Papin S, Tschopp J, Werner S, Beer HD. The estrogen-responsive B box protein: a novel enhancer of interleukin-1 β secretion. *Cell Death Differ* 2006; 11:1938-1949.
 51. Hotchkiss RS, Chang KC, Swanson PE, Tinsley KW, Hui JJ, Klender P, Xanthoudakis S, Roy S, Black C, Grimm E, Aspiotis R, Han Y, Nicholson DW, Karl IE. Caspase inhibitors improve survival in sepsis: a critical role of the lymphocyte. *Nat Immunol* 2000; 6:496-501.
 52. Hotchkiss RS, Karl IE. The pathophysiology and treatment of sepsis. *N Engl J Med* 2003; 2:138-150.
 53. Wesche DE, Lomas-Neira JL, Perl M, Chung CS, Ayala A. Leukocyte apoptosis and its significance in sepsis and shock. *J Leukoc Biol* 2005; 2:325-337.
 54. Sarkar A, Hall MW, Exline M, Hart J, Knatz N, Gatson NT, Wewers MD. Caspase-1 regulates *Escherichia coli* sepsis and splenic B cell apoptosis independently of interleukin-1 β and interleukin-18. *Am J Respir Crit Care Med* 2006; 9:1003-1010.
 55. Wang H, Bloom O, Zhang M, *et al.* HMG-1 as a late mediator of endotoxin lethality in mice. *Science* 1999; 5425:248-251.
 56. Yang H, Ochani M, Li J, *et al.* Reversing established sepsis with antagonists of endogenous high-mobility

- group box 1. Proc Natl Acad Sci USA 2004; 1:296-301.
57. Qin S, Wang H, Yuan R, *et al.* Role of HMGB1 in apoptosis-mediated sepsis lethality. J Exp Med 2006; 7:1637-1642.
58. Shi Y, Evans JE, Rock KL. Molecular identification of a danger signal that alerts the immune system to dying cells. Nature 2003; 6957:516-521.
59. Agostini L, Martinon F, Burns K, McDermott MF, Hawkins PN, Tschopp J. NALP3 forms an IL-1 β -processing inflammasome with increased activity in Muckle-Wells autoinflammatory disorder. Immunity 2004; 3:319-325.
60. Hull KM, Shoham N, Chae JJ, Aksentijevich I, Kastner DL. The expanding spectrum of systemic autoinflammatory disorders and their rheumatic manifestations. Curr Opin Rheumatol 2003; 1:61-69.
61. Tanji T, Ip YT. Regulators of the Toll and Imd pathways in the *Drosophila* innate immune response. Trends Immunol 2005; 4:193-198.
62. Stoven S, Silverman N, Junell A, Hedengren-Olcott M, Erturk D, Engstrom Y, Maniatis T, Hultmark D. Caspase-mediated processing of the *Drosophila* NF- κ B factor Relish. Proc Natl Acad Sci USA 2003; 10:5991-5996.
63. Igaki T, Kanda H, Yamamoto-Goto Y, Kanuka H, Kuranaga E, Aigaki T, Miura M. *Eiger*, a TNF superfamily ligand that triggers the *Drosophila* JNK pathway. Embo J 2002; 12:3009-3018.
64. Geuking P, Narasimamurthy R, Basler K. A genetic screen targeting the tumor necrosis factor/*Eiger* signaling pathway: identification of *Drosophila* TAB2 as a functionally conserved component. Genetics 2005; 4:1683-1694.
65. Johansson KC, Metzendorf C, Soderhall K. Microarray analysis of immune challenged *Drosophila* hemocytes. Exp Cell Res 2005; 1:145-155.
66. Brandt SM, Dionne MS, Khush RS, Pham LN, Vigdal TJ, Schneider DS. Secreted bacterial effectors and Host-produced *eiger*/TNF drive death in a Salmonella-infected fruit fly. PLoS Biol 2004; 12:e418.
67. Schneider DS, Ayres JS, Brandt SM, Costa A, Dionne MS, Gordon MD, Mabery EM, Moule MG, Pham LN, Shirasu-Hiza MM. *Drosophila eiger* mutants are sensitive to extracellular pathogens. PLoS Pathog 2007; 3:e41.
68. Kim KD, Zhao J, Auh S, Yang X, Du P, Tang H, Fu YX. Adaptive immune cells temper initial innate responses. Nat Med 2007; 10:1248-1252.
69. Aballay A, Ausubel FM. Programmed cell death mediated by *ced-3* and *ced-4* protects *Caenorhabditis elegans* from *Salmonella typhimurium*-mediated killing. Proc Natl Acad Sci USA 2001; 5:2735-2739.

(Received February 18, 2008; Accepted February 22, 2008)

Original Article

Pharmacologic action of oseltamivir on the nervous system

Kenichi Ishii¹, Hiroshi Hamamoto², Takuya Sasaki¹, Yuji Ikegaya¹, Kenzo Yamatsugu¹, Motomu Kanai¹, Masakatsu Shibasaki¹, Kazuhisa Sekimizu^{1,*}

¹ Graduate School of Pharmaceutical Sciences, The University of Tokyo, Tokyo, Japan;

² Genome Pharmaceuticals Institute, Co., Ltd., Tokyo, Japan.

ABSTRACT: Oseltamivir, an antiviral drug used for the treatment of influenza, contains the *L*-glutamic acid motif in its chemical structure. We focused on this structural characteristic of oseltamivir and examined the pharmacologic effects of the drug on the nervous system in invertebrate and vertebrate animal models. Injection of oseltamivir or *L*-glutamic acid into silkworm (*Bombyx mori*) larvae induced muscle relaxation. Oseltamivir and *L*-glutamic acid inhibited kainate-induced rapid muscle contraction, but neither drug affected insect cytokine paralytic peptide-induced slow muscle contraction. In the mammalian system, mice (*Mus musculus*) treated intracerebrally with oseltamivir developed convulsive seizures. Hydrolyzed oseltamivir, the active form containing a carboxylic acid, evoked epileptiform firing of hippocampal neurons in rat (*Rattus norvegicus*) organotypic hippocampal slice cultures. These results are the first to demonstrate that oseltamivir exerts pharmacologic effects on the nervous system in insects and mammals.

Keywords: Oseltamivir, Nervous system, *L*-Glutamic acid, Kainite, Pharmacologic effect

1. Introduction

Influenza is a highly transmissible viral disease. The recent emergence of fatal influenza virus types, especially H5N1-type, has raised concerns over a future global influenza pandemic (1). Oseltamivir phosphate (Tamiflu[®]; Figure 1, 1) is the most widely used therapeutic agent for influenza (2). Oseltamivir exerts its activity through potent inhibition of neuraminidase

localized on the surface of the influenza virus by mimicking the transition state of sialic acid hydrolysis (3-5). Because this process is essential for influenza transmission (6-8) oseltamivir is considered consistently effective against new types of influenza. To protect human beings from a future pandemic, the development of a novel synthetic route for 1 that enables efficient mass production has been studied intensively (9-15). Other than rare cases of asthma provocation in patients with hepatic dysfunction (16), oseltamivir is considered to be a safe drug without severe side effects (17,18). Recently in Japan, however, where 80% of the world supply of oseltamivir is consumed, it was reported that oseltamivir might cause abnormal behavior (such as hallucinations and impulsive behavior) in children under the age of 20. Comprehensive statistical investigations are now underway to clarify the relationship between the abnormal behavior and oseltamivir administration (19). To date, molecular-level or cellular-level studies that have addressed the pharmacologic effects of oseltamivir on the nervous system are limited. Izumi recently reported the pharmacologic effects of oseltamivir using juvenile rats and hippocampal slices of rats (20). In this paper, we describe the *L*-glutamic acid-like activities of oseltamivir in the nervous system of three animals (silkworms, mice, and rats).

2. Materials and Methods

2.1. Chemical synthesis of Tamiflu[®]

Tamiflu[®] (Figure 1, 1), Ro64-0802 (Figure 1, 2), and its enantiomer (Figure 1, 4) were synthesized by the previously reported method (15). For details, see Supplementary data.

2.2. Silkworm larvae muscle contraction assay

Silkworm eggs (*Bombyx mori*, Hu•Yo × Tukuba•Ne) were purchased from Ehime Sanshu (Ehime, Japan). Silkworm larvae were reared on an artificial diet (Silkmate 2S, Nihon Nosan, Kanagawa, Japan)

*Correspondence to: Dr. Kazuhisa Sekimizu, Graduate School of Pharmaceutical Sciences, The University of Tokyo, 7-3-1 Hongo, Bunkyo-ku, Tokyo 113-0033, Japan;
e-mail: sekimizu@mol.f.u-tokyo.ac.jp

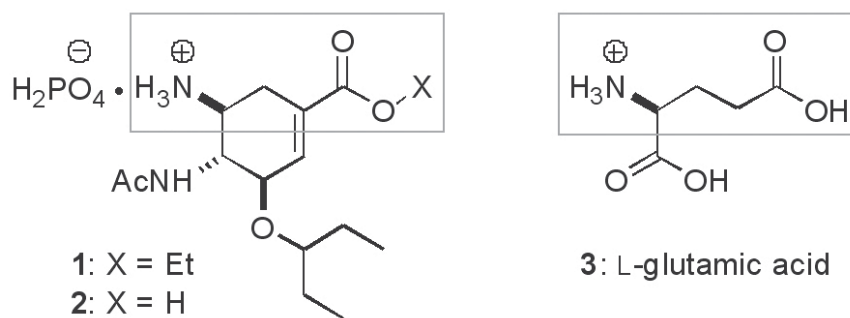


Figure 1. Structural analogy between oseltamivir and L-glutamic acid.

at 27°C. The measurement of muscle contraction activity using silkworms was described previously (21). Briefly, the heads of 5th instar silkworm larvae (3-4 g) were cut off and the peritrophic membranes removed. Each specimen was tied and attached to a transducer to measure isotonic contraction with a load of 27 g. Test samples were dissolved or suspended in phosphate-buffered saline, and injected into the body fluid of a specimen with a 1-mL syringe attached to a 27-gauge needle (Terumo, Tokyo, Japan). The intensity of the muscle contraction was expressed as the contraction value, calculated by measuring the maximum length of each specimen before (x cm) and after (y cm) the injection using the formula $(x-y)/x$. The muscle contraction stimulant kainate monohydrate was purchased from Wako (Osaka, Japan), and insect cytokine paralytic peptide (2.5 kDa) was synthesized using the solid-phase Fmoc method (22). To test the effects of the inhibitors, 50 μ L each of two samples (inhibitor and stimulant) were successively injected with an interval of 5 to 10 sec.

2.3. Injection into cerebral ventricles of mice

ICR mice (female, 6-week-old) were anesthetized with 300 μ L of 1/10 diluted Nembutal (*i.p.*), and scalps were dissected to expose the cranial bones. After 3 to 5 h, 20 μ L of the indicated samples were injected intracerebrally. Behaviors of mice were observed for at least 30 min after injection.

2.4. Whole-cell patch-clamp recordings from rat hippocampal slices

Organotypic cultures of hippocampal slices: Postnatal day 7 Sprague Dawley rats (SLC, Shizuoka, Japan) were deeply anesthetized by hypothermia, and their brains were aseptically removed (23), according to National Institutes of Health guidelines for laboratory animal care and safety. The posterior part of the brain was cut into 300- μ m-thick transverse slices using a DTK-1500 vibratome (Dosaka, Japan) in aerated, ice-cold Gey's balanced salt solution supplemented with 25 mM glucose. The entorhino-hippocampi were

dissected out under stereomicroscopic control and cultured using membrane interface techniques (24,25). Briefly, slices were placed on sterile 30-mm diameter membranes (Millicell-CM; Millipore, Bedford, MA, USA) and transferred into six-well tissue culture trays. Cultures were fed with 1 mL of 50% minimal essential medium (Invitrogen, Gaithersburg, MD, USA), 25% horse serum (Cell Culture Lab, Cleveland, OH, USA), and 25% Hank's Balanced Salt Solution and were maintained in a humidified incubator at 37°C in 5% CO₂. The medium was changed every 3.5 days.

Electrophysiologic recordings: Slices were placed in a recording chamber, perfused with artificial cerebrospinal fluid consisting of: 127 mM NaCl, 26 mM NaHCO₃, 1.6 mM KCl, 1.24 mM KH₂PO₄, 1.3 mM MgSO₄, 2.4 mM CaCl₂, and 10 mM glucose, bubbled with 95% O₂ and 5% CO₂ or Neurobasal (Gibco BRL, Gaithersburg, MD) at a rate of 2 to 3 mL/min. Whole-cell patch-clamp recordings were performed with glass pipettes (6-8 M Ω) filled with intracellular solution containing 120 mM K-gluconate, 20 mM KCl, 10 HEPES, 0.1 mM CaCl₂, 4 mM Mg-ATP, and 0.2 mM EGTA (pH 7.4, 280-300 mOsm). Recordings were performed with Axopatch 200B amplifiers (Molecular Devices, Union City, CA, USA). CA1 pyramidal cells were identified using an Olympus BX50WI microscope (Tokyo, Japan) and a 40 \times objective under phase contrast control with a Cascade cooled CCD camera (Roper Scientific, Tucson, AZ, USA). Pipette seal resistances were typically >1 G Ω , and pipette capacitive transients were minimized prior to breakthrough. Postsynaptic currents were studied in voltage-clamp mode at -30 mV holding potential. Signals were low-pass filtered at 1 kHz, digitized at 10 kHz, and analyzed with pCLAMP 8.0 software (Molecular Devices). Drugs were applied locally via a puffer pipette placed near (20-50 μ m) the patched neuron (50-70 hPa).

3. Results and Discussion

Oseltamivir (**1**) is a prodrug, and its biologically active form is the corresponding carboxylic acid **2** (Ro64-0802), which is produced through the hydrolysis of **1** by plasma and liver esterase (26,27).

The identification of an *L*-glutamic acid motif in the chemical structure of **2** (Figure 1) led us to hypothesize that oseltamivir has *L*-glutamic acid-like biologic activity. *L*-Glutamic acid is a major excitatory neurotransmitter in the vertebrate nervous system. Agonists of glutamic acid receptors induce hallucinative behaviors (28) and epileptic seizures (29,30) in experimental animals.

To examine our hypothesis experimentally, we first examined the pharmacologic effect of oseltamivir in an invertebrate model. Some of the authors of the present study previously proposed that silkworms (*Bombyx mori*) could serve as a useful invertebrate model for drug screening and evaluation, as the effects and pharmacologic kinetics in silkworms are generally comparable to those in mammalian models (31-34). In our previous work, we reported the biologic activity of *L*-glutamic acid in silkworms; kainate, a putative neurotransmitter receptor agonist in silkworm, induces muscle contraction in silkworm larvae, which is inhibited by *L*-glutamic acid, and *L*-glutamic acid itself causes muscle relaxation (21). Oseltamivir (2.5 mg) injected into the body fluid of silkworm larvae induces paralysis accompanied by muscle relaxation. This response resembles the effect of *L*-glutamic acid ($ED_{50} = 15 \mu\text{g}$). In addition, prior injection of 5 mg oseltamivir into silkworm larvae significantly inhibits kainate (2 μg)-induced muscle contraction (Supplementary data). On the other hand, another muscle contraction pathway independent of nervous system excitation (thus, not affected by *L*-glutamic acid), *i.e.*, the insect cytokine paralytic peptide pathway (35) is not affected by

oseltamivir (Supplementary data). These results support our hypothesis that oseltamivir has a specific effect, similar to *L*-glutamic acid, on the nervous system.

Next we investigated the pharmacologic effect of oseltamivir on the mammalian central nervous system. Injection of 0.3 mg *L*-glutamic acid into the lateral ventricle of mice (*Mus musculus*) induced acute epileptiform convulsions, which lasted from several to 30 min (Figure 2). Intracerebral injection of more than 0.5 mg of oseltamivir caused intense convulsions, similar to those induced by *L*-glutamic acid (Figure 2). Phosphate-buffered saline, the solvent for both drugs, did not induce seizures in mice (Figure 2). Thus, oseltamivir acts as a convulsant agent in the central nervous system. We also performed whole-cell patch-clamp recordings from CA1 pyramidal cells in rat (*Rattus norvegicus*) cultured organotypic hippocampal slices to evaluate the electrophysiologic responses to the active form **2** (Figure 3). Results varied from neuron to neuron, and three types of responses were observed; i) generation of burst-like action potentials ($n = 6$), ii) subthreshold depolarization of membrane potentials ($n = 4$), and iii) no electrical response ($n = 3$), whereas *L*-glutamic acid (1 mM) induced burst-like action potentials in all neurons tested. The heterogeneous reactions induced by **2** are likely due to the diversity of neurons in the various parts of neural microcircuits. In tissue section cultures, the observed reactions could be induced not only by application of the drug to a single cell, but also by the complex activity of a large number of surrounding cells. Recently, the importance of experimental systems reflecting complex effects

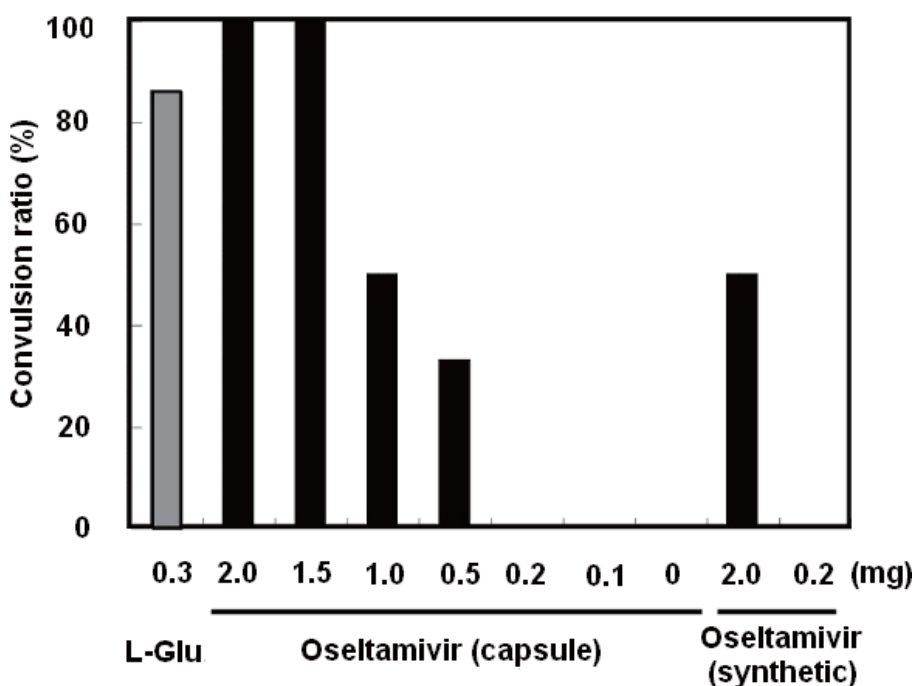


Figure 2. Convulsion induced by intracerebral injection of *L*-glutamic acid (*L*-Glu), oseltamivir (capsule), or synthetic oseltamivir in mice. Synthetic oseltamivir was administered at a dose of 0.2 mg ($n = 5$) and 2.0 mg ($n = 6$). Oseltamivir (capsule) was administered at a dose of 0.1 to 1.5 mg ($n = 6$), 2.0 mg ($n = 8$), and 0 mg ($n = 7$). Seven mice were injected with 0.3 mg *L*-glutamic acid.

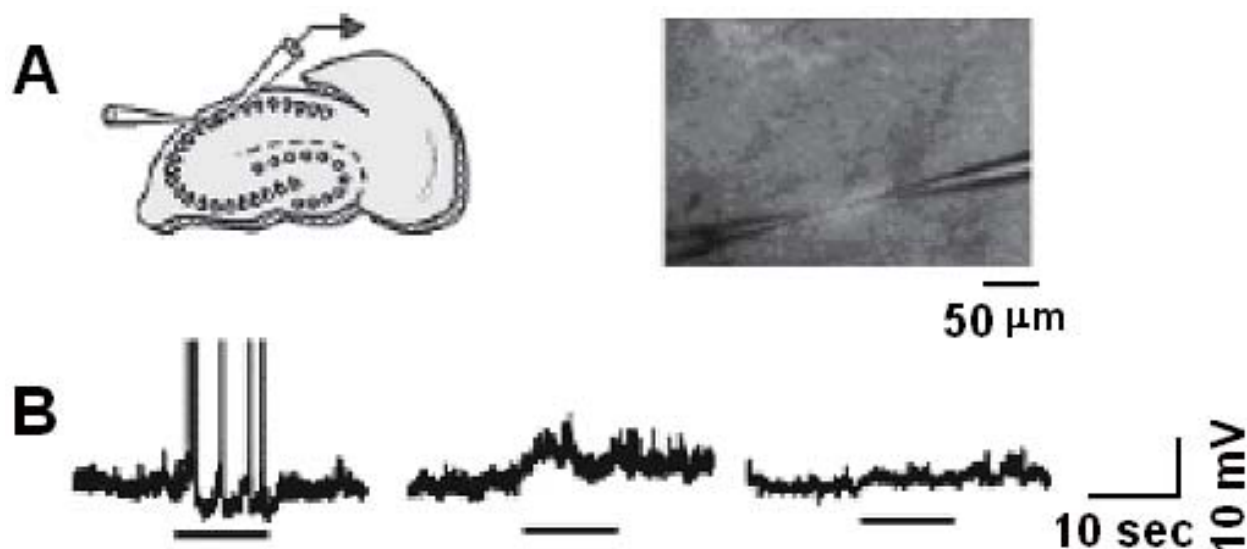


Figure 3. Excitatory effect of acid-form oseltamivir (**2**) on neurons in rat hippocampal slice cultures. A) Illustration and photograph of experimental procedures. Electrophysiologic responses were recorded from CA1 pyramidal cells through the right electrode in the current-clamp mode. Drugs were locally applied from the left electrode. B) Voltage responses to 1 mM acid form-oseltamivir (**2**). Underlines indicate periods of drug treatment. Representatives of three types of responses are shown.

in cell clusters for examination of the pharmacologic effects and toxicity of neuroactive substances has been emphasized (36). To identify the cells and receptors that interact with oseltamivir, studies using large-scale systems linked with the whole neuron networks are necessary. Importantly, the enantiomer of **2** (for the synthetic route, see Supplementary data) (1 mM) did not affect membrane potentials of hippocampal neurons ($n = 5$). This finding clearly indicated that the electrophysiologic effects of oseltamivir on neurons were stereospecific, and thus induced by specific interactions with biologic molecules.

The results of the above three types of experiments all demonstrated that oseltamivir induces specific responses in the nervous system identical to those induced by *L*-glutamic acid. Mammalian glutamate receptors are highly expressed in cortical and hippocampal neurons, and are classified into three subtypes; *N*-methyl-D-aspartate (NMDA) receptors, α -amino-3-hydroxy-5-methyl-isoxazole-4-propionic acid (AMPA)/kainate receptors, and metabotropic receptors. Agonists of these receptors excite neurons and induce seizures in mammals (37). Based on the results described here, oseltamivir may act on these receptors, thereby causing membrane depolarization in excitatory neurons and systemic seizures. In conclusion, these findings are the first to demonstrate that oseltamivir exerts *L*-glutamic acid-like effects in experimental systems reflecting higher biologic activities, *i.e.*, muscle contraction assay in silkworm larvae, seizure assay in mice, and electrophysiologic *ex vivo* membrane potential recordings. The C1 carboxylate, C4 acetamide, C5 amino moieties, and the position of the double bond of oseltamivir are important for the interaction between oseltamivir and viral neuraminidase (3). Modifying other parts of the molecule might eliminate

the *L*-glutamic acid-like effects of oseltamivir without inducing a loss of its affinity to neuraminidase. Detailed studies toward mechanistic elucidation of oseltamivir's pharmacologic effects on the nervous system (especially, glutamate receptor subtype selectivity) and its chemical structure modification are ongoing in our group.

Acknowledgements

Financial support was provided by a grant from Genome Pharmaceuticals Institute Co., Ltd, and a Grant-in-Aid for Specially Promoted Research of MEXT. K.Y. thanks JSPS for a research fellowship.

References

1. Normile D, Enserink M. Avian influenza. With change in the seasons, bird flu returns. *Science* 2007; 315:448.
2. De Clercq E. Antiviral agents active against influenza A viruses. *Nat Rev Drug Discov* 2006; 5:1015-1025.
3. Kim CU, Lew W, Williams MA, Liu H, Zhang L, Swaminathan S, Bischofberger N, Chen MS, Mendel DB, Tai CY, Laver WG, Stevens RC. Influenza neuraminidase inhibitors possessing a novel hydrophobic interaction in the enzyme active site: design, synthesis, and structural analysis of carbocyclic sialic acid analogues with potent anti-influenza activity. *J Am Chem Soc* 1997; 119:681-690.
4. Russell RJ, Haire LF, Stevens DJ, Collins PJ, Lin YP, Blackburn GM, Hay AJ, Gamblin SJ, Skehel JJ. The structure of H5N1 avian influenza neuraminidase suggests new opportunities for drug design. *Nature* 2006; 443:45-49.
5. Wei DQ, Du QS, Sun H, Chou KC. Insights from modeling the 3D structure of H5N1 influenza virus neuraminidase and its binding interactions with ligands. *Biochem Biophys Res Commun* 2006; 344:1048-1055.
6. Herlocher ML, Carr J, Ives J, Elias S, Truscon R, Roberts N, Monto AS. Influenza virus carrying an R292K

- mutation in the neuraminidase gene is not transmitted in ferrets. *Antiviral Res* 2002; 54:99-111.
7. Matrosovich MN, Matrosovich TY, Gray T, Roberts NA, Klenk HD. Neuraminidase is important for the initiation of influenza virus infection in human airway epithelium. *J Virol* 2004; 78:12665-12667.
 8. Ohuchi M, Asaoka N, Sakai T, Ohuchi R. Roles of neuraminidase in the initial stage of influenza virus infection. *Microbes Infect* 2006; 8:1287-1293.
 9. Abrecht S, Harrington P, Iding H, Karpf M, Trussardi R, Wirz B, Zutter U. The synthetic development of the anti-influenza neuraminidase inhibitor oseltamivir phosphate (Tamiflu®): A challenge for synthesis & process research. *Chimia* 2004; 58:621-629.
 10. Fukuta Y, Mita T, Fukuda N, Kanai M, Shibasaki M. De novo synthesis of Tamiflu *via* a catalytic asymmetric ring-opening of meso-aziridines with TMSN₃. *J Am Chem Soc* 2006; 128:6312-6313.
 11. Yeung YY, Hong S, Corey EJ. A short enantioselective pathway for the synthesis of the anti-influenza neuraminidase inhibitor oseltamivir from 1,3-butadiene and acrylic acid. *J Am Chem Soc* 2006; 128:6310-6311.
 12. Bromfield KM, Gradén H, Hagberg DP, Olsson T, Kann N. An iron carbonyl approach to the influenza neuraminidase inhibitor oseltamivir. *Chem Commun* 2007; 30:3183-3185.
 13. Mita T, Fukuda N, Roca FX, Kanai M, Shibasaki M. Second generation catalytic asymmetric synthesis of Tamiflu: Allylic substitution route. *Org Lett* 2007; 9:259-262.
 14. Satoh N, Akiba T, Yokoshima S, Fukuyama T. A practical synthesis of (-)-oseltamivir *Angew Chem Int Ed Engl* 2007; 46:5734-5736.
 15. Yamatsugu K, Kamijo S, Suto Y, Kanai M, Shibasaki M. A concise synthesis of Tamiflu: third generation route via the Diels-Alder reaction and the Curtius rearrangement. *Tetrahedron Lett* 2007; 48:1403-1406.
 16. Kaji M, Fukuda T, Tanaka M, Aizawa H. A side effect of neuraminidase inhibitor in a patient with liver cirrhosis. *J Infect Chemother* 2005; 11:41-43.
 17. Hayden FG, Treanor JJ, Fritz RS, Lobo M, Betts RF, Miller M, Kinnersley N, Mills RG, Ward P, Straus SE. Use of the oral neuraminidase inhibitor oseltamivir in experimental human influenza: randomized controlled trials for prevention and treatment. *JAMA* 1999; 282:1240-1246.
 18. Nicholson KG, Aoki FY, Osterhaus AD, Trottier S, Carewicz O, Mercier CH, Rode A, Kinnersley N, Ward P. Efficacy and safety of oseltamivir in treatment of acute influenza: a randomised controlled trial. Neuraminidase Inhibitor Flu Treatment Investigator Group. *Lancet* 2000; 355:1845-1850.
 19. Fuyuno I. Tamiflu side effects come under scrutiny. *Nature* 2007; 446:358-359.
 20. Izumi Y, Tokuda K, O'Dell KA, Zorumski CF, Narahashi T. Neuroexcitatory actions of Tamiflu and its carboxylate metabolite. *Neurosci Lett* 2007; 426:54-58.
 21. Sekimizu K, Larranaga J, Hamamoto H, Sekine M, Furuchi T, Katane M, Homma H, Matsuki N. D-Glutamic acid-induced muscle contraction in the silkworm, *Bombyx mori*. *J Biochem (Tokyo)* 2005; 137:199-203.
 22. Ha SD, Nagata S, Suzuki A, Kataoka H. Isolation and structure determination of a paralytic peptide from the hemolymph of the silkworm, *Bombyx mori*. *Peptides* 1999; 20:561-568.
 23. Mizuhashi S, Nishiyama N, Matsuki N, Ikegaya Y. Cyclic nucleotide-mediated regulation of hippocampal mossy fiber development: a target-specific guidance. *J Neurosci* 2001; 21:6181-6194.
 24. Yamamoto T, Shiosaka S, Whittaker ME, Hertzberg EL, Nagy JJ. Gap junction protein in rat hippocampus: light microscope immunohistochemical localization. *J Comp Neurol* 1989; 281:269-281.
 25. Stoppini L, Buchs PA, Muller D. A simple method for organotypic cultures of nervous tissue. *J Neurosci Methods* 1991; 37:173-182.
 26. Li W, Escarpe PA, Eisenberg EJ, Cundy KC, Sweet C, Jakeman KJ, Merson J, Lew W, Williams M, Zhang L, Kim CU, Bischofberger N, Chen MS, Mendel DB. Identification of GS 4104 as an orally bioavailable prodrug of the influenza virus neuraminidase inhibitor GS 4071. *Antimicrob Agents Chemother* 1998; 42:647-653.
 27. Lindegardh N, Davies GR, Tran TH, Farrar J, Singhasivanon P, Day NP, White NJ. Rapid degradation of oseltamivir phosphate in clinical samples by plasma esterases. *Antimicrob Agents Chemother* 2006; 50:3197-3199.
 28. Kitsikis A, Steriade M. Immediate behavioral effects of kainic acid injections into the midbrain reticular core. *Behav Brain Res* 1981; 3:361-380.
 29. Johnston GA. Convulsions induced in 10-day-old rats by intraperitoneal injection of monosodium glutamate and related excitant amino acids. *Biochem Pharmacol* 1973; 22:137-140.
 30. Chapman AG. Glutamate and epilepsy. *J Nutr* 2000; 130:1043S-1045S.
 31. Kaito C, Akimitsu N, Watanabe H, Sekimizu K. Silkworm larvae as an animal model of bacterial infection pathogenic to humans. *Microb Pathog* 2002; 32:183-190.
 32. Hamamoto H, Kurokawa K, Kaito C, Kamura K, Manitra Razanajatovo I, Kusuhara H, Santa T, Sekimizu K. Quantitative evaluation of the therapeutic effects of antibiotics using silkworms infected with human pathogenic microorganisms. *Antimicrob Agents Chemother* 2004; 48:774-779.
 33. Orihara Y, Hamamoto H, Kasuga H, Shimada T, Kawaguchi Y, Sekimizu K. A silkworm-baculovirus model for assessing the therapeutic effects of anti-viral compounds: characterization and application to the isolation of anti-virals from traditional medicines. *J Gen Virol* 2008; 89:188-194.
 34. Hamamoto H, Kamura K, Razanajatovo IM, Murakami K, Santa T, Sekimizu K. Effects of molecular mass and hydrophobicity on transport rates through non-specific pathways of the silkworm larva midgut. *Int J Antimicrob Agents* 2005; 26:38-42.
 35. Ishii K, Hamamoto H, Kamimura M, Sekimizu K. Activation of the silkworm cytokine by bacterial and fungal cell wall components via a reactive oxygen species-triggered mechanism. *J Biol Chem* 2008; 283:2185-2191.
 36. Faingold CL. Emergent properties of CNS neuronal networks as targets for pharmacology: application to anticonvulsant drug action. *Prog Neurobiol* 2004; 72:55-85.
 37. Peeters BW, Ramakers GM, Vossen JM, Coenen AM. The WAG/Rij rat model for nonconvulsive absence epilepsy: involvement of nonNMDA receptors. *Brain Res Bull* 1994; 33:709-713.

(Received November 15, 2007; Accepted November 20, 2007)

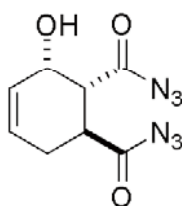
Supplementary Data

Synthesis of Tamiflu®

Overall Scheme

Tamiflu® (**1**), Ro64-0802 (**2**), and its enantiomer **4** were synthesized by the previously reported method (*1*).

(1S*,2R*,3S*)-3-Hydroxy-cyclohex-4-ene-1,2-dicarbonyl diazide (S-1):

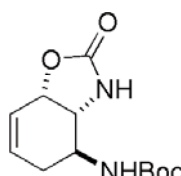


Fumaryl chloride (37.7 g, 247 mmol) was added slowly to a stirred solution of 1-(trimethylsilyloxy)-1,3-butadiene (40 g, 281 mmol) in THF (1,240 mL) at room temperature, and the mixture was stirred for 2 h. TMSN₃ (68.7 mL,

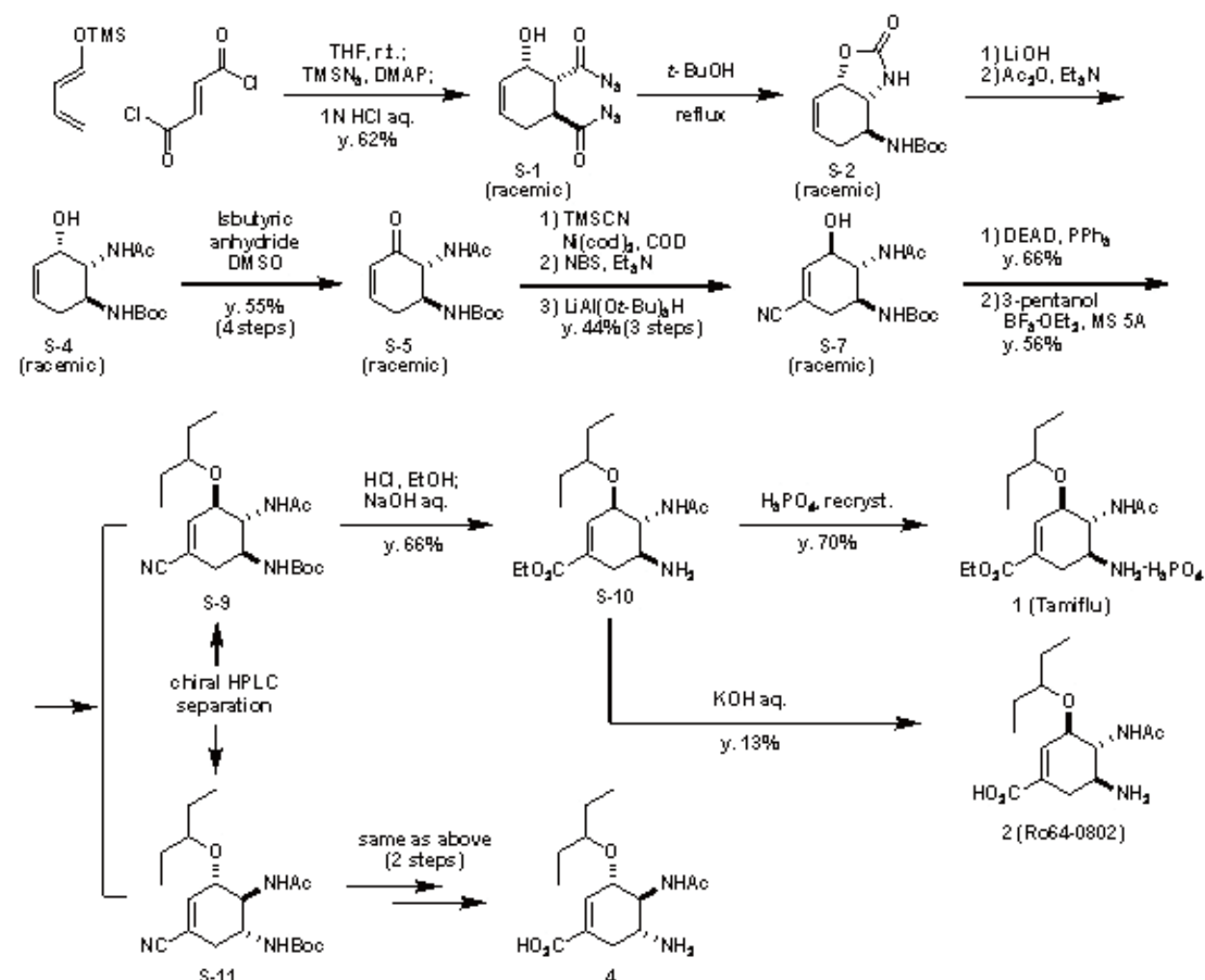
519 mmol) and DMAP (3 g, 24.7 mmol) were carefully added at room temperature, and the mixture was stirred for 2 h. After cooling to 4°C, 1 N HCl aq. (25.0 mL, 25.0 mmol) was carefully added, and the mixture was stirred at the same temperature for 10 min. The

organic layer was separated and the aqueous layer was extracted twice with AcOEt (1,500 mL). The combined organic layers were washed with saturated NaHCO₃ solution (500 mL) and brine (500 mL), dried over Na₂SO₄, and concentrated to give crude **S-1**, which was purified by silica gel column chromatography (neutral SiO₂, 1,000 g, hexane /AcOEt = 4/1 to 2/1) to give **S-1** (36.0 g, 152.4 mmol; 62% yield) as a colorless oil. ¹H NMR (CDCl₃, 500 MHz) δ 6.92-5.86 (m, 2H), 4.48 (m, 1H), 2.96 (ddd, *J* = 5.3, 11.6, 12.0 Hz, 1H), 2.87 (dd, *J* = 4.0, 12.0 Hz, 1H), 2.49 (ddd, *J* = 5.2, 5.3, 17.7 Hz, 1H), 2.10-2.03 (m, 1H); ¹³C NMR (CDCl₃, 125 MHz) δ 181.9, 179.3, 128.7, 127.0, 63.8, 49.6, 37.9, 28.7; IR (neat, cm⁻¹) 3412, 2260, 2146, 1710; FAB-HRMS Calcd for C₈H₉N₆O₃ [M+H]⁺: 237.0731, Found: 237.0726.

(2-Oxo-2,3,3aβ,4α,5,7aβ-hexahydro-benzoxazol-4-yl)-carbamic acid tert-butyl ester (S-2):



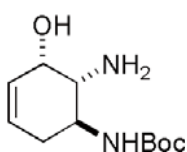
The solution of **S-1** (36.0 g, 152.4 mmol) in distilled *t*-BuOH (305 mL) was stirred at refluxing temperature for 15 h. Removal of the solvent under reduced pressure gave crude



Scheme 1. Overall synthetic scheme.

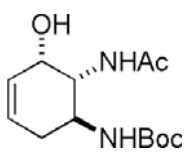
S-2 (38.8 g, 152.4 mmol) as a white solid, which was used for the next reaction without further purification. $^1\text{H NMR}$ (CD_3OD , 500 MHz) δ 6.10 (m, 1H), 5.88-5.86 (m, 1H), 5.04-5.03 (m, 1H), 3.77-3.73 (m, 1H), 3.55-3.50 (m, 1H), 2.37 (ddd, $J = 5.2, 5.5, 17.2$ Hz, 1H), 2.01-1.96 (m, 1H), 1.44 (s, 9H); $^{13}\text{C NMR}$ (CD_3OD , 125 MHz) δ 161.4, 158.1, 132.7, 123.7, 80.5, 75.3, 56.4, 51.0, 29.8, 28.7; IR (KBr, cm^{-1}) 3370, 3243, 1747, 1683; ESI-MS m/z 277 [$\text{M} + \text{Na}$] $^+$; FAB-HRMS Calcd for $\text{C}_{12}\text{H}_{19}\text{N}_2\text{O}_4$ [$\text{M} + \text{H}$] $^+$: 255.1339, Found: 255.1332.

(1S*,5S*,6R*)-(6-Amino-5-hydroxy-cyclohex-3-enyl)-carbamic acid *tert*-butyl ester (S-3):



$\text{LiOH}\cdot\text{H}_2\text{O}$ (32 g, 763 mmol) was added to a stirred solution of **S-2** (38.8 g, 152.4 mmol) in $\text{MeOH}/\text{H}_2\text{O}$ (1/1, 1,530 mL) at room temperature, and the mixture was stirred at 65°C for 16 h. After evaporation of MeOH , $\text{CHCl}_3/\text{MeOH} = 9/1$ solution (500 mL) and brine (300 mL) were added. The aqueous layer was extracted with $\text{CHCl}_3/\text{MeOH} = 9/1$ solution (1,500 mL). The combined organic layers were dried over Na_2SO_4 , and concentrated to give crude **S-3** (31.2 g, 136.7 mmol) as a pale brown solid, which was used for the next reaction without further purification. $^1\text{H NMR}$ (CD_3OD , 500 MHz) δ 5.77 (m, 2H), 4.11 (m, 1H), 3.66 (m, 1H), 2.61 (dd, $J = 11.0, 11.0$, 1H), 2.62-2.40 (m, 1H), 1.97-1.90 (m, 1H), 1.45 (s, 9H); $^{13}\text{C NMR}$ (CD_3OD , 125 MHz) δ 158.6, 129.6, 129.0, 80.1, 67.8, 67.8, 56.0, 33.7, 28.8; IR (KBr, cm^{-1}) 3301, 1675; ESI-MS m/z 229 [$\text{M} + \text{H}$] $^+$; FAB-HRMS Calcd for $\text{C}_{11}\text{H}_{21}\text{N}_2\text{O}_3$ [$\text{M} + \text{H}$] $^+$: 229.1547, Found: 229.1550.

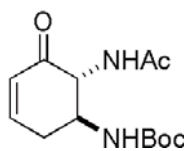
(1S*,5S*,6R*)-(6-Acetylamino-5-hydroxy-cyclohex-3-enyl)-carbamic acid *tert*-butyl ester (S-4):



Et_3N (37.9 mL, 273.4 mmol) and Ac_2O (12.9 mL, 136.7 mmol) were slowly added to a stirred solution of **S-3** (31.2 g, 136.7 mmol) in THF (1,370 mL) at 4°C . The mixture was stirred at the same temperature for 15 min. The reaction was diluted with AcOEt (300 mL) and quenched with saturated NH_4Cl solution (150 mL). The organic layer was separated, and the aqueous layer was extracted with AcOEt (1,200 mL). The combined organic layers were washed with brine (300 mL), dried over Na_2SO_4 , and concentrated to give crude **S-4** (37.0 g, 136.7 mmol) as a pale brown solid, which was used for the next reaction without further purification. $^1\text{H NMR}$ (CDCl_3 , 500 MHz) δ 6.89 (d, $J = 8.3$ Hz, 1H), 5.81-5.74 (m, 2H), 5.14 (d, $J = 8.6$ Hz, 1H), 4.08 (m, 1H), 4.08-3.90 (m, 2H), 2.48 (ddd, $J = 4.7, 4.7, 17.7$ Hz, 1H), 2.02-1.96 (m, 4H), 1.36 (s, 9H); $^{13}\text{C NMR}$ (CDCl_3 , 125 MHz) δ 171.2, 156.8, 129.1, 127.4, 79.5, 66.6, 54.1, 46.2, 33.0,

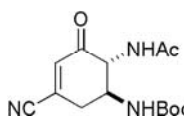
28.3, 23.1; IR (KBr, cm^{-1}) 3364, 3290, 1686, 1663; ESI-MS m/z 293 [$\text{M} + \text{Na}$] $^+$; FAB-HRMS Calcd for $\text{C}_{13}\text{H}_{23}\text{N}_2\text{O}_4$ [$\text{M} + \text{H}$] $^+$: 271.1652, Found: 271.1657.

(1S*,6R*)-6-Acetylamino-5-oxo-cyclohex-3-enyl)-carbamic acid *tert*-butyl ester (S-5):



Dimethylsulfoxide (117 mL, 1640 mmol) was added to a stirred solution of **S-4** (37.0 g, 136.7 mmol) in AcOEt (1,370 mL) at room temperature. The reaction temperature was raised to refluxing temperature, and isobutyric anhydride (64 mL, 386.0 mmol) was added. The mixture was stirred at the same temperature for 25 h. The reaction was quenched with saturated NaHCO_3 solution (150 mL), the organic layer was separated, and the aqueous layer was extracted with AcOEt (1,000 mL). The combined organic layers were washed with brine (300 mL), dried over Na_2SO_4 , and concentrated to give crude **S-5**, which was purified by recrystallization from hexane/2-propanol to afford **S-5** (17.0 g, 63.2 mmol). The filtrate was evaporated and purified by silica gel column chromatography (neutral SiO_2 , 450 g, hexane/ $\text{AcOEt} = 1/4$ to AcOEt) to afford **S-5** (5.39 g, 20.1 mmol) as a white crystal. Both were combined and used for the next reaction (22.4 g, 83.3 mmol; 55% yield for 4 steps). $^1\text{H NMR}$ (CDCl_3 , 500 MHz) δ 6.96-6.93 (m, 1H), 6.37 (d, $J = 6.6$ Hz, 1H), 6.11 (dd, $J = 2.9, 9.9$ Hz, 1H), 5.70 (d, $J = 7.6$ Hz, 1H), 4.58 (dd, $J = 6.6, 13.0$ Hz, 1H), 3.94-3.86 (m, 1H), 2.92 (ddd, $J = 5.5, 5.5, 18.9$ Hz, 1H), 2.45-2.39 (m, 1H), 2.06 (s, 3H), 1.39 (s, 9H); $^{13}\text{C NMR}$ (CDCl_3 , 125 MHz) δ 194.8, 172.3, 155.8, 148.6, 128.5, 79.7, 59.7, 53.5, 34.1, 28.3, 23.1; IR (KBr, cm^{-1}) 3329, 3283, 1689, 1664, 1626; ESI-MS m/z 291 [$\text{M} + \text{Na}$] $^+$; FAB-HRMS Calcd for $\text{C}_{13}\text{H}_{21}\text{N}_2\text{O}_4$ [$\text{M} + \text{H}$] $^+$: 269.1496, Found: 269.1493.

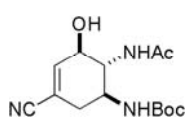
(1S*,6R*)-6-Acetylamino-3-cyano-5-oxo-cyclohex-3-enyl)-carbamic acid *tert*-butyl ester (S-6):



THF solution of **S-5** (0.17 M, 2.21 mL, 0.37 mmol), THF solution of 1,5-cyclooctadiene (0.40 M, 0.489 mL, 0.19 mmol), and distilled TMSCN (150 μL , 1.12 mmol) were added to a THF (1.98 mL) solution of $\text{Ni}(\text{cod})_2$ (51.3 mg, 0.19 mmol) in a flame-dried flask at room temperature with stirring. The mixture was stirred at 65°C for 1 h. After the starting material was consumed, the mixture was filtered through a celite pad, and the filtrate was evaporated. The residue was dissolved in THF (3.73 mL), and cooled to 4°C . *N*-bromosuccinimide (69.7 mg, 0.39 mmol) was added to this solution, and the mixture was stirred at the same temperature for 1 h. The reaction temperature was raised to room temperature, and Et_3N (103 μL , 0.74 mmol) was added. The reaction

temperature was raised to refluxing temperature and stirred for 12 h. After cooling to room temperature, the mixture was diluted with AcOEt (5 mL), and quenched with 5% NaH₂PO₄ aqueous solution (2 mL). The organic layer was separated, and aqueous layer was extracted with AcOEt (15 mL). The combined organic layers were dried over Na₂SO₄ and concentrated to give crude **S-6**, which was passed through a silica gel (neutral SiO₂ 5 g, hexane/AcOEt = 1/1 to 1/2 to 1/6) to afford semi-purified **S-6** (73 mg). It was used for the next reaction without further purification.

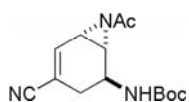
(1S*,5R*,6R*)-(6-Acetylamino-3-cyano-5-hydroxy-cyclohex-3-enyl)-carbamic acid tert-butyl ester (S-7):



LiAl(O*t*-Bu)₃H (1.0 M in THF, 448 μL, 0.45 mmol) was added to a stirred solution of semi-purified **S-6** (66 mg) in THF (1.12 mL) at 4°C.

The mixture was stirred at the same temperature for 45 min. The reaction was quenched with saturated NH₄Cl solution (1 mL), the organic layer was separated, and the aqueous layer was extracted with AcOEt (10 mL). The combined organic layers were washed with brine (5 mL), dried over Na₂SO₄, and concentrated to give crude **S-7**, which was purified by silica gel column chromatography (neutral SiO₂ 3 g, AcOEt/MeOH = 100/1 to 50/1) to afford **S-7** (48 mg, 0.16 mmol; 44% yield for 3 steps) as a white solid. ¹H NMR (CDCl₃) δ 7.12 (d, *J* = 5.2 Hz, 1H), 6.49 (s, 1H), 5.01 (d, *J* = 2.3 Hz, 1H), 4.82 (d, *J* = 8.0 Hz, 1H), 4.28-4.21 (m, 1H), 3.92-3.81 (m, 1H), 3.78-3.70 (m, 1H), 2.63 (dd, *J* = 16.9, 5.0 Hz, 1H), 2.32-2.22 (m, 1H), 2.00 (s, 3H), 1.44 (s, 9H); ¹³C NMR (CDCl₃) δ 173.6, 157.3, 145.3, 117.2, 109.8, 81.3, 73.1, 59.5, 47.3, 32.7, 28.2, 23.0; IR (KBr, cm⁻¹) 3322, 2979, 2225, 1683, 1625, 1571; ESI-MS: *m/z* 318 [M+Na]⁺; FAB-HRMS: *m/z* calcd for C₁₄H₂₂N₃O₄ [M+H]⁺: 296.1605, Found: 296.1602.

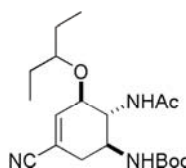
(1R*,2S*,6S*)-(7-Acetyl-4-cyano-7-azabicyclo[4.1.0]hept-4-en-2-yl)-carbamic acid tert-butyl ester (S-8):



Diethyl azodicarboxylate (40% in toluene, 0.72 mL, 1.58 mmol) was added to a solution of triphenylphosphine (414 mg, 1.58 mmol) in THF (7.9 mL) at -20°C. Then **S-7** (234 mg, 0.79 mmol) in THF (2.5 mL) was added dropwise to the reaction mixture over 15 min at the same temperature. After stirring for 1 h, the reaction mixture was concentrated *in vacuo*. The residue was purified by flash column chromatography twice (first [removal of triphenylphosphine oxide]; hexane/AcOEt = 1/4 to AcOEt, and then AcOEt/MeOH = 20/1, second [removal of the residue derived from DEAD]; Et₂O/hexane = 3/1 to 5/1) to afford **S-8** (144 mg, 0.521 mmol; 66% yield)

as an amorphous substance. ¹H NMR (CDCl₃) δ 6.88 (dd, *J* = 3.5, 3.7 Hz, 1H), 4.54 (brs, 2H), 3.12-3.04 (m, 2H), 2.53 (brd, *J* = 17.0 Hz, 1H), 2.35 (brd, *J* = 17.0, 1H), 2.13 (s, 3H), 1.43 (s, 9H); ¹³C NMR (CDCl₃) δ 180.8, 154.8, 140.0, 118.1, 112.3, 80.5, 41.3, 40.5, 31.4, 30.0, 28.3, 23.1; IR (neat, cm⁻¹) 3322, 2978, 2218, 1703, 1525; ESI-MS: *m/z* 300 [M+Na]⁺; FAB-HRMS: *m/z* calcd for C₁₄H₂₀N₃O₃ [M+H]⁺: 278.1499, Found: 278.1500.

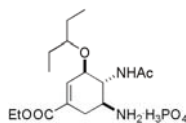
(1S,5R,6R)-[6-Acetylamino-3-cyano-5-(1-ethylpropoxy)-cyclohex-3-enyl]-carbamic acid tert-butyl ester (S-9):



BF₃•OEt₂ (1 M in 3-pentanol, 0.65 mL, 0.645 mmol) was added dropwise over 15 min to a slurry of **S-8** (119.3 mg, 0.430 mmol) and activated molecular sieves 5A (430 mg) in 3-pentanol (4.3 mL) at -20°C.

After stirring for 1 h, water (10 mL) was added at -20°C. The aqueous layer was extracted with AcOEt (15 mL) twice. The combined organic layers were washed with brine (15 mL), dried over Na₂SO₄, and concentrated to give crude **S-9**, which was purified by flash column chromatography (hexane /AcOEt = 2/1 to 3/2 to 1/1) to afford **S-9** (88.1 mg, 0.241 mmol; 56% yield) as a white solid. Enantiomers were separated by chiral HPLC [Daicel Chiralpak AD-H, 2-propanol/hexane 1/20, flow 0.7 mL/min, detection at 220 nm; *t_R* 13.6 min (*ent*-**S-9**, [α]_D²⁷ +84.2 (*c* 0.180, CHCl₃)) and 19.4 min (**S-9**, [α]_D²⁷ -109.3 (*c* 0.140, CHCl₃))]. ¹H NMR (CDCl₃) δ 6.47 (s, 1H), 5.66 (brd, *J* = 8.6 Hz, 1H), 5.12, (brd, *J* = 8.6 Hz, 1H), 4.09-4.01 (m, 1H), 3.95-3.90 (m, 1H), 3.87-3.78 (m, 1H), 3.29 (quintet, *J* = 5.8 Hz, 1H), 2.60 (dd, *J* = 5.5, 18.1 Hz, 1H), 2.37-2.29 (m, 1H), 1.97 (s, 3H), 1.47 (quintet, *J* = 7.5 Hz, 4H), 1.40 (s, 9H), 0.87 (t, *J* = 7.5 Hz, 3H), 0.86 (t, *J* = 7.5 Hz, 3H); ¹³C NMR (CDCl₃) δ 170.9, 156.1, 143.7, 117.5, 111.6, 82.6, 80.0, 75.0, 53.6, 48.3, 32.6, 28.3, 26.0, 25.6, 23.2, 9.4, 9.1; IR (KBr, cm⁻¹): 3335, 3287, 2968, 2220, 1686, 1654, 1541; ESI-MS: *m/z* 388 [M+Na]⁺; FAB-HRMS: *m/z* calcd for C₁₉H₃₂N₃O₄ [M+H]⁺: 366.2393, Found: 366.2401.

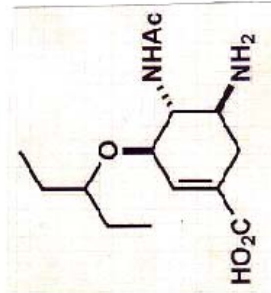
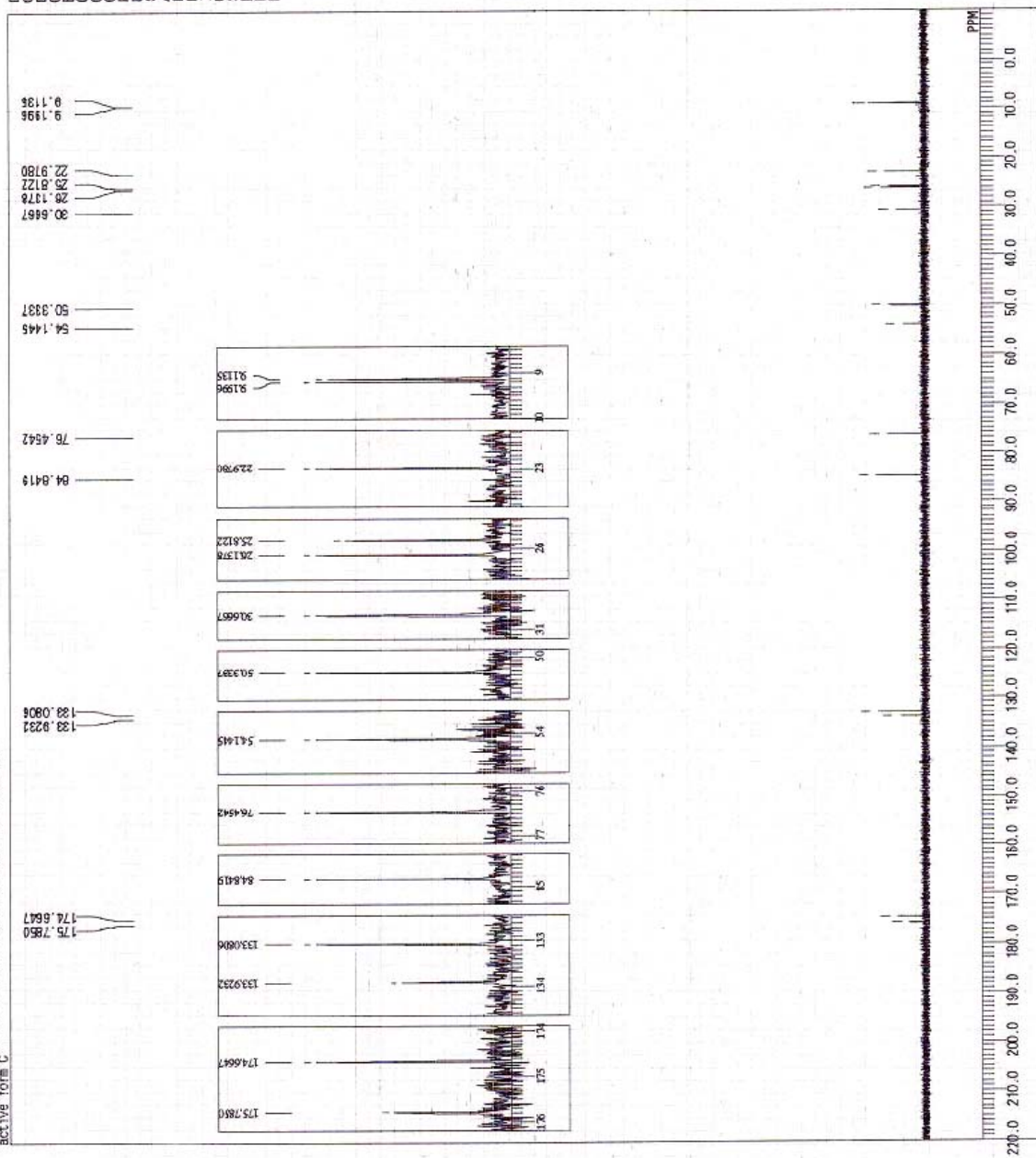
Ethyl (3R,4R,5S)-4-Acetamide-5-amino-3-(1-ethylpropoxy)cyclohexene-1-carboxylate phosphate (I) (Tamiflu®):



The solution of **S-9** (29.8 mg, 0.082 mmol) in 4.2 M HCl/EtOH (3.3 mL) was stirred at room temperature for 24 h. After cooling to 4°C, water (3.3 mL) was added to decompose the imino ester, and the mixture was stirred for 7 h. After addition of CH₂Cl₂ (6.6 mL), the mixture was stirred for a couple of minutes and the CH₂Cl₂ layer was removed. The aqueous layer was basified by 2 M NaOH aqueous

C:\My Documents\FP0use\Hyanatsugu\Hami flu_active_form_C.als
active form C

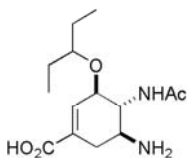
DFILE C:\My Documents\FP0use\Hyanatsugu\Hami flu_active_form_C.als
 COUNT active form C
 DATE 17-09-2007 14:49:21
 ORNUC 13C
 QXNUM 1000
 QXRES 14.45
 QRES 4.00
 POINT 26214
 FREQ 31244.52 Hz
 SCANS 1847
 ACQTH 0.8389 sec
 PD 2.0000 sec
 PW 3.57 usec
 IRNUC 1H
 CTMP 21.7 C
 SLVT D2O
 EXNF 77.00 ppm
 BF 0.12 Hz
 RGAIN 80



solution to pH = 10, extracted with CH₂Cl₂, washed with brine, dried over Na₂SO₄, and concentrated to give the free base **S-10** (16.9 mg, 0.054 mmol; 66% yield). The free base (**S-10**, 74.6 mg, 0.239 mmol) in EtOH (1.44 mL) was slowly added to a solution of H₃PO₄ (85%, 33.1 mg, 0.287 mmol) in EtOH (2.41 mL) at 60°C. Crystallization commenced after a few minutes, and the suspension was cooled to 0°C. The crystal was collected and washed with acetone twice to afford Tamiflu® (**1**) (68.6 mg, 0.167 mmol; 70% yield) as a colorless crystal. ¹H NMR (D₂O) δ 6.91 (s, 1H), 4.39 (brd, *J* = 7.4 Hz, 1H), 4.34-4.26 (m, 2H), 4.11 (dd, *J* = 8.9, 11.6 Hz, 1H), 3.69-3.56 (m, 2H), 3.02 (dd, *J* = 5.1, 17.2 Hz, 1H), 2.62-2.53 (m, 1H), 2.14 (s, 3H), 1.64-1.46 (m, 4H), 1.35 (t, *J* = 7.2 Hz, 3H), 0.94 (t, *J* = 7.3 Hz, 3H), 0.90 (t, *J* = 7.3 Hz, 3H); ¹³C NMR (D₂O) δ 178.1, 170.3, 140.7, 130.5, 87.2, 77.9, 65.3, 55.5, 52.0, 31.0, 28.3, 27.9, 25.2, 16.1, 11.4, 11.3; ³¹P NMR (D₂O) δ 2.85; IR (KBr, cm⁻¹): 3195, 1718, 1661, 1551, 1246, 1127, 513; mp: 184-186°C; ESI-MS: *m/z* 313 [M-H₃PO₄+H]⁺; FAB-HRMS: *m/z* calcd for C₁₆H₂₉N₂O₄ [M-H₃PO₄+H]⁺: 313.2127. Found: 313.2124. [α]_D²² -30.5 (*c* 0.480, H₂O).

This analytical data completely matched with the reported one (2).

(3*R*,4*R*,5*S*)-4-Acetylamino-5-amino-3-(1-ethyl-propoxy)-cyclohex-1-enecarboxylic acid (2) (Ro64-0802):



Aqueous KOH (1M; 0.320 mL, 0.320 mmol) was added to a THF (1.60 mL) solution of free-base **S-10** (50.0 mg, 0.160 mmol) at room temperature. The resulting solution was stirred at the same temperature

for 1 h. The reaction mixture was acidified to pH = 4 with Amberlyst 15-DRY®, and filtered. The filtrate was evaporated, to afford the crude **2**, which was purified by reverse-phase PTLC (H₂O/CH₃CN = 20/1) to afford **2** (5.8 mg, 0.0204 mmol; 13% yield). ¹H NMR (D₂O) δ 6.46 (m, 1H), 4.24-4.22 (m, 1H), 3.97 (dd, *J* = 11.5, 9.2 Hz, 1H), 3.51-3.41 (m, 2H), 2.83 (dd, *J* = 17.2, 5.2 Hz, 1H), 2.44-2.38 (m, 1H), 2.05 (s, 3H), 1.57-1.40 (m, 4H), 0.86 (t, *J* = 7.5 Hz, 3H), 0.82 (t, *J* = 7.5 Hz, 3H). ¹³C NMR (D₂O) δ 175.0, 174.7, 133.9, 133.1, 84.8, 76.5, 54.1, 50.3, 30.7, 26.1, 25.8, 23.0, 9.20, 9.11. IR (KBr, cm⁻¹): 3434, 1656, 1560; ESI-MS: *m/z* 307 [M+Na]⁺.

This analytical data completely matched with the reported one (3).

The enantiomer **4** [(3*S*,4*S*,5*R*)-4-Acetylamino-5-amino-3-(1-ethyl-propoxy)-cyclohex-1-enecarboxylic acid] was synthesized in the same way as **2**.

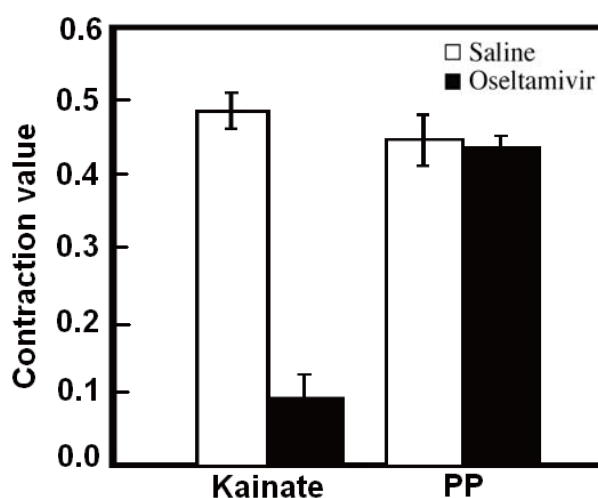
Paralytic effect of oseltamivir on silkworm larvae

The paralysis and muscle relaxation of 5th instar



silkworm larvae induced immediately after injection of 0.9% NaCl or 2.5 mg oseltamivir (Tamiflu®, Chugai Pharmaceutical Co. Ltd., Tokyo, Japan) are shown.

Inhibitory effect of oseltamivir on kainate-induced muscle contraction of silkworm larval specimen



Vehicle (50 μL, 0.9% NaCl) or oseltamivir (50 μL, 100 mg/mL capsule) was injected into a silkworm larval muscle specimen, and successively, 50 μL of kainate (40 μg/mL) or paralytic peptide (4 μg/mL) was injected. Contraction values were calculated as described above. Values represent the mean ± S.D., *n* = 3.

References

- Rohloff JC, Kenneth MK, Postich MJ, Becker MW, Chapman HH, Kelly DE, Lew W, Louie MS, McGee LR, Prisbe EJ, Schultze LM, Yu RH, Zhang LJ. Practical total synthesis of the anti-influenza drug GS-4104. *J Org Chem* 1998; 63:4545-4550.
- Kim CU, Lew W, Williams MA, Liu H, Zhang L, Swaminathan S, Bischofberger N, Chen MS, Mendel DB, Tai CY, Laver WG, Stevens RC. Influenza neuraminidase inhibitors possessing a novel hydrophobic interaction in the enzyme active site: design, synthesis, and structural analysis of carbocyclic sialic acid analogues with potent anti-influenza activity. *J Am Chem Soc* 1997; 119:681-690.
- Yamatsugu K, Kamijo S, Suto Y, Kanai M, Shibasaki M. A concise synthesis of Tamiflu: third generation route via the Diels-Alder reaction and the Curtius rearrangement. *Tetrahedron Lett* 2007; 48:1403-1406.

Original Article**Immunosuppressive effect of ER-38925, a retinoic acid receptor subtype α -selective agonist, in mouse models of human graft-*vs*-host disease**Takayuki Hida^{1,2}, Kohdoh Shikata¹, Naoki Tokuhara¹, Akira Ishibashi¹, Mitsuo Nagai¹, Toshihiko Yamauchi^{1,*}, Seiichi Kobayashi¹¹ Tsukuba Research Laboratories, Eisai Co., Ltd., Tsukuba-shi, Ibaraki, Japan;² Current address, Morphotek Inc., 210 Welsh Pool Road, Exton, PA, USA.

ABSTRACT: Graft-*vs*-host disease (GVHD) is a devastating disorder that determines the prognosis of patients who receive a bone marrow transplant. GVHD is caused by donor cells responding to host disparate MHC alleles. In this report, we demonstrate that ER-38925, a newly discovered retinoid agonist with selectivity to retinoic acid receptor subtype α (RAR- α), is a potent immunosuppressive agent in mouse models of human GVHD. In a mouse model of lethal acute GVHD (aGVHD), ER-38925 prolonged the lifespan of the recipient mice in a dose-dependent manner. Its effect at 1 mg/kg was almost comparable to that of cyclosporin A at 30 mg/kg. ER-38925 profoundly prevented the development of anti-allogeneic cytotoxic T lymphocyte (CTL) response in the mouse model of aGVHD at 0.1 and 0.3 mg/kg. It strongly inhibited *in vitro* proliferation of alloantigen-stimulated donor T lymphocytes, and RAR- α seemed to play an exclusive role in this effect since inhibition by all-trans retinoic acid, which can activate all subtypes of RAR, was completely reversed by an RAR- α selective antagonist. Moreover, it significantly inhibited the elevation of serum IL-12 and IFN- γ and LPS-induced serum TNF- α elevation, all of which are known to be crucial disease-exacerbating factors in this model and human GVHD, in the mouse model of aGVHD. These results suggest that ER-38925 prevents the development of aGVHD through substantial inhibition of anti-allogeneic responses of donor T lymphocytes. In addition, *in vivo* administration of ER-38925 also blocked serum anti-DNA autoantibody production in a mouse model of human chronic GVHD. This is the first report to clearly show the

remarkable immunosuppressive effects of an RAR- α selective agonist in mouse models of human GVHD. These findings may allow an RAR- α selective agonist like ER-38925 to serve as a novel therapy to prevent both acute and chronic types of human GVHD.

Keywords: Graft-*vs*-host disease, Bone marrow transplantation, Retinoid, Therapy

Introduction

Graft-*vs*-host disease (GVHD) occurs after bone marrow transplantation (BMT) and can be found in acute and chronic forms. In patients who received BMT, acute GVHD (aGVHD) takes place within about 60 days post-transplantation and results in damage to the skin, liver, and gut due to the action of cytotoxic lymphocytes. Chronic GVHD (cGVHD) occurs later and is a systemic autoimmune disease that primarily affects the skin, resulting in the polyclonal activation of B cells and hyperproduction of immunoglobulin (Ig) and various kinds of autoantibodies, including anti-DNA autoantibody. The current method of preventing GVHD is to irradiate donor bone marrow cells or deplete mature T lymphocytes before transferring them to the host. BMT patients are systemically treated with various kinds of immunosuppressive drugs, including glucocorticoid, cyclosporin A, and cyclophosphamide. Despite their undesirable and severe toxicity, none of those therapies completely blocks GVHD development, and more effective and safer remedies are desired for this disease.

GVHD is studied in experimental systems by transferring T lymphocytes into allogeneic or semiallogeneic immunoincompetent recipients. In both types of GVHD model, donor T lymphocytes recognize and respond to the host disparate MHC antigens and

*Correspondence to: Dr. Toshihiko Yamauchi, Discovery Research Laboratories I, Tsukuba Research Labs., Eisai Co. Ltd., 5-1-3 Tokodai, Tsukuba-Shi, Ibaraki 300-2635, Japan;
e-mail: t-yamauchi@hhc.eisai.co.jp

initiate immunological disorders. In the mouse aGVHD model, animals die within 1-3 weeks after suffering from severe wasting, diarrhea, and skin lesions. In those mice, serum interferon- γ , IL-12 and TNF- α are significantly elevated, as also reported in human GVHD patients. On the other hand, in mouse cGVHD models, host B cells are polyclonally activated and produce excess amount of Ig and autoantibodies through cognate interaction between allospecific donor helper T cells (Th) and host B cells (1,2). Pathological features of those mouse models of GVHD closely resemble the pathological changes in human patients with either acute or chronic GVHD. This enables the use of those animals as models of human GVHD.

Retinoids are vitamin A derivatives used for the treatment of vitamin A deficiency and dermatological disorders as well as for chemoprevention and therapy for certain cancers (3). Retinoids regulate gene expression through the action of retinoic acid receptors (RARs) and retinoid-X receptors (RXRs), both of which belong to the family of nuclear hormone receptors (4). Both RARs and RXRs consist of 3 subtypes, *i.e.* α , β , γ . Those subtypes are expressed in various organs in a specially and/or temporally regulated manner and mediate pleiotropic effects of retinoids, including either beneficial or adverse effects. Many RAR and RXR pan- or subtype specific-modulators have been developed as drugs, mainly targeting cancer and metabolic diseases (5).

In addition, retinoids, like 4-hydroxyretinamide, all-trans, and 13-cis retinoic acid were reported to be effective in some immunological disease models like rat adjuvant arthritis (6) and experimental allergic encephalomyelitis (7), both of which are believed to be caused by cell-mediated immunity. Am80, a ligand with an affinity selective for RAR α , was reported to inhibit rat collagen-induced arthritis with a prominent reduction of anti-collagen IgG titers (8) and also inhibit experimental allergic encephalomyelitis in rats (9). In light of these findings, retinoids, and especially RAR α -selective ones, are expected to be a new remedy for intractable human immunological diseases.

ER-38925 is an RAR- α selective retinoid synthesized in the authors' laboratory (10). It has profound immunosuppressive activities in various kinds of models, like mouse cardiac allograft transplantation (11), and mouse lupus nephritis in female (NZB/NZW)F1 mice (12). These findings prompted an investigation of whether ER-38925 would inhibit various kinds of immunological disorders in mouse models of human GVHD.

Materials and Methods

Mice

C57BL/6 (B6; H-2^b), DBA/2 (D2; H-2^d) and B6D2F1

(BDF1; H-2^{b/d}) were purchased from Charles River Japan (Kanagawa, Japan) and maintained in a specific pathogen-free environment in the animal facility at Eisai Tsukuba Research Labs. All mice used in this study were female and 7 to 12 weeks old. All animal experiments were approved by the Animal Care and Use Committee of Eisai.

Drugs

ER-38925 (4-{5-[4,7-dimethyl-benzo[*b*]furan-2-yl]-1*H*-2-pyrrolyl}benzoic acid) was synthesized at Eisai Tsukuba Laboratories with a structure as shown in Figure 1. ER-50891 was also synthesized at Eisai and is an RAR- α selective antagonist as reported previously (13). Am80, a well-known RAR- α selective agonist, was purchased from WAKO Pure Chemical (Osaka, Japan). ER-38925 and Am80 were suspended in 0.5% methyl cellulose solution for *in vivo* administration. Cyclosporin A (CyA, Sandimmun[®] concentrate for infusion, lot.4197, Novartis, Switzerland) was diluted with physiological saline to the appropriate concentration. Recipient mice were administered appropriate doses of ER-38925 and Am80 orally or CyA subcutaneously at a volume of 10 mL of drug solution per kg of body weight.

Induction of aGVHD

Acute GVHD was induced according to the methods previously reported (1). To induce lethal GVHD, BDF1 recipients were lethally irradiated (10 Gy) and intravenously injected with 2×10^7 bone marrow cells and 5×10^7 spleen cells obtained from B6 donors. Parental B6 mice were anesthetized and killed by cervical dislocation prior to removal of the spleen and femur. Dissociated bone marrow and spleen cells were washed and resuspended in D-PBS for intravenous injection into the BDF1 hybrid. After bone marrow transplantation (BMT), recipients were given sterile chow and water, and the survival of each mouse was monitored daily. In other experiments, 5×10^7 B6 spleen cells were intravenously infused into non-irradiated BDF1 mice as a means of examining the induction of cytotoxic T lymphocyte (CTL) against a disparate MHC allele (H-2^d).

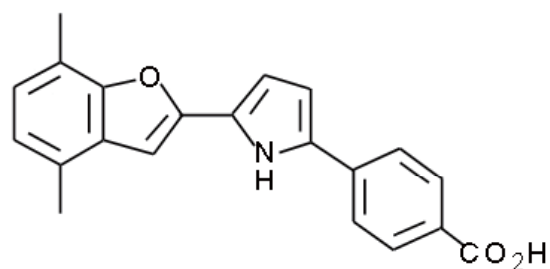


Figure 1. Chemical structure of ER-38925.

Induction of cGVHD

To induce cGVHD, BDF1 recipients were intravenously injected with 5×10^7 DBA/2 spleen cells. Preparation and transfer of the spleen cells were carried out as described in the previous (aGVHD) section. Two weeks after the transfer, mice were bled and their sera were collected for the determination of anti-single stranded DNA (ssDNA) autoantibody titers.

Assessment of CTL activity

Ten to twelve days after the injection of B6 spleen cells, recipients were anesthetized and killed by cervical dislocation prior to removal of the spleen. After dissociation, spleen cells were washed and resuspended in RPMI-1640 at various cell densities. Suspended in 200 μ L of complete RPMI-1640 (supplemented with 10% FCS (lot S07300, Sanko Junyaku, Tokyo, Japan) and 50 μ M 2-mercaptoethanol, 5,000 U/mL penicillin and 5,000 U/mL streptomycin) were 1×10^7 target tumor cells, P-815 (H-2^d, mouse mastocytoma), and EL-4 (H-2^b, mouse T-lymphoma), which were then labeled with 0.1 mCi of ⁵¹Cr (Cat. No. NEZ-030(S), DuPont NEN, Boston, MA) for 1 h at 37°C, 5% CO₂. Cells were then washed thoroughly and resuspended at 1×10^5 cells/mL in complete RPMI-1640. Labeled target cells were plated at 1×10^4 per well on a 96-well round bottom plate with effector cells at an effector/target (E/T) ratio of 80:1, 40:1, 20:1, 10:1, 5:1, and 2.5:1. The plates were incubated at 37°C, 5% CO₂ for 4 h. After incubation, these plates were centrifuged at 1,500 rpm for 5 min, and an aliquot of cell-free supernatant was collected from each well and transferred onto LumaPlates™ (Packard) to determine radioactivity with a TopCount™ Microplate Scintillation Counter (Packard). Percent-specific lysis is defined as $(a-b)/(c-b)$, where *a* equals cpm released by target cells incubated with effector cells, *b* equals cpm released by target cells incubated with medium only (spontaneous release), and *c* equals cpm released by target cells incubated with 1% of Triton X-100 (100% release). No nonspecific cytotoxicity was observed after effector cells were incubated with MHC-matched target cells (EL-4).

Anti-ssDNA IgG

For anti-ssDNA, ELISA plates (Costar, Cambridge, MA, Cat #3590) were first coated at room temperature with 10 mg/mL poly-L-lysine (Sigma, St. Louis, MO) for 0.5 h and then incubated overnight at 4°C with ssDNA preparation (heat-inactivated calf thymus DNA) at 5 μ g/mL. After wells were washed with washing buffer (0.05% Tween 20-0.1 M phosphate buffer (pH 7.4)) and blocked with 50% FCS-PBS (37°C, 2 h), 50 μ L of serially diluted serum sample were added and

plates were incubated at 37°C for 2 h. After washing, biotinylated goat anti-mouse IgG (Amersham) diluted with ELISA buffer (10% normal rabbit serum, 0.05% Tween 20-PBS (-)) at 1:1000 was added and plates were incubated further (37°C, 2 h). Anti-DNA IgG was detected with horseradish peroxidase-labeled streptavidin (Amersham, Buckinghamshire, England) and developed with o-phenylenediamine dihydrochloride. About 30 min later, the reaction was stopped by adding 50 μ L of sulphuric acid, and plates were read at an OD of 490 nm with a Micro Plate Reader. The amount of anti-ssDNA activity in each sample was expressed as units/mL in reference to standard serum obtained from an old female (NZB/NZW)F1 mouse, which was defined as having 1,000 U/mL of activity.

Serum cytokines

For the detection of serum cytokines, B6 spleen cells were transferred to BDF1 mice, which were treated with the drugs from the day of disease induction. Two weeks later, half of these mice were bled from the retro-orbital vein under diethyl ether anesthesia, and their sera were obtained for the detection of IL-12 and IFN- γ . The other half were intravenously injected with 30 μ g of lipopolysaccharide (LPS) and sera were obtained 3 h later for the detection of TNF- α . ELISA kits for mouse IL-12(p40), IFN- γ , and TNF- α were all purchased from BioSource International (Camarillo, CA), and assays were carried out according to the manufacturer's instructions.

aGVHD-type mixed lymphocyte reaction

Single cell suspensions of B6 and BDF1 spleen were prepared as described above. BDF1 spleen cells were growth-arrested by treating with mitomycin C (Sigma) prior to incubation. Suspended in 180 μ L of complete RPMI-1640 medium were 2×10^5 of B6 and 1×10^5 of mitomycin C-treated BDF1 spleen cells, which were then incubated at 37°C, 5% CO₂ for 5 days. Drugs were dissolved and diluted at appropriate concentrations in complete RPMI-1640 containing 0.1% DMSO and added to the culture in a volume of 20 μ L at the beginning of the culture. After incubation, each well was pulsed with 0.5 μ Ci of ³H-thymidine and further incubated for 16 h. Radioactivity incorporated in each well was determined with a beta-plate counter (Pharmacia, Uppsala, Sweden). Results are expressed as the mean cpm for triplicate cultures.

Statistics

In a lethal aGVHD model, the difference between the control and drug-treatment group in days of survival was analyzed with a Log-rank test. In cytokine

production assays, the difference between vehicle- and drug-treated groups was analyzed with a Mann-Whitney test. In cGVHD, the difference between dosage groups in serum anti-ssDNA titer was analyzed with one-way ANOVA followed by a Dunnett-type multiple comparison. A probability value of 5% (two-sided) was considered statistically significant. All statistical analyses were conducted using the SAS6.12 software package (SAS Institute Japan, Tokyo, Japan).

Results

Effect of ER-38925 on survival in the aGVHD model

Vehicle-treated BDF1 mice that were lethally irradiated and infused with bone marrow and spleen cells of B6 mice developed lethal aGVHD and began to die as of 12 days after the cell transfer. In this group, all mice were dead by day 22 after the cell transfer. Mice treated with ER-38925 at 1, 3, and 10 mg/kg had a significantly prolonged lifespan compared with the vehicle control ($p < 0.05$ by Log-rank test, Figure 2). During 4-week treatment, no mice in ER-38925 groups, except for one at 1 mg/kg, died from aGVHD. After the termination of the treatment, however, mice in those groups eventually died from aGVHD and no animal survived longer than 70 days post-disease induction. Reproducibility of the improvement in this parameter as a result of ER-38925 at 1 mg/kg was observed in an additional experiment (data not shown). In addition, ER-38925 at 0.3 mg/kg also significantly improved the survival of aGVHD mice in a separate experiment ($p < 0.05$ by Log-rank test, data not shown). ER-38925 at 1 mg/kg, p.o. again prolonged the survival of aGVHD mice almost as potently as CyA at 30 mg/kg, s.c., and both drugs had a

statistically significant effect ($p < 0.05$ by Log-rank test, Figure 3).

Effect of ER-38925 on cytotoxic T lymphocyte (CTL) induction in aGVHD mice

aGVHD is associated with the marked induction of anti-allogeneic donor CTL, and such CTLs are thought to play a crucial role in the induction of various disorders in aGVHD. The effect of ER-38925 on the lethality of aGVHD may result from the inhibition of CTL in this model. To assess this possibility, CTL activity was compared in control and drug-treated aGVHD mice. aGVHD was induced by injection of B6 spleen cells into non-irradiated BDF1 recipients. As shown in Figure 4a, on 12 day following the transfer of donor cells, a vigorous anti-allogeneic (anti-H-2^d) CTL response was detected. Treatment of mice with ER-38925 at 0.1 and 0.3 mg/kg from the day of transfer prevented the induction of this CTL response. ER-38925 suppressed the response by about 50% and 80% at 0.1 and 0.3 mg/kg, respectively. This inhibitory effect of ER-38925 at 0.3 mg/kg was fully consistent with its improvement of the survival of aGVHD mice, as mentioned before. Administration of CyA also prevented CTL induction in aGVHD models, and the inhibition of CyA at 10 mg/kg was almost comparable to that of 0.1 mg/kg of ER-38925 (Figure 4a, b). All-trans retinoic acid (ATRA) inhibited CTL response at 10 and 30 mg/kg (Figure 4b). Moreover, oral administration of another RAR- α selective retinoid, Am80, at 1 mg/kg also prevented CTL generation (Figure 4c). Hence, the inhibition of anti-allogeneic CTL induction in the aGVHD model seems to be a common feature for various types of retinoids.

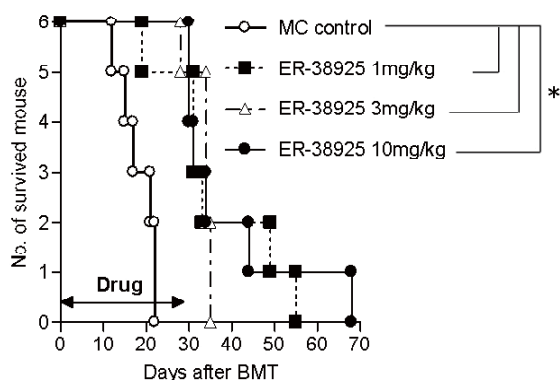


Figure 2. Effect of ER-38925 on the survival of aGVHD mice. Lethal aGVHD was developed in lethally irradiated female BDF1 mice by transferring bone marrow and spleen cells of B6 mice. Mice were administered either vehicle (0.5% MC) or ER-38925 (1, 3 or 10 mg/kg) for 4 weeks from the day of disease induction. Each group consisted of 6 animals at the beginning of the study. Respective lines indicate survival for each treatment group. ER-38925 prolonged the lifespan of aGVHD mice starting at 1 mg/kg. A statistically significant difference was found between the control and each ER-38925 treatment group. * $p < 0.05$ by Log-rank test.

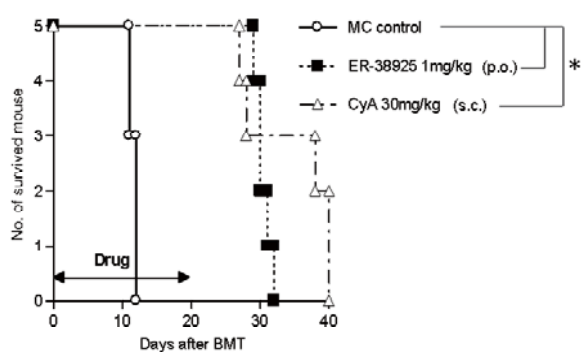


Figure 3. Effect of ER-38925 and CyA on the survival of aGVHD mice. aGVHD were induced in female BDF1 mice as described in Figure 2, and those mice were divided into 3 groups and administered vehicle (0.5% MC), ER-38925 (1mg/kg, p.o.), or CyA (30 mg/kg, s.c.) respectively, for 20 days from the day of disease induction. Each group consisted of 5 animals at the beginning of the study. Respective lines indicate survival for each treatment group. Both ER-28925 and CyA significantly improved survival at the dose tested. * $p < 0.05$ by Log-rank test.

Effect of ER-38925 on alloantigen-induced proliferation of donor spleen cells

In aGVHD, parental T lymphocytes recognize and respond to disparate MHC alleles resulting in a massive proliferative response and cytokine secretion. To ascertain the mechanisms by which retinoids inhibit CTL induction in the aGVHD model, the effect of compounds on the anti-allogeneic proliferation of donor

spleen cells was studied. As shown in Figure 5, B6 donor spleen cells profoundly proliferated *in vitro* in the presence of host (BDF1) spleen cells (open circles in Figure 5a, b). ATRA and ER-38925 inhibited this response in a concentration-dependent manner, and their IC₅₀ values in this assay were 0.62 and 1.64 nM, respectively (Figure 5a). The next assay investigated whether inhibition of these retinoids is mediated via RAR- α or not. ER-50891 is a retinoid synthesized in this laboratory and is defined as an RAR- α specific

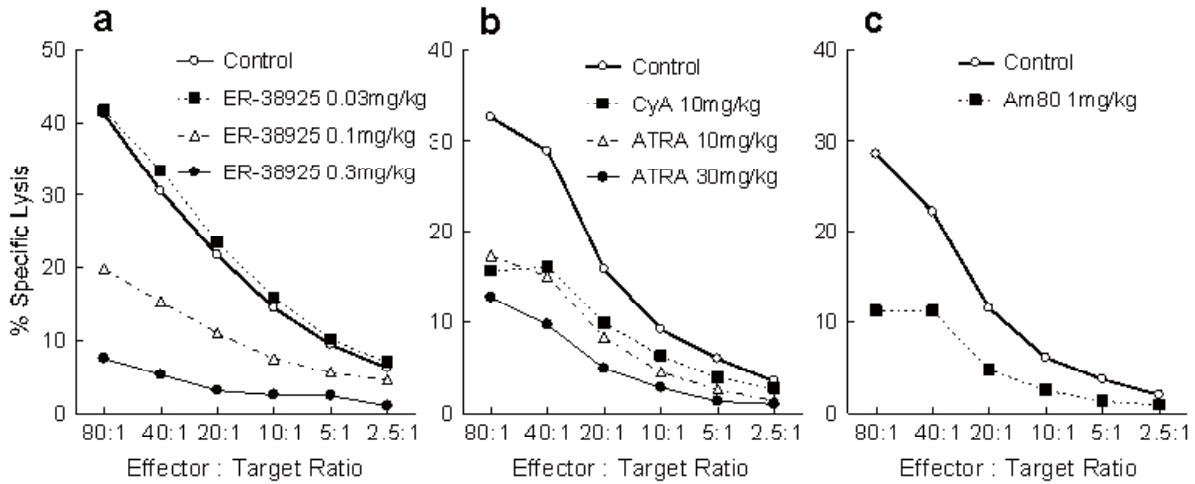


Figure 4. Effect of ER-38925, ATRA and CyA on the CTL induction in aGVHD mice. Anti-alloantigen (H-2^d) specific CTL was induced in female BDF1 mice by transferring spleen cells of B6 mice. Mice were divided into groups consisting of 5 animals and administered with drugs at various doses from the day of cell transfer, as indicated in Figure 4a, 4b, and 4c. Control mice received the vehicle only (0.5% MC). Twelve days after the cell transfer, anti-allogeneic CTL activity was determined by measuring the cytotoxicity against P815 target cells (H-2^d). Each point represents the mean CTL activity of 5 animals. **a.** ER-38925 inhibited the response starting at 0.1 mg/kg. **b.** CyA and ATRA inhibited the response at 10 mg/kg and 10 mg/kg, respectively. **c.** Am80 inhibited the response at 1 mg/kg.

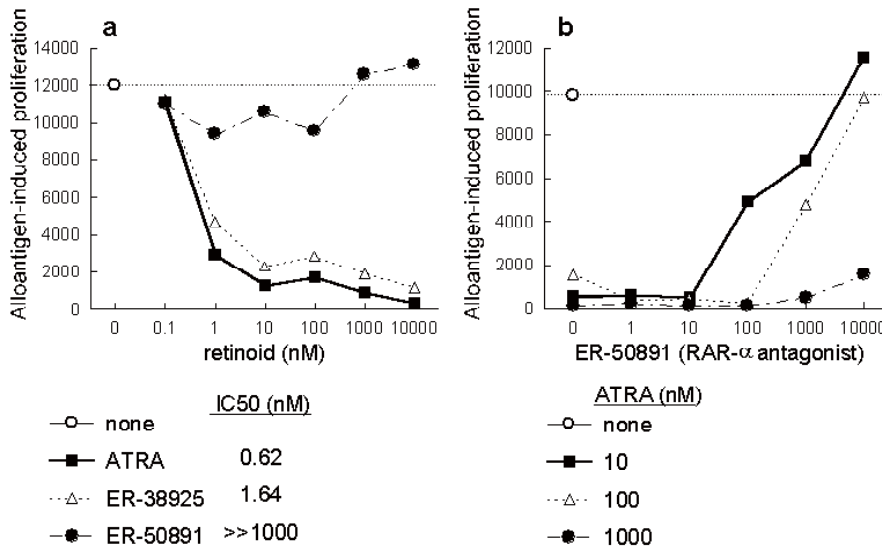


Figure 5. *In vitro* effect of retinoids on alloantigen induced proliferation of donor spleen cells. Anti-alloantigenic (anti-H-2^d) proliferation of donor spleen cells was induced by coculturing B6 spleen cells (2×10^5) and mitomycin C-treated BDF1 spleen cells (1×10^5). Each compound was added at the beginning of the culture. Five days later, each culture was pulsed with 0.5 mCi of ³H-thymidine for the final 16 h. Each point represents the mean of radioactivity incorporated into triplicate cultures. **a.** ATRA and ER-38925 inhibited the response in a concentration-dependent manner, while ER-50891, an RAR- α selective antagonist, did not, up to the highest concentration tested. **b.** ATRA inhibited the response almost completely starting at 10 nM. Inhibition of the response by ATRA at 10 and 100 nM was completely reversed by ER-50891 at 10,000 nM.

antagonist, as reported previously (13). This compound did not alter the response up to 10,000 nM (Figure 5a). The inhibition of ATRA at either 10 or 100 nM was reversed by ER-50891 in a concentration-dependent manner and completely recovered in the presence of 10,000 nM of ER-50891 (Figure 5b). Hence, the RAR- α receptor seems to play a crucial role in the suppression of alloantigen-induced proliferation of donor lymphocytes by retinoids in the aGVHD model.

Effect of ER-38925 on cytokine production in aGVHD hosts

A well-known fact is that various kinds of cytokines are produced in aGVHD hosts and work as disease-exacerbating factors in both human GVHD patients

and murine GVHD models. In particular, cytokines produced by type 1 T-helper cells (Th1), *i.e.* IL-12, IFN- γ , and TNF- α are known to play a crucial role in the development of aGVHD and are regarded as promising targets for disease intervention (14-17). As shown in Figure 6, as of 14 days after disease induction BDF1 mice with aGVHD had elevated serum IL-12 (p40) and IFN- γ when compared with intact controls that received spleen cells from a syngeneic strain (BDF1). The elevation of IL-12 in aGVHD mice was statistically significant. aGVHD control mice had much higher serum IFN- γ than intact controls, although this difference was not statistically significant due to a large data variation among the control animals. Compared to the aGVHD control, ER-38925 decreased serum IL-12 by about 30%, and the decrease was statistically

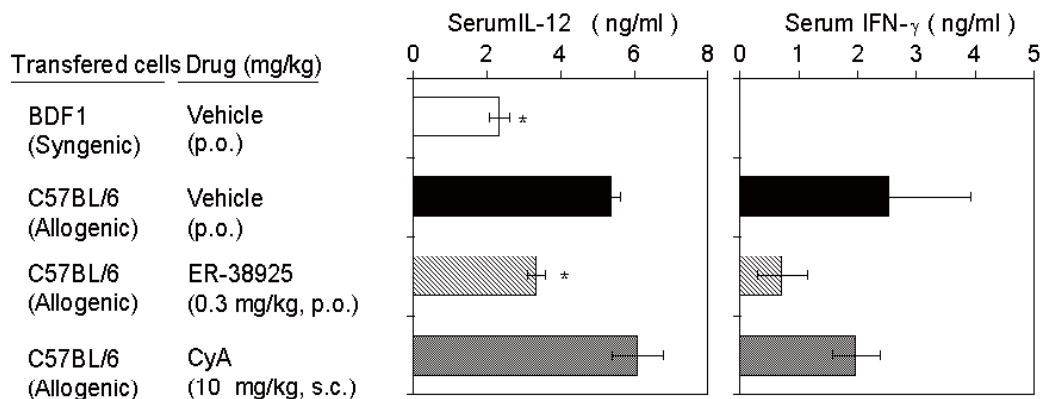


Figure 6. Effect of retinoids on cytokine production in aGVHD mice. Sera were collected from BDF1 mice with aGVHD at day 14 post-disease induction. Serum IL-12 (p40) and IFN- γ content was determined by ELISA as described in the Methods section. Each mouse was administered either ER-38925, CyA, or the vehicle once daily from the day of cell transfer. The dose and route of administration for each drug are indicated in the figure. BDF1 mice transferred with spleen cells from the syngeneic strain served as an intact control (open column). Each column represents the mean \pm S.E.M. of 5 animals. A significant difference from the aGVHD control as indicated by a Mann-Whitney test is shown in the figure, * $p < 0.05$. ER-38925 inhibited the elevation of serum IL-12 and IFN- γ in the aGVHD model while CyA did not.

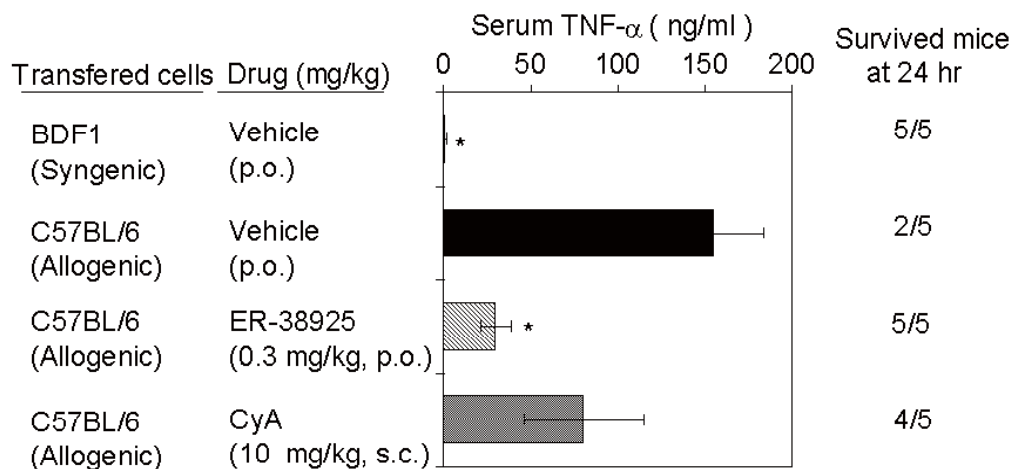


Figure 7. Effect of retinoids on TNF- α production in aGVHD mice. BDF1 mice with aGVHD were intravenously challenged with LPS (30 μ g/mouse) at day 14 post-disease induction. Three hours later, serum was collected from each mouse, and its TNF- α content was determined by ELISA. The number of mice alive at 24 h post-LPS injection is indicated on the right of each column. Mice were treated with drugs or the vehicle in the same manner as described in Figure 6. Each column represents the mean \pm S.E.M. of 5 animals. A significant difference from the aGVHD control as indicated by a Mann-Whitney test is shown in the figure, * $p < 0.05$. ER-38925 significantly inhibited LPS-induced serum TNF- α elevation and improved the survival after LPS challenge in the aGVHD model. These effects were more significant than those of CyA at 10 mg/kg.

significant ($p < 0.05$ by Mann-Whitney test, Figure 6). It also reduced serum IFN- γ in aGVHD mice by about 60%, but this effect was not statistically significant, again due to a large data variation among aGVHD controls. In contrast to ER-38925, CyA had no effect on serum IL-12 content, and it decreased serum IFN- γ only moderately, with no statistical significance to the decrease. In addition to the above Th1-type cytokines, aGVHD mice are known to produce TNF- α when challenged with microorganic components like lipopolysaccharide (LPS). This phenomenon may be mediated by activated monocytes or macrophages primed by IFN- γ and represent the accelerated vulnerability to septic shock after systemic infection in GVHD patients (18). The current aGVHD mice also produced a large amount of TNF- α in sera after challenge with LPS, and 3 out of 5 animals died from septic shock within 24 h, although neither response was observed in intact controls used in the same assay (Figure 7). Mice treated with ER-38925 at 0.3 mg/kg produced less TNF- α in sera, and this effect was statistically significant ($p < 0.05$ by Mann-Whitney test, Figure 7). Additionally, none of these mice died after the LPS challenge. The effect of ER-38925 on these parameters was more prominent than CyA at 10 mg/kg.

Effect of ER-38925 on cGVHD

cGVHD is characterized by a systemic autoimmune disease that primarily affects the skin and results in the

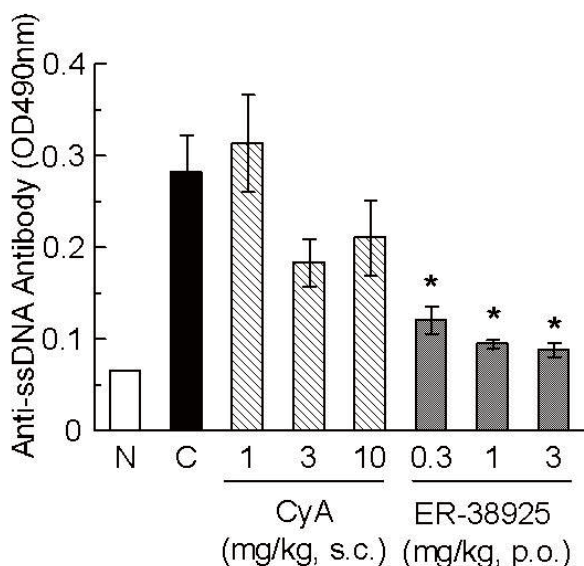


Figure 8. Effect of ER-38925 and CyA on autoantibody induction in a cGVHD model. cGVHD was developed in female BDF1 mice by transferring spleen cells of DBA2. After the cell transfer, those mice were divided into groups each consisting of 5 animals and administered the vehicle (0.5% MC, p.o.), ER-38925 (0.3, 1 or 3 mg/kg, p.o.) or CyA (1, 3 or 10 mg/kg, s.c.) from the day of cell transfer. Intact control mice were left untreated throughout the study period. Two weeks later, mice were bled and serum anti-ssDNA titer was determined by specific ELISA as described in the Methods section. A significant difference between the control and drug treatment group was noted in One-way ANOVA, * $p < 0.05$. ER-38925 inhibited the elevation of serum anti-ssDNA titer in a dose-dependent manner in the cGVHD model while CyA did not.

polyclonal activation of B cells and hyperproduction of Ig, including IgE and anti-DNA autoantibodies (1,19). To investigate the effect of ER-38925 on cGVHD, parental DBA/2 spleen cells were transferred to BDF1 hybrids. In vehicle-treated cGVHD hosts, the serum anti-ssDNA autoantibody titer was substantially elevated. ER-38925 significantly inhibited the elevation of anti-ssDNA starting at a dose of 0.3 mg/kg ($p < 0.05$ by One-way ANOVA, Figure 8). The effect of ER-38925 was much more marked than that of CyA since the latter did not significantly inhibit this parameter even at 10 mg/kg.

Discussion

The present study clearly shows that retinoids, and especially RAR- α selective retinoids, can inhibit mouse GVHD responses both *in vitro* and *in vivo*. ER-38925 significantly prolonged the lifespan of aGVHD hosts starting at 1 mg/kg (Figure 2), and this effect was almost comparable to 30 mg/kg of CyA (Figure 3). Moreover, it potently inhibited anti-ssDNA autoantibody production in the cGVHD model (Figure 8). To the extent known, this report is the first to clearly indicate the remediating effect of a retinoid on various GVHD-related disorders.

The authors' RAR- α selective retinoid effectively inhibited anti-allogeneic CTL induction in aGVHD hosts starting at 0.1 mg/kg (Figure 4). Since ATRA and Am80 also inhibited this response, this effect seems to be common among various types of retinoids. Retinoid-induced inhibition of CTL induction in aGVHD hosts seems to be mediated, at least partly, through the massive inhibition of donor cell proliferation since ER-38925 and ATRA inhibited the alloantigen-induced *in vitro* proliferation of B6 donor spleen cells in a concentration-dependent manner (Figure 5a). Moreover, inhibition of this response by ATRA was totally reversed by an excessive amount of an RAR- α selective antagonist, ER-50891 (Figure 5b). Therefore, RAR- α seems to play a pivotal role in the anti-proliferative effect of retinoids on alloantigen-stimulated murine lymphocytes, and may also play a role in the inhibition of CTL induction by retinoids.

IFN- γ , a representative Th1 cytokine, is critical to promoting CTL induction in murine GVHD models (20). Hayes and his colleagues observed increased IFN- γ and decreased IL-4 and IL-5 secretion in vitamin A-deficient mice, and such an imbalance was reversed by the administration of retinoic acid (21-23). They also reported that retinoic acid inhibits IFN- γ production by a Th1 cell line via a CD28 co-stimulatory signal blockade (24). Retinoid-mediated suppression of human (25) and murine (26) IFN- γ production is exerted at the transcriptional level. Consistent with these reports, ER-38925 reduced the serum IFN- γ level that was upregulated in the aGVHD model (Figure 6).

In addition, retinoids have recently been reported to inhibit IL-12 production by activated macrophages through functional interactions between their receptors (RXR and RAR) and NF- κ B, a crucial transcription factor for IL-12 gene expression (27). Fully consistent with this report, elevation of serum IL-12 was markedly suppressed in ER-38925-treated aGVHD mice (Figure 6). The inhibitory effect of ER-38925 on serum IL-12 and IFN- γ upregulation was observed at 0.3 mg/kg, the dose also effective in inhibiting CTL induction. Taken together, these findings indicate that the current retinoid must have inhibited Th1 differentiation in the aGVHD models and thereby reduced the secretion of Th1 cytokines like IL-12 and IFN- γ . These effects must have contributed to its potent suppression of CTL induction (Figure 4) since both cytokines have been reported to be critical to allo-specific CTL induction (20,28,29).

TNF- α is the other disease-exacerbating factor of GVHD in humans and rodents (17,18), and its serum level is known to correlate well with the severity of human GVHD (30,31). LPS is a component of endogenous bowel flora and a potent inducer of pro-inflammatory cytokine release from monocytes or macrophages. Translocation of LPS across damaged gut mucosa to systemic circulation is believed to take place during both experimental and clinical GVHD, and the serum level of LPS was elevated in BMT patients with GVHD (32). Once translocated into systemic circulation, LPS triggers monocytes or macrophages that have been primed by IFN- γ produced by activated T cells to produce a cytopathic amount of inflammatory cytokines like TNF- α or IL-1 (33). Together with activated T cells, those cytokines cause organ damage in GVHD hosts (34). This pathway must also be crucial in human GVHD, since the severity of GVHD is effectively reduced by germ-free conditions or antibiotic therapy in BMT recipients (35). In this study, ER-38925 reduced the production of TNF- α in LPS-injected aGVHD hosts and thereby improved their survival (Figure 7). This result suggests that ER-38925 inhibited the production of IFN- γ by activated donor T cells and thereby prevented the activation of monocytes or macrophages in aGVHD hosts (see Figure 6). This effect, together with ER-38925's potent inhibition of CTL activity, must largely contribute to its disease remediation in the aGVHD model.

In addition to aGVHD, ER-38925 intensely inhibited autoantibody production in cGVHD mice. Its effect excelled over that of CyA. The mechanism(s) by which ER-38925 suppress autoimmune disease in cGVHD remains to be elucidated. Nevertheless, anti-DNA production is also reported to be abrogated in IFN- γ R knock-out (NZB \times NZW)F1 mice, which are known to be a model of human SLE (36). Hence, ER-38925 may inhibit anti-ssDNA production via massive inhibition of IFN- γ production in cGVHD. This possibility warrants future study.

While the immunosuppressive mechanism of RAR- α selective retinoids is not precisely understood at the cellular level, recent studies indicate that retinoids induce the CD4⁺CD25⁺ regulatory T cell (Treg) subset (37,38) in mice in an RAR- α -dependent manner (39,40). Research has also suggested that Treg plays an important role in determining the prognosis of patients who receive a haematopoietic cell transplant. Namely, Treg decreases the incidence and severity of mouse GVHD (41,42) and promotes donor bone marrow engraftment by protecting these cells from host rejection (43) in mouse models. These findings suggest that ER-38925 suppressed GVHDs by inducing Treg cells in the semiallogeneic GVHD models used in this study. This possibility remains to be elucidated in future studies.

The present results suggest that retinoids, and especially RAR- α selective retinoids including ER-38925, may serve as a new remedy for preventing and/or treating GVHD in human BMT patients.

References

1. Durie HF, Aruffo A, Ledbetter J, Crassi, MK, Green WR, Fast DL, Noelle JR. Antibody to the ligand of CD40, gp39, blocks the occurrence of the acute and chronic forms of graft-*vs*-host disease. *J Clin Invest* 1994; 94:1333-1338.
2. Morris SC, Cheek RL, Cohen PL, Eisenberg RA. Autoantibodies in chronic graft versus host result in cognate T-B interactions. *J Exp Med* 1983; 171:503-517.
3. Hong WK, Itri LM. Retinoids and human cancer. In: THE RETINOIDS: Biology, Chemistry and Medicine (Sporn MB, Roberts AB, Goodman DS, eds.). Raven Press, Ltd., New York, NY, USA, 1994; pp. 597-630.
4. Mangelsdorf DJ, Evans RM. The RXR heterodimers and orphan receptors. *Cell* 1995; 83:841-850.
5. Altucci L, Leibowitz MD, Ogilvie KM, de Lera AR, Gronemeyer H. RAR and RXR modulation in cancer and metabolic disease. *Nat Rev Drug Discov* 2007; 6:703-810.
6. Brinckerhoff CE, Coffy JW, Sullivan AC. Inflammation and collagenase production in rats with adjuvant arthritis reduced with 13-*cis*-retinoic acid. *Science* 1983; 221:756-758.
7. Racke MK, Burnett D, Pak SH, Albert PS, Cannella B, Raine CS, McFarlin DE, Scott DE. Retinoid treatment of experimental allergic encephalomyelitis. IL-4 production correlates with improved disease course. *J Immunol* 1995; 154:450-458.
8. Kuwabara K, Shudo K, Hori Y. Novel synthetic retinoic acid inhibits rat collagen arthritis and differentially affects serum immunoglobulin subclass levels. *FEBS Lett* 1996; 378:153-156.
9. Wang T, Niwa S, Bouda K, Matsuura S, Homma T, Shudo K, Nagai H. The effect of Am-80, one of retinoids derivatives on experimental allergic encephalomyelitis in rats. *Life Sci* 2000; 67:1869-1879.
10. Yoshimura H, Kikuchi K, Hibi S, Tagami K, Satoh T, Yamauchi T, Ishibashi A, Tai K, Hida T, Tokuhara N, Nagai M. Discovery of novel and potent retinoic acid

- receptor alpha agonists: Syntheses and evaluation of benzofuranyl-pyrrole and benzothiophenyl-pyrrole derivatives. *J Med Chem* 2000; 43:2929-2937.
11. Seino K, Yamauchi T, Shikata K, Kobayashi S, Nagai M, Taniguchi M, Fukao K. Prevention of acute and chronic allograft rejection by a novel retinoic acid receptor-alpha-selective agonist. *Int Immunol* 2004; 16:665-673.
 12. Yamauchi T, Ishibashi A, Shikata K, Tokuhara N, Seino K, Kobayashi S, Nagai M. Effect of E6060 [4-{5-[7-fluoro-4-(trifluoromethyl)benzo[*b*]furan-2-yl]-1*H*-2-pyrrolyl}benzoic acid], a novel subtype-selective retinoid, on lupus-like nephritis in female (NZBxNZW)F1 mice. *J Pharmacol Exp Ther* 2005; 312:938-944.
 13. Kikuchi K, Tagami K, Hibi S, Yoshimura H, Tokuhara N, Tai K, Hida T, Yamauchi T, Nagai M. Synthesis and evaluation of quinoline derivatives as novel retinoic acid receptor α antagonists. *Bioorg Med Chem Lett* 2001; 11:1215-1218.
 14. Williamson E, Garside P, Bradley A, Mowat AM. IL-12 is a central mediator of acute graft-versus-host disease in mice. *J Immunol* 1996; 157:689-699.
 15. Mowat AM. Antibodies to IFN- γ prevent immunologically mediated intestinal damage in murine graft-versus-host reaction. *Immunology* 1989; 68:18-23.
 16. Huchet R, Bruley-Rosset M, Mathiot C, Grandjon D, Halle-Pannenko O. Involvement of INF- γ and transforming growth factor- β in graft-versus-host reaction associated immunosuppression. *J Immunol* 1993; 157:2517-2524.
 17. Cooke KR, Hill GR, Crawford JM, Bungard D, Brinson YS, Delmonte J Jr, Ferrara JLM. Tumor necrosis factor- α production to lipopolysaccharide stimulation by donor cell predicts the severity of experimental acute graft-versus-host disease. *J Clin Invest* 1998; 10:1882-1891.
 18. Nestel FP, Price KS, Seemayer TA, Lapp WS. Macrophage priming and lipopolysaccharide-triggered release of tumor necrosis factor- α during graft-versus-host disease. *J Exp Med* 1995; 175:405-413.
 19. Dautreleont JM, Moser M, Leo O, Abramowicz D, Vanderhaegen ML, Urbain J, Goldman M. Hyper IgE in stimulatory graft-versus-host disease: role of interleukin-4. *Clin Exp Immunol* 1991; 83:133-136.
 20. Puliaev R, Nguyen P, Finkelman FD, Via CS. Differential requirement for IFN-gamma in CTL maturation in acute murine graft-versus-host disease. *J Immunol* 2004; 173:910-919.
 21. Carman JA, Hayes CE. Abnormal regulation of INF- γ secretion in vitamin A deficiency. *J Immunol* 1991; 147:1247-1252.
 22. Cantorna MT, Nashold FE, Hayes CE. In Vitamin A deficiency multiple mechanisms establish a regulatory helper T cell imbalance with excess Th1 and insufficient Th2 function. *J Immunol* 1994; 152:1515-1522.
 23. Cantorna MT, Nashold FE, Hayes CE. Vitamin A deficiency results in a priming environment conducive for Th1 cell development. *Eur J Immunol* 1995; 25:1673-1679.
 24. Cantorna MT, Nashold FE, Chun TE, Hayes CE. Vitamin A down-regulation of IFN- γ synthesis in cloned mouse Th1 lymphocytes depends on the CD28 costimulatory pathway. *J Immunol* 1996; 156:2676-2679.
 25. Cippitelli M, Ye J, Viggiano V, Sica A, Ghosh P, Gulino A, Santoni A, Young HA. Retinoic acid-induced transcriptional modulation of the human interferon- γ promoter. *J Biol Chem* 1996; 271:26783-26793.
 26. Felli MP, Vacca A, Meco D, Screpanti I, Farina AR, Maroder M, Martinotti S, Petrangeli E, Frati L, Gulino A. Retinoic acid-induced down regulation of the interleukin-2 promoter via cis-regulatory sequences containing an octamer motif. *Mol Cell Biol* 1991; 11:4771-4778.
 27. Na SY, Kang BY, Chung SW, Han SJ, Ma X, Trinchieri G, Im SY, Lee JW, Kim TS. Retinoids inhibit interleukin-12 production in macrophages through physical associations of retinoid X receptor and NFkappaB. *J Biol Chem* 1999; 274:7674-7680.
 28. Piccotti JR, Li K, Chan SY, Eichwald EJ, Bishop DK. Interleukin-12 (IL-12)-driven alloimmune responses *in vitro* and *in vivo*. Requirement for B1 subunit of the IL-12 receptor. *Transplantation* 1999; 67:1453-1460.
 29. Diamond AS, Gill RG. An essential contribution by IFN-gamma to CD8⁺ T cell-mediated rejection of pancreatic islet allografts. *J Immunol* 2000; 165:247-255.
 30. Holler E, Kolb HJ, Möller A, Kempeni J, Liesenfeld S, Pechumer H, Lehmacher W, Ruckdeschel G, Gleixner B, Riedner C. Increased serum levels of tumor necrosis factor alpha precede major complications of bone marrow transplantation. *Blood* 1990; 75:1011-1016.
 31. Symington FW, Pepe MS, Chen AB, Deliganis A. Serum tumor necrosis factor alpha associated with acute graft-versus-host disease in humans. *Transplantation* 1990; 50:518-521.
 32. Cooke KR, Gerbitz A, Crawford JM, Teshima T, Hill GR, Tesolin A, Rossignol DP, Ferrara JL. LPS antagonism reduces graft-versus-host disease and preserves graft-versus-leukemia activity after experimental bone marrow transplantation. *J Clin Invest* 2001; 107:1581-1589.
 33. Nestel FP, Price KS, Seemayer TA, Lapp WS. Macrophage priming and lipopolysaccharide-triggered release of tumor necrosis factor alpha during graft-versus-host disease. *J Exp Med* 1992; 175:405-413.
 34. Piguet PF, Grau GE, Allet B, Vassali P. Tumor necrosis factor/cachectin in an effector of skin and gut lesions of acute phase of graft-versus-host disease. *J Exp Med* 1987; 166:1280-1289.
 35. Storb R, Prentice RL, Buckner CD, Clift RA, Appelbaum F, Deeg J, Doney K, Hansen JA, Mason M, Sanders JE, Singer J, Sullivan KM, Witherspoon RP, Thomas ED. Graft-versus-host disease and survival in patients with aplastic anaemia treated by marrow grafts from HLA-identical siblings. Beneficial effect of a protective environment. *N Eng J Med* 1983; 308:302-307.
 36. Haas C, Ryffel B, Le Hir M. IFN-gamma receptor deletion prevents autoantibody production and glomerulonephritis in lupus-prone (NZB x NZW)F1 mice. *J Immunol* 1998; 160:3713-3718.
 37. Mucida D, Park Y, Kim G, Turovskaya O, Scott I, Kronenberg M, Cheroutre H. Reciprocal TH17 and regulatory T cell differentiation mediated by retinoic acid. *Science* 2007; 317:256-260.
 38. Benson MJ, Pino-Lagos K, Roseblatt M, Noelle RJ. All-trans retinoic acid mediates enhanced T reg cell growth, differentiation, and gut homing in the face of high levels of co-stimulation. *J Exp Med* 2007; 204:1765-1774.
 39. Kang SG, Lim HW, Andrisani OM, Broxmeyer HE, Kim CH. Vitamin A metabolites induce gut-homing FoxP3⁺ regulatory T cells. *J Immunol* 2007; 179:3724-3733.
 40. Schambach F, Schupp M, Lazar MA, Reiner SL.

- Activation of retinoic acid receptor-alpha favors regulatory T cell induction at the expense of IL-17-secreting T helper cell differentiation. *Eur J Immunol* 2007; 37:2396-2399.
41. Taylor PA, Noelle RJ, Blazar BR. CD4(+)CD25(+) immune regulatory cells are required for induction of tolerance to alloantigen via costimulatory blockade. *J Exp Med* 2001; 193:1311-1318.
42. Cohen JL, Trenado A, Vasey D, Klatzmann D, Salomon BL. CD4(+)CD25(+) immunoregulatory T Cells: new therapeutics for graft-versus-host disease. *J Exp Med* 2002; 196:401-406.
43. Hanash AM, Levy RB. Donor CD4⁺CD25⁺ T cells promote engraftment and tolerance following MHC-mismatched hematopoietic cell transplantation. *Blood* 2005; 105:1828-1836.

(Received December 27, 2007; Revised January 21, 2008; Accepted January 24, 2008)

Original Article**A new method of preparing TRH derivative-loaded poly(dl-lactide-co-glycolide) microspheres based on a solid solution system**

Akihiro Matsumoto*, Yasuhisa Matsukawa, Yukiko Nishioka, Masanobu Harada, Yuji Horikiri, Hiroshi Yamahara

Tanabe Seiyaku Co., Ltd., Osaka, Japan.

ABSTRACT: We investigated a new method of preparing peptide-loaded poly(dl-lactide-co-glycolide) microspheres with high encapsulation efficiency, low initial burst, and long-term sustained release by dissolving a peptide in a polymer by applying a solid solution system to the preparation of an oil phase. Solid solutions were prepared by dissolving a polymer (poly(dl-lactide-co-glycolide)) and a peptide (TRH derivative) in mixed solvents and then evaporating the solvents. Microspheres were prepared by an O/W emulsion solvent evaporation method, using the solution of the solid solution in dichloromethane as an oil phase. The state of the peptide in the solid solution and in the microspheres was evaluated by X-ray diffraction analysis. Release of the peptide from the microspheres was evaluated by an *in vitro* drug release test. Observation of the oil phase, X-ray diffraction analysis, and DSC analysis revealed that the peptides were dispersed in a molecular state in the solid solution and in microspheres with peptide loading of up to 15%. Encapsulation efficiency was over 90% for microspheres with peptide loading of up to 15%. The release of the peptide from the microspheres lasted over 21 days at least with the limited initial burst *in vitro*. High encapsulation efficiency, low initial burst, and long-term sustained release can be accomplished with microspheres prepared by a method based on a solid solution system.

Keywords: Microspheres, Peptide, Poly(dl-lactide-co-glycolide), Solid solution, Controlled release

Introduction

The technologies of long-term sustained release systems are useful in maximizing the efficacy of peptides,

*Correspondence to: Dr. Akihiro Matsumoto, Tanabe Seiyaku Co., Ltd., 2-10, Dosho-machi 3-Chome, Chuo-ku, Osaka 541-8505, Japan;
e-mail: pinebook@tanabe.co.jp

which have very short biological half-lives. Among the long-term sustained release systems, implantable microspheres made from biodegradable polymers such as polylactide and poly(lactide-co-glycolide) have been investigated by many researchers because of the ease of administration and their complete disappearance in the body. Although the polymers are insoluble in water, the polymers gradually degrade and erode in the body, releasing the microencapsulated drug.

Common techniques of microencapsulation are a phase separation method (1,2), a solvent evaporation method (3,4), and a spray-drying method (5,6). For phase separation, a poor solvent for polymers is added into the polymeric solution containing drug particles (oil phase); consequently, microspheres are prepared by precipitating polymers around the drug particles. For solvent evaporation, a polymeric solution containing drug particles (oil phase) is emulsified into another liquid (*e.g.* water, oil); the microspheres are prepared by evaporating the solvent from the oil phase. For spray-drying, the polymeric solution containing drug particles (oil phase) is sprayed through a nozzle; the microspheres are prepared by drying the oil droplets in the air. Regardless of the technique chosen, preparation of the oil phase that serves as the polymeric solution containing the drug is crucial.

The preparation of an oil phase is one of the most important processes in the microencapsulation process. The state of a drug in an oil phase influences its state in microspheres. If fine particles are dispersed well in an oil phase, microspheres with a uniformly dispersed drug can be obtained. If large particles or aggregates are dispersed in an oil phase, microspheres with an ununiformly distributed drug may be obtained. The distribution of a drug in microspheres is responsible for the property of those microspheres. Microspheres with large particles or aggregates of a drug often have low encapsulation efficiency and a high initial burst (7,8).

For most peptide drugs, the preparation of an oil phase is complicated in terms of the insolubility in the solvents used for the oil phase. Two major methods were reported for the preparation of an oil phase

containing peptides; the peptide particles were dispersed in organic solvents (9,10) or a peptide aqueous solution was emulsified in organic solvents (11,12). Whichever method is chosen, the particles or droplets must be reduced in size in order to obtain microspheres with high encapsulation efficiency and a preferable release profile (13,14). There are, however, few methods of reducing the size of peptide particles, such as the crystallization method. Moreover, fine particles easily aggregate, which leads to an increase in apparent particle size. With a peptide aqueous solution, particle size can be reduced by higher-speed emulsification, but the resulting droplets readily join with one another, which leads to an increase in droplet size.

In the field of the drug dissolution and absorption, an approach involving a solid dispersion system has been investigated for several decades in order to reduce drug particle size. Solid dispersion refers to the dispersion of one or more active ingredients in an inert carrier or matrix in a solid state (15). A solid dispersion system can suppress the growth of crystals to provide fine particles. Specifically, dispersing a drug in a molecular state in a matrix refers to a "solid solution" (15). In other words, a solid solution is the state in which a drug is dissolved in a matrix. If a solid solution system can be used to prepare an oil phase, then peptides should be dispersed as extremely fine particles (a molecular state) in an oil phase because the viscosity of the polymer hampers aggregation.

This study sought to develop a new method of preparing peptide-loaded microspheres by focusing on the use of a solid solution system. This study sought to demonstrate that a method of preparation based on a solid solution system would be useful in preparing peptide-loaded microspheres with high encapsulation efficiency, low initial burst, and long-term sustained release of a drug. Taltirelin, a TRH derivative (Figure 1), was chosen as a model peptide. Poly(dl-lactide-co-glycolide) (PLGA) served as a biodegradable polymer.

Materials and Methods

Materials

Poly(dl-lactide-co-glycolide) (PLGA, MW20,000, lactide:glycolide = 1:1; Wako Pure Chemicals Industries Ltd., Japan) was used as a polymer. Poly(vinyl alcohol) (PVA, EG-40; Nihon Synthetic Chemical Industries Ltd., Japan) was used as an emulsifier. Taltirelin was synthesized at Tanabe Seiyaku Co. Ltd., Japan. All other materials or solvents were of reagent grade.

Selection of mixed solvents for preparation of solid solution

Taltirelin and polymer (total amount: 0.5 g or 1.0 g) were dissolved in 2-2.5 mL of the mixed solvents,

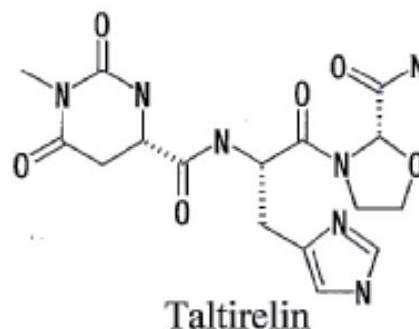


Figure 1. Structure of Taltirelin.

which consisted of a good solvent for the polymer and a good solvent for Taltirelin. The obtained solutions were evaporated under a nitrogen stream at 40°C and dried completely under vacuum overnight.

Preparation of microspheres

The procedure for preparation of microspheres is shown in Figure 2. Microspheres were basically prepared by an O/W emulsion solvent evaporation method. Briefly, the solid solution (0.5-1 g) [prepared from a mixture of the solvents dichloromethane and ethanol (4/1)] was dissolved in dichloromethane (1-2 g) to obtain an oil phase. The oil phase was emulsified into the PVA solution (150 mL or 400 mL) by a homogenizer (Polytron[®], Kinematica Ag Littau, Switzerland) for 3 min at 8,000 rpm at 15°C. Then, the temperature was gradually increased to 30°C with stirring to remove dichloromethane. The hardened microspheres were washed with deionized water and collected by centrifugation. The obtained microspheres were re-dispersed in deionized water and lyophilized.

X-ray diffraction analysis

The intensity of X-ray diffraction from the solid solution and the microspheres was measured as a function of diffraction angles by X-ray powder diffraction (MXP3VA, Mac Science Ltd.).

Measurement of glass transition (T_g) of microspheres

The T_g of microspheres was measured by Differential Scanning Calorimetry (DSC, Thermo Flex, Rigaku Corporation) with a temperature elevation rate of 10°C.

Microscopic observation

The cross section of microspheres was prepared by slicing microspheres with razor-edge manually. The microspheres and the cross section of the microspheres were coated with gold-palladium by sputtering at 15

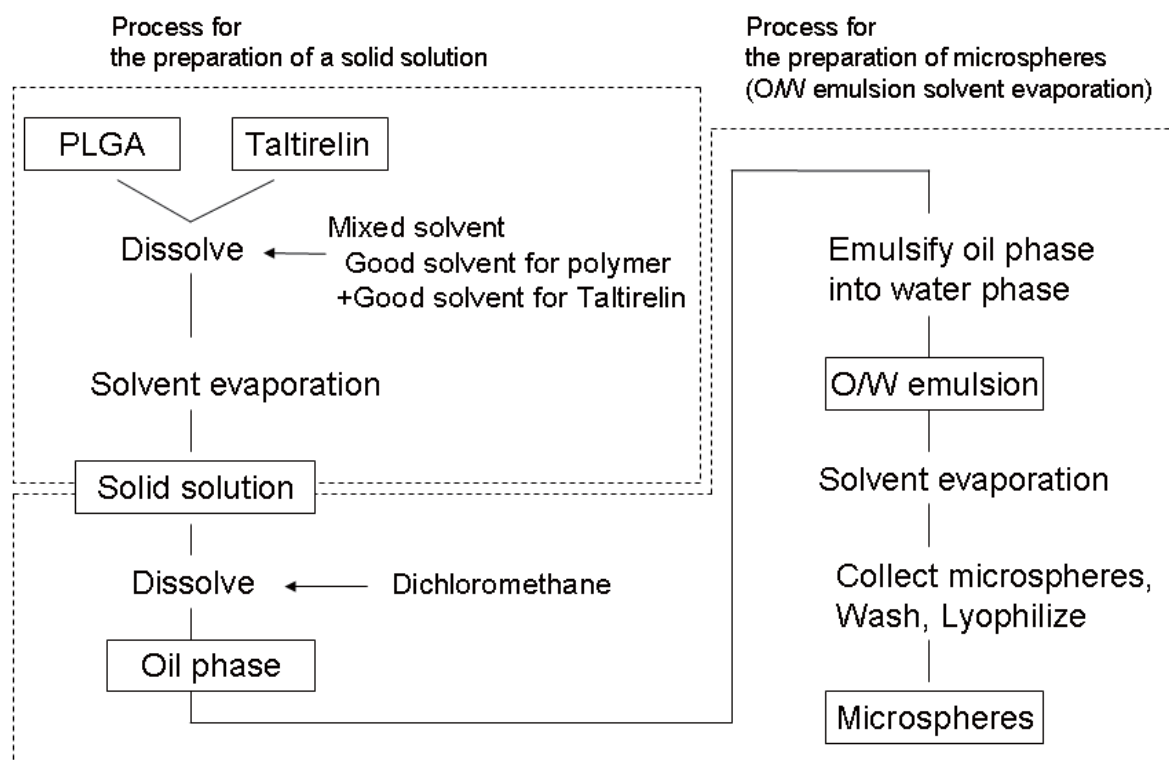


Figure 2. Procedure of the preparation for microspheres based on solid solution system.

mA for 3 min. The resulting samples were observed with a scanning electron microscope (S-2250N, Hitachi Ltd., Japan).

Determination of microsphere size

The size of microspheres was determined using a laser diffraction particle size analyzer (SALD-1100, Shimadzu Co. Ltd., Japan).

Determination of peptide contents in microspheres

The microspheres containing Taltirelin (10 mg) were dissolved in dichloromethane (2 mL) and extracted with phosphate buffer ($\mu = 0.15$, pH 7.4) (5 mL) for 30 min. The aqueous layer was assayed for the Taltirelin concentration by the HPLC method described in "Determination of peptides by the UV-HPLC method."

In vitro release study

Microspheres containing Taltirelin were weighed out in test tubes. The test tubes were filled with phosphate buffer ($\mu = 0.15$, pH 7.4) (10 mL) and then stirred at 25 rpm in an air chamber kept at $37 \pm 1^\circ\text{C}$. Each test tube was taken out at the predetermined interval. The buffer was removed and the residual Taltirelin in microspheres was determined by the method described in "Determination of peptide contents in microspheres."

Although the recovery of Taltirelin remained almost 100% during the release study, the release of Taltirelin in this study was calculated based on the difference between initial peptide content and residual peptide content.

Determination by the UV-HPLC method

Samples were analyzed with a 5C18 Nucleosil analytical column (4.6×150 mm, GL science). HPLC conditions for the determination of Taltirelin were as follows: flow rate, 1.0 mL/min; injection volume, 50 μL ; detection wavelength, 210 nm; column temperature, 40°C ; eluent, a mixture of acetonitril and 50 mM phosphate buffer (pH 2.5) (5:40) containing 0.13% sodium 1-octansulphonic acid.

Results

Preparation of solid solutions and oil phases

Solid solutions were prepared from a mixture of solvent A (good solvent for the drug) and solvent B (good solvent for the polymer). Table 1 shows the solvents mixed to prepare samples and the state of the samples in dichloromethane (oil phase). At 10% of Taltirelin loading, all samples, except for those prepared from ethyl acetate-ethanol (4:1) and dichloromethane alone, appeared transparent when

Table 3. Effect of the composition of the mixed solvents on the state of oil phase

Composition of mixed solvents	The mixed solvents (Taltirelin + PLGA)	Loading % of Taltirelin	State of oil phase
Ethanol/Dichloromethane (1/4)	2.5 mL/0.5 g	10%	transparent
Water/Acetonitrile (1/10)	2.5 mL/0.5 g	10%	transparent
Methanol/Acetonitrile (1/4)	2.5 mL/0.5 g	10%	transparent
Ethanol/Acetonitrile (1/4)	2.5 mL/0.5 g	10%	transparent
Ethanol/Ethyl acetate (1/4)	2.5 mL/0.5 g	10%	Suspension
Dichloromethane*	2.0 mL/1.0 g	10%	Suspension
Ethanol/Dichloromethane (1/4)	2.0 mL/1.0 g	2.5%	transparent
Ethanol/Dichloromethane (1/4)	2.0 mL/1.0 g	15%	transparent
Ethanol/Dichloromethane (1/4)	2.0 mL/1.0 g	20%	Suspension
Ethanol/Dichloromethane (1/4)	2.0 mL/1.0 g	30%	Suspension
Ethanol/Dichloromethane (1/4)	2.0 mL/1.0 g	50%	Suspension

* not dissolve Taltirelin.

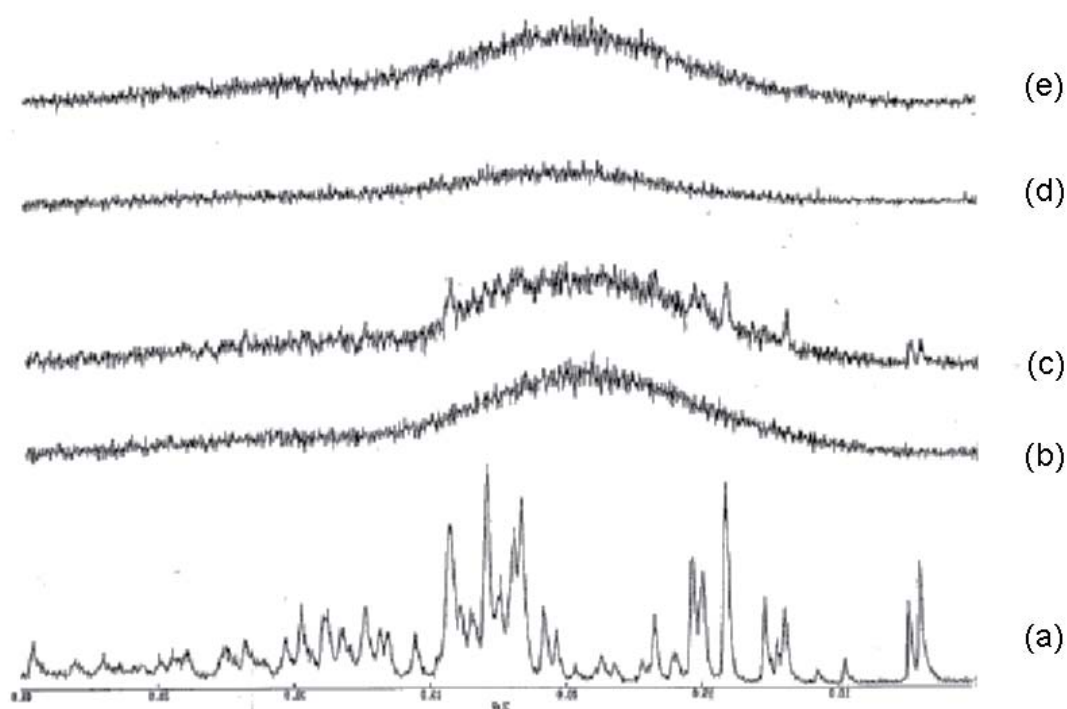


Figure 3. X-ray diffraction spectra. (a) Taltirelin, (b) PLGA, (c) physical mixture (Taltirelin: PLGA5020 = 1:9), (d) solid solution (Taltirelin: PLGA = 1:9), (e) Taltirelin-loaded microspheres (Taltirelin: PLGA = 1:9).

dissolved in dichloromethane. The resultants prepared from dichloromethane and ethanol (4:1) provided a transparent oil phase at a Taltirelin loading of up to 15%. The obtained sample prepared by dichloromethane and ethanol (4:1) at 10% of Taltirelin loading was analyzed by X-ray powder diffraction. No peaks of Taltirelin were detected for the solid solution although peaks of Taltirelin were detected for the physical mixture, as shown in Figure 3.

Characteristics of microspheres

The morphological features of microspheres prepared from the transparent oil phase, are shown in Figure 4.

No drug particles were found on the surface and the inside of the microspheres. X-ray powder diffraction analysis showed no peak in Taltirelin, as shown in Figure 3.

The T_g of the microspheres increased for Taltirelin loading of up to 15% (Figure 5). The microspheres have 50% greater size of approximately 15 μm (Figure 6).

Encapsulation efficiency and *in vitro* release of Taltirelin

The efficiency of Taltirelin encapsulation in the microspheres prepared from the oil phase of the solid solutions was over 90% for Taltirelin loading of up to

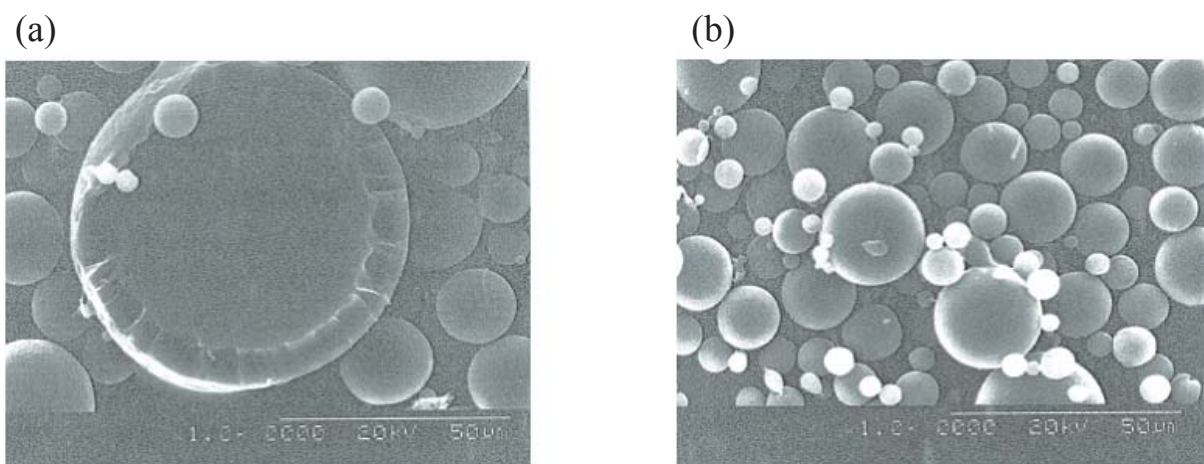


Figure 4. Scanning electron photomicrograph of Taltirelin-loaded microspheres; (a) cross section, (b) surface.

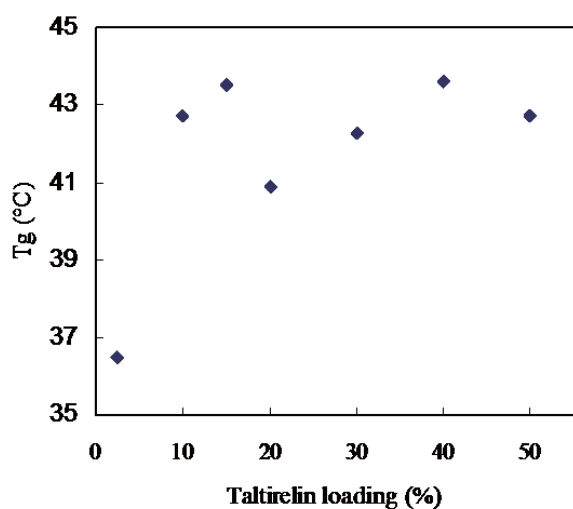


Figure 5. Effect of Taltirelin-loading on the T_g of Taltirelin-loaded microspheres.

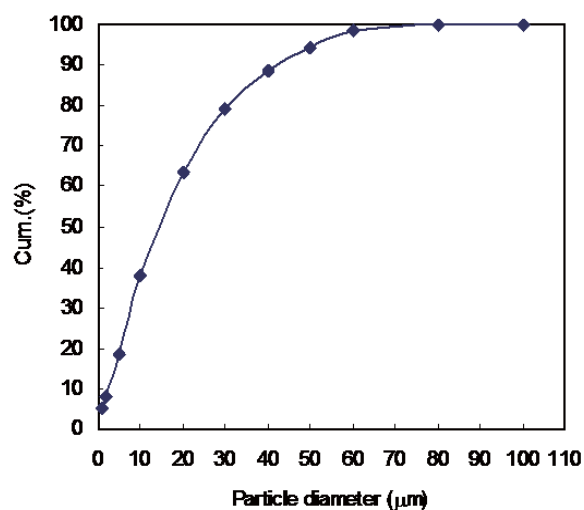


Figure 6. Particle diameter of Taltirelin-loaded microspheres (Taltirelin: PLGA = 1:9).

Table 2. Effect of drug loading on encapsulation efficiency

Loading of Taltirelin (%)	Encapsulation efficiencies
2.5	103.5
10	90.1
15	101.7
20	62.9
30	43.0
50	18.3

15% (Table 2), while that in microspheres from the conventional oil phase (dispersing peptide in solid) was 46.7% for 10% loading. The *in vitro* release of Taltirelin from microspheres is shown in Figure 7. The amount of Taltirelin released on day 1 was $7.7 \pm 5.7\%$ of microencapsulated Taltirelin ($n = 3$ batch). The release of Taltirelin from microspheres lasted over 21 days.

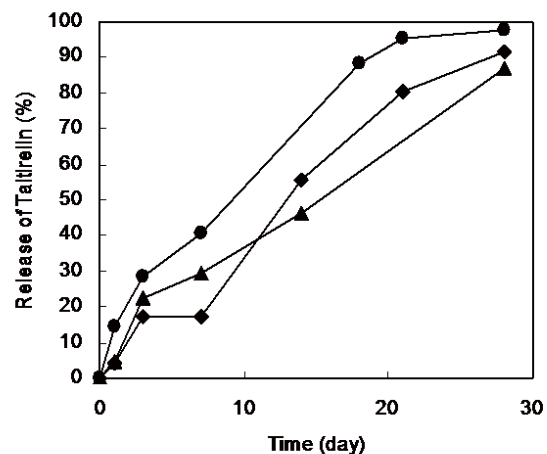


Figure 7. Release profiles of Taltirelin from Taltirelin-loaded microspheres (Taltirelin: PLGA = 1:9). ●:batch1, ◆:batch2, ▲:batch3.

Discussion

Preparation of solid solutions and oil phases

In the field of microencapsulation, some problems still remain despite the amount of research conducted. One problem is low encapsulation efficiency. Another is 'initial burst,' which is the phenomenon whereby a large portion of the encapsulated drug is released in a short time just after administration. Low encapsulation efficiency leads to an increase in manufacturing costs and initial burst is suspected of leading to side effects. Dispersing fine particles in an oil phase without aggregation is believed to be an effective way of avoiding these problems (13,14). The current study investigated the use of a solid solution system in the preparation of microspheres. A solid solution system is a type of solid dispersion system. A solid dispersion system is thought to be able to provide reduced particle size for a drug in a polymer because it can suppress the growth of drug crystals because of the viscosity of the polymer. Among solid dispersion systems, a solid solution system is thought to result in a dispersed drug in a polymer in a molecular state. Solid dispersions / solid solutions can be obtained by the following processes: melting drugs and excipients and then cooling and solidifying (melting method), or dissolving drugs and excipients in solvents and then evaporating the solvents (solvent method) (15). The melting method requires high temperatures. In contrast, the solvent method can provide solid dispersions/solid solutions even at low temperatures. Here, a solvent method was used to prepare solid solutions because this method is thought to be suitable for peptides in terms of avoiding their thermal decomposition.

In this study, the resultants from the mixtures of dichloromethane or acetonitril (good solvent for polymer and poor solvent for Taltirelin) and water, methanol, or ethanol (good solvent for Taltirelin and poor solvent for polymer) appeared transparent when dissolved in dichloromethane, which is a poor solvent for Taltirelin. This is the most important finding of this study. Namely, the peptide was apparently dissolved in an oil phase, of which dichloromethane was a poor solvent for the peptide. This indicates that Taltirelin can be dispersed in a molecular state in PLGA by a solid solution system. This is confirmed by the fact that X-ray diffraction analysis did not detect Taltirelin particles in resultants.

Production of the Taltirelin-PLGA solid solution was limited by the choice of the mixed solvents and the % of drug loading. A mixture of solvents using ethyl acetate did not provide resultants that appeared to be transparent when dissolved in dichloromethane. With regard to drug loading, a preparation with Taltirelin loading of over 20% did not provide resultants that appeared to be transparent when dissolved in

dichloromethane.

Characteristics of microspheres, encapsulation efficiency, and in vitro release of Taltirelin

In the microspheres prepared from the Taltirelin-PLGA solid solution, microscopic observation and X-ray diffraction analysis revealed that Taltirelin was dispersed in a molecular state in the matrix of the microspheres. The state of Taltirelin in the solid solution reflected the state of the peptide in the microspheres.

Drugs are often reported to precipitate during the evaporation process of microencapsulation, even if the drugs are dissolved in an oil phase (16). This phenomenon is due to the removal of the solvents that dissolve the drugs. In the case of the oil phase of the solid solution, the precipitation of Taltirelin did not occur as a result of the removal of solvent dichloromethane because it was unable to dissolve Taltirelin. Although Taltirelin apparently dissolved in the oil phase in this study, this is believed to be due to peptide-polymer interaction and not to dissolution of Taltirelin in dichloromethane. Regarding peptide-loaded microspheres, the following points have been noted: (a) the interaction between a peptide and a PLGA occurs through $-NH_2$ and $-COOH$, and (b) the interaction between the peptide and polymer contributes to long-term sustained release (17). The finding that the T_g of microspheres increased for Taltirelin loading of up to 15% supports the interaction between Taltirelin and PLGA.

Regarding the characterization of microspheres, the present study revealed that the obtained microspheres show high encapsulation efficiencies and long-term sustained release without initial burst *in vitro* as a result of use of the solid solution system in the microencapsulation of Taltirelin. Efficient interaction is believed to have led to the high encapsulation efficiency, low initial burst, and long-term sustained release.

Advantages of the current method

In light of its use in the current study, there are several major advantages of a method based on a solid solution system. Peptides that can only be dissolved in water and water-miscible solvents (*e.g.* ethanol) can be microencapsulated in water-insoluble polymers such as polylactide and PLGA by an O/W emulsion solvent evaporation method. Another advantage is that an oil phase with a high viscosity can be obtained. An oil phase consisting of mixed solvents [a good solvent for the peptide (*e.g.* ethanol) and a good water-immiscible solvent for the polymer (*e.g.* dichloromethane)] can be used in an O/W emulsion solvent evaporation method for microencapsulation. However, the oil phase of the mixed solvent may have lower viscosity because

a larger amount of the mixed solvents is needed to dissolve both the peptide and polymer. An oil phase with a low viscosity tends to leak its drug during the manufacture of microspheres (18). Moreover, a large amount of solvents results in longer time for the emulsion to harden. Therefore, the oil phase of the mixed solvents may provide the microspheres with lower encapsulation efficiency. In contrast, the new method based on a solid solution system requires less solvent to prepare an oil phase to dissolve both the polymer and drug. This leads to higher encapsulation efficiency because an oil phase with higher viscosity can be obtained.

The new method is useful because it takes advantage of the properties of peptides, namely (i) solubility in solvents that solve polymers and (ii) stability in solvents. This preliminary study confirmed that several peptides (e.g. LH-RH and calcitonin) can be used in microencapsulation via the new method.

Conclusion

Results indicated that a solid solution system substantially reduced the particle size of Taltirelin and resulted in its apparent dissolution in the oil phase. Using a Taltirelin-PLGA solid solution to prepare microspheres provided peptide-loaded microspheres with high encapsulation efficiency, low initial burst, and long-term sustained release. These findings suggest that a method of preparation based on a solid solution system should prove useful in the microencapsulation of peptides.

Acknowledgements

The authors wish to thank Dr. Hiroyuki Yoshino and Mr. Takehiko Suzuki for their valued advice regarding this study.

References

1. Deasy P. Microencapsulation *via* coacervation-phase separation. National Industrial Research Conference, Land O'Lakes, WI, 1966. June.
2. Ruiz JM, Tissier B, Benoit JP. Microencapsulation of peptide: A study of the phase separation of poly(dl-lactic acid-co-glycolic acid) copolymers 50/50 by silicone oil. *Int J Pharm* 1989; 49:69-77.
3. Beck LR, Cowsar DR, Lewis DH, Cosgrove RJ, Riddle CT, Lowry SL, Epperly T. A new long-acting injectable microcapsule system for the administration of progesterone. *Fertil Steril* 1979; 31:545-551.
4. Bodmeier R, McGinity JW. The preparation and evaluation of drug containing poly(dl-lactide) microspheres formed by the solvent evaporation. *Pharm Res* 1987; 4:465-471.
5. Bodmeier R, McGinity JW. Preparation of biodegradable polylactide microspheres using a spray-drying technique. *J Pharm Pharmacol* 1988; 40:754-757.
6. Nielsen F. Spray drying pharmaceuticals. *Manuf Chem* 1982; 53:38-39.
7. Yang YY, Chung TS, Ng NP. Morphology, drug distribution, and *in vitro* release profiles of biodegradable polymeric microspheres containing protein fabricated by double-emulsion solvent extraction/evaporation method. *Biomaterials* 2001; 22:231-241.
8. Wischke C, Borchert HH. Influence of the primary emulsification procedure on the characteristics of small protein-loaded PLGA microparticles for antigen delivery. *J Microencapsul* 2006; 23:435-448.
9. Kwong AK, Chou S, Sun AM, Sefton MV, Goosen MFA. *In vitro* and *in vivo* release of insulin from poly(lactic acid) microbeads and pellets. *J Control Rel* 1986; 4:47-62.
10. Bao W, Zhou J, Luo J, Wu D. PLGA microspheres with high drug loading and high encapsulation efficiency prepared by a novel solvent evaporation technique. *J Microencapsul* 2006; 23:471-479.
11. Gombotz W, Healy M, Brown. L. Very low temperature casting of controlled release microspheres. 1991; US Patent 5019400.
12. Okada H, Ogawa Y, Yashiki T. Prolonged release microcapsule and its production. 1987; US Patent 4652441.
13. Ogawa Y, Yamamoto M, Okada H, Yashiki T, Shimamoto T. A new technique to efficiently entrap leuprolide acetate into microcapsules of polylactic acid or copoly(lactic/glycolic) acid. *Chem Pharm Bull* 1988; 36:1095-1103.
14. Shukla AJ, Price JC. Effect of drug (core) particle size on the dissolution of Theophylline from microspheres made from low molecular weight cellulose acetate propionate. *Pharm Res* 1989; 6:418-421.
15. Chiou WL, Riegelman S. Pharmaceutical applications of solid dispersion system. *J Pharm Sci* 1971; 60:1281-1302.
16. Kyo M, Hyon SH, Ikada Y. Effects of preparation conditions of cisplatin-loaded microspheres on the *in vitro* release. *J Control Release* 1995; 35:73-82.
17. Heya T, Okada H, Tanigawara Y, Ogawa Y, Toguchi H. Effect of counteranion of TRH and loading amount on control of TRH release from copoly(dl-lactic/glycolic acid) microspheres prepared by an in water drying method. *Int J Pharm* 1991; 69:69-75.
18. Herrmann J, Bdmeier R. Biodegradable, somatostatin acetate containing microspheres prepared by various aqueous and non-aqueous solvent evaporation methods. *Eur J Pharm Biopharm* 1998; 45:75-82.

(Received December 13, 2007; Revised February 5, 2008; Accepted February 13, 2008)

Original Article**3D-QSAR study with pharmacophore-based molecular alignment of hydroxamic acid-related phosphinates that are aminopeptidase N inhibitors**Huawei Zhu¹, Hao Fang¹, Luyao Wang², Wenxiang Hu², Wenfang Xu^{1,*}¹Institute of Medicinal Chemistry, School of Pharmaceutical Sciences, Shandong University, Ji'nan, Shandong, China;²Department of Chemistry, Capital Normal University, Beijing, China.

ABSTRACT: 3D-QSAR models for a series of aminopeptidase N inhibitors were developed based on comparative molecular field analysis (CoMFA) and comparative molecular similarity analysis (CoMSIA). GALAHAD, a pharmacophore generation module involving a genetic algorithm, was used to generate the pharmacophore model of the series of inhibitors. Molecules both in the training set and test set were aligned to the pharmacophore model. Values for the CoMFA model were $r^2 = 0.992$, $q^2 = 0.586$, SEE = 0.111, and F (8, 10) = 191.263. Values for the CoMSIA model were $r^2 = 0.990$, $q^2 = 0.776$, SEE = 0.123, and F (7, 11) = 156.68. This model can help not only in improving current understanding of enzyme-ligand interactions but also in predicting the activity of derivatives and designing new compounds with better potency.

Keywords: Aminopeptidase N, 3D-QSAR, CoMFA, CoMSIA

Introduction

Aminopeptidase N (APN)/CD13 (EC 3.4.11.2) is a transmembrane protease belonging to the M1 family of Zinc-dependent metalloexopeptidase (1,2). It is widely expressed on the surface of a variety of human tissues and cell types and especially on renal and intestinal brush border cells (1,3,4). It is also considered to be the receptor of TGEV and HEV229E and *Bacillus thuringiensis* Cry1A toxin (5-7). Furthermore, many studies have indicated that APN is overexpressed on tumor cells and plays an essential role in extracellular matrix degradation and invasion of tumor cells (8,9).

*Correspondence to: Dr. Wenfang Xu, Institute of Medicinal Chemistry, School of Pharmaceutical Sciences, Shandong University, Ji'nan, Shandong, China; e-mail: xuwenf@sdu.edu.cn

Therefore, APN inhibitors have been used to suppress tumor cell invasion (10). Bestatin, which is the sole APN inhibitor on the market to date, can treat leukemia with an inhibiting capacity in the micromole range (11,12). Thus, a number of laboratories are designing and synthesizing APN inhibitors with a new scaffold, expecting with greater APN inhibiting ability. A series of hydroxamic acid-related phosphinates compounds designed and synthesized by Marcin Drag and his co-workers has shown good APN-inhibiting activity (13). Here, 3D-QSAR analysis with molecular alignment based on a pharmacophore model has been performed on this series of APN inhibitors, using comparative molecular field analysis (CoMFA) and comparative molecular similarity indices analysis (CoMSIA) with partial least-square fit to predict the steric, electrostatic, hydrophobic and H-bond molecular field interactions for this activity (14,15).

Materials and Methods

Computer modeling was conducted on a Dell Precision workstation. All calculations were done with the programs SYBYL7.0 (16) and SYBYL7.3 (17) with default values except those specially referred to. A set of 23 hydroxamic acid-related phosphinates derivatives (13) has been chosen for 3D-QSAR study. The affinity of compounds binding to APN was represented by the IC₅₀ value (μM) in the literature (Table 1). Log (1/IC₅₀) values (pIC₅₀) were used to derive 3D-QSAR models (see Table 3).

Pharmacophoric conformation determination

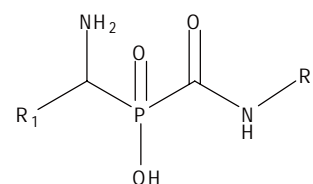
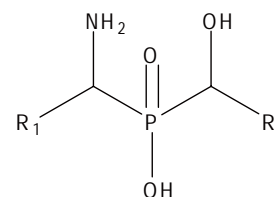
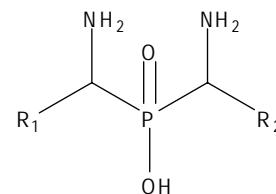
Compounds described in the literature were racemic mixtures, with two chiral carbon atoms included in each. The pharmacophoric conformation of the compounds was first determined. Compound **16** was selected as the template molecule because it had the greatest activity. The four isomers of compound **16** were built with a SYBYL/Sketch module and the

Table 1. Structure of compounds used in this study and their bioactivity

Compounds	R ₁	R ₂	IC ₅₀ (μM)
1	-C ₆ H ₅ (Phenylglycine)	-H (Gly)	42
2	-C ₆ H ₅ (Phenylglycine)	-CH ₃ (Ala)	46
3	-C ₆ H ₅ (Phenylglycine)	-CH ₂ CH ₂ CH ₃ (nor-Val)	17
4	-C ₆ H ₅ (Phenylglycine)	-CH ₂ CH(CH ₃) ₂ (Leu)	4
5	-C ₆ H ₅ (Phenylglycine)	-C ₆ H ₅ (Phenylglycine)	0.6
6	-C ₆ H ₅ (Phenylglycine)	-CH ₂ CH ₂ Phe (hPhe)	0.71
7	-CH ₂ CH ₂ Phe (hPhe)	-CH ₂ CH ₂ Phe (hPhe)	0.83
8	-CH ₂ CH(CH ₃) ₂ (Leu)	-H (Gly)	76
9	-CH ₂ CH(CH ₃) ₂ (Leu)	-CH ₃ (Ala)	155
10	-CH ₂ CH(CH ₃) ₂ (Leu)	-CH ₂ CH ₂ CH ₃ (nor-Val)	50
11	-CH ₂ CH(CH ₃) ₂ (Leu)	-CH ₂ CH(CH ₃) ₂ (Leu)	50

Compounds	R ₁	R ₂	IC ₅₀ (μM)
12	-C ₆ H ₅ (Phenylglycine)	-CH ₃ (Ala)	48
13	-C ₆ H ₅ (Phenylglycine)	-(CH ₂) ₃ CH ₃ (nor-Leu)	28
14	-C ₆ H ₅ (Phenylglycine)	-CH ₂ CH(CH ₃) ₂ (Leu)	12
15	-C ₆ H ₅ (Phenylglycine)	-C ₆ H ₅ (Phenylglycine)	0.55
16	-C ₆ H ₅ (Phenylglycine)	-CH ₂ CH ₂ Phe (hPhe)	0.24
17	-CH(CH ₃) ₂ (Val)	-CH ₂ CH ₂ Phe (hPhe)	0.5
18	-CH ₂ CH(CH ₃) ₂ (Leu)	-(CH ₂) ₃ CH ₃ (nor-Leu)	3
19	-CH ₂ CH(CH ₃) ₂ (Leu)	-CH ₂ CH ₂ Phe (hPhe)	1

Compounds	R ₁	R ₂	IC ₅₀ (μM)
20	-CH ₂ CH(CH ₃) ₂ (Leu)	-C ₆ H ₅ (Phenylglycine)	35
21	-CH ₂ CH(CH ₃) ₂ (Leu)	-CH ₂ Phe (Phe)	0.53
22	-CH(CH ₃) ₂ (Val)	-C ₆ H ₅ (Phenylglycine)	160
23	-CH(CH ₃) ₂ (Val)	-CH ₂ Phe (Phe)	0.93



Powell method was used with a Tripos force field in the energy-minimization process; convergence criterion was 4.184 J/mol and a Gasteiger-Hückel charge was given. Then, the compounds were docked into the active site of *E. coli* APN (PDB Code: 2DQM) using the SYBYL/FlexX module. The docking result suggested both chiral carbon atoms had an *S*-configuration when the binding model was consistent with that described in literature (Figure 1). The other 22 molecules were built and minimized based on the template.

Pharmacophore-based molecular alignment

The series of compounds reported in the literature can be divided into three subtypes according to their scaffold, but alignment by traditional molecular alignment methods, such as fit atoms or match atoms, is difficult. Under such conditions, pharmacophore-based molecular alignment is an ideal way to align molecules in different scaffolds. The SYBYL new pharmacophore alignment module GALAHAD (Genetic Algorithm with Linear Assignment for Hypermolecular Alignment of Datasets) (18) aligns a set of molecules that share a common mode of biological activity and develops corresponding pharmacophore models. Using a sophisticated genetic algorithm and a multi-objective

scoring function, GALAHAD takes into account energetics, steric similarity, and pharmacophoric overlap, while accommodating conformational flexibility, ambiguous stereochemistry, alternative ring configurations, multiple partial match constraints, and alternative feature mappings among molecules. Here compounds **5**, **6**, **16**, **17**, and **21** were chosen as the data source to generate pharmacophore models with GALAHAD (Figures 2 and 3). Compounds both in the training set and test set were aligned to the pharmacophore model using the Align Molecules to Template Individually method. The alignment conformation of all molecules is shown in Figure 4.

3D-QSAR analysis

3D-QSAR analysis was performed on the aligned compounds using the CoMFA and CoMSIA methods. In the CoMFA model, a hybrid sp³ carbon atom with a positive charge was used as a probe to compute the CoMFA steric and electrostatic fields. The lattice size and probe step size were adjusted automatically. Default parameters were used for other values. Partial least squares (PLS) regression was separately performed on the compounds. The Leave-One-Out method, with 2.0 kcal/mol as the column filtering value, was first used

Figure 1. Compound 16 docked into the activity site of E.coli APN with the two chiral carbon atoms in an S-configuration.

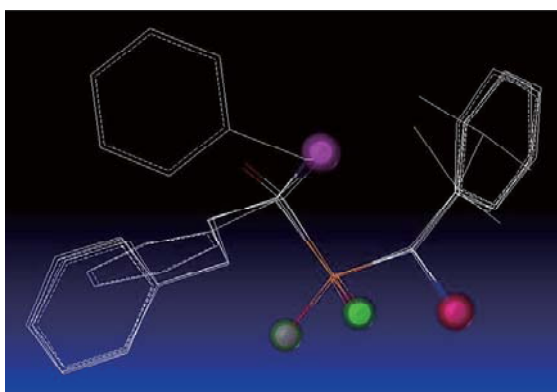
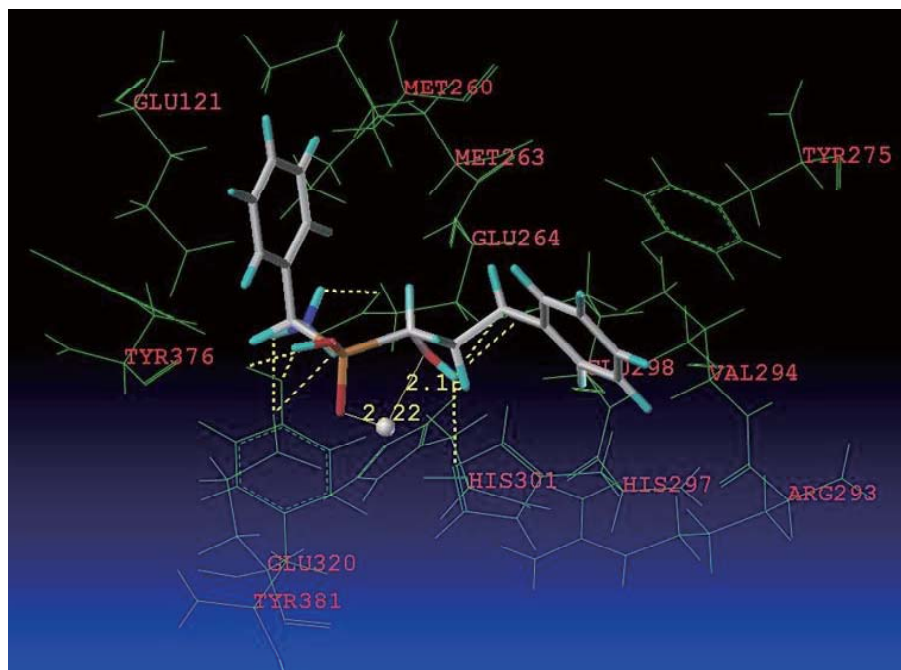


Figure 2. Pharmacophore model generated by GALAHAD with compounds 5, 6, 16, 17 and 21.

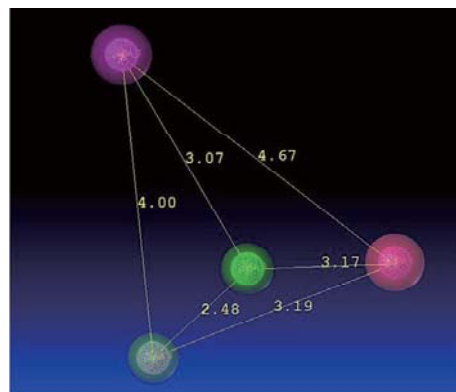
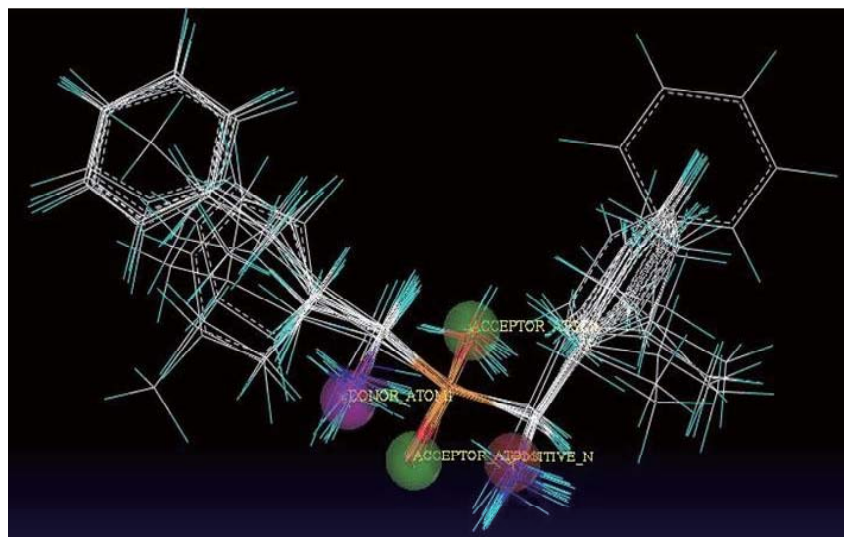


Figure 3. The relative spatial locations of the pharmacophore elements. Pink for positive nitrogen, magenta for H-bond donor, green for H-bond acceptor. The yellow line represents the relative distance of each element, with length in angstroms.

Figure 4. Pharmacophore-based alignment of the training set and the test set.



to obtain the optimum number of components (ONC), and then the CoMFA model was computed with non-cross-validation PLS at the ONC. Computation of the CoMSIA model was similar to that for the CoMFA model, and apart from steric and electrostatic fields the CoMSIA model took into account hydrophobic and H-bond fields.

Results and Discussion

Pharmacophore model

Four elements were included in the pharmacophore model which generated from compounds **5**, **6**, **16**, **17**, **21**, including two H-bond acceptors (AA1, AA2), one H-bond donor (DA), and one positive nitrogen site (PN). Their relative locations and relative distance are shown in Figure 3.

Table 2. Summary of PLS results

Statistical parameters	CoMFA	CoMSIA
r^2_{cv}	0.586	0.776
ONC	7	6
r^2	0.992	0.990
SEE	0.111	0.123
F_{ratio}	191.263	156.68
Fraction of field contributions		
Steric	59.4%	13.9%
Electrostatic	40.6%	39%
Hydrophobic	-	30%
Donor	-	11.8%
Acceptor	-	15.3%

CoMFA and CoMSIA models

PLS analysis was performed on CoMFA/CoMSIA field values and experimental bioactivity values (IC_{50}) of the training set. The CoMFA and CoMSIA statistical analysis is summarized in Table 2. Statistical data show an r^2_{cv} of 0.586 for the CoMFA model and 0.776 for the CoMSIA model, which indicates good internal predictive ability for both models. The models developed also displayed an r^2_{NCV} of 0.992 and 0.990 for the CoMFA and CoMSIA models, respectively.

QSAR model verification

To test the predictive ability of the models, 19 molecules in a training set and a test set of 4 molecules excluded from the model derivation were used (Table 3). For the test set, a predictive correlation coefficient r^2_{pred} of 0.772 for the CoMFA model and 0.839 for the CoMSIA model indicates good external predictive ability for the models. Figure 5 shows the scatterplot of the actual pIC_{50} vs predicted pIC_{50} .

Contour analysis

The contour maps of CoMFA (electrostatic and steric) and CoMSIA (electrostatic, steric, hydrophobic, donor, and acceptor) are shown in Figure 6.

The steric contour maps of the CoMFA and CoMSIA models are shown in Figure 6a and 6c. The phenyl group on the R_2 substitute site was located in the green region, which suggested that bulky group substitution would help to increase potency. For example,

Table 3. Actual activity versus predicted activity and their residuals

Compounds	Actual pIC_{50}	CoMFA Predicted pIC_{50}	Residuals (CoMFA)	CoMSIA Predicted pIC_{50}	Residuals (CoMSIA)
1	4.38	4.35	0.03	4.38	0
2	4.34	4.42	-0.08	4.34	0
3*	4.77	4.68	0.09	4.51	0.26
4	5.40	5.18	0.22	5.21	0.19
5	6.22	6.20	0.02	6.19	0.03
6	6.15	6.12	0.03	6.13	0.02
7	6.08	6.12	-0.04	6.01	0.07
8	4.12	4.11	0.01	4.13	-0.01
9	3.81	3.81	0	3.87	-0.06
10*	4.30	4.98	-0.68	4.75	-0.45
11	4.30	4.35	-0.05	4.31	-0.01
12	4.32	4.34	-0.02	4.36	-0.04
13	4.55	4.46	0.09	4.46	0.09
14	4.92	5.11	-0.19	5.05	-0.13
15	6.26	6.31	-0.05	6.31	-0.05
16*	6.62	5.95	0.67	6.11	0.51
17	6.30	6.28	0.02	6.35	-0.05
18*	5.52	5.71	-0.19	4.98	0.54
19	6.00	6.00	0	5.97	0.03
20	4.46	4.32	0.14	4.19	0.27
21	6.28	6.39	-0.11	6.21	0.07
22	3.80	3.93	-0.13	4.09	-0.29
23	6.03	5.92	0.11	6.07	-0.04

* Molecules in test set.

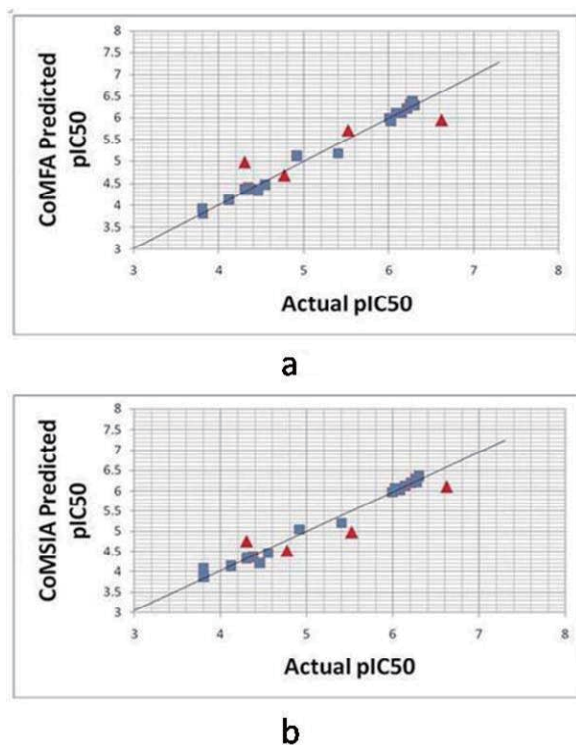


Figure 5. Scatterplot of actual pIC_{50} vs CoMFA (a) and CoMSIA (b) predicted pIC_{50} . ■, Training set; ▲, Test set.

compounds **1** ($pIC_{50} = 4.38$), **2** ($pIC_{50} = 4.34$), **8** ($pIC_{50} = 4.12$), and **9** ($pIC_{50} = 3.81$ M) exhibited low inhibitory activity due to the lack of a steric bulk substituent in the R_2 position. While the compounds with $pIC_{50} > 6$, such as compounds **5** ($pIC_{50} = 6.22$), **6** ($pIC_{50} = 6.15$), **7** ($pIC_{50} = 6.08$), **15** ($pIC_{50} = 6.26$), **16** ($pIC_{50} = 6.62$), **17** ($pIC_{50} = 6.3$), and **21** ($pIC_{50} = 6.28$), have phenyl or phenethyl group substitution in the R_2 position. The yellow contour maps existed near the R_1 substitute site, which indicate that bulky group substitution at this position will lower potencies, such as compounds **10** ($pIC_{50} = 4.30$) and **11** ($pIC_{50} = 4.30$) with a long and flexible isobutyl group in the R_1 substitute.

CoMFA and CoMSIA electrostatic contour maps are shown in Figure 6b and 6d. Both electron positive and electron negative substitution in the R_2 position significantly affect inhibitory activity because most blue and red regions are located around the R_2 position. CoMSIA H-bond donor/acceptor contour maps (Figure 6e and 6f) indicate favoring of a H-bond acceptor rather than H-bond donor groups near the hydroxyl group of compound **15**.

CoMSIA hydrophobic contour maps are shown in Figure 6g. The yellow and white contour maps highlight areas where hydrophobic and hydrophilic properties are preferred. The presence of a large yellow contour map beside the R_2 substituent suggests that its occupancy by hydrophobic groups would favor inhibitory activity. In the most active compounds R_2 was a phenyl group (*i.e.*, compounds **5** and **15**) or a phenethyl group (*i.e.*, compounds **6**, **7**, **16**, and **17**).

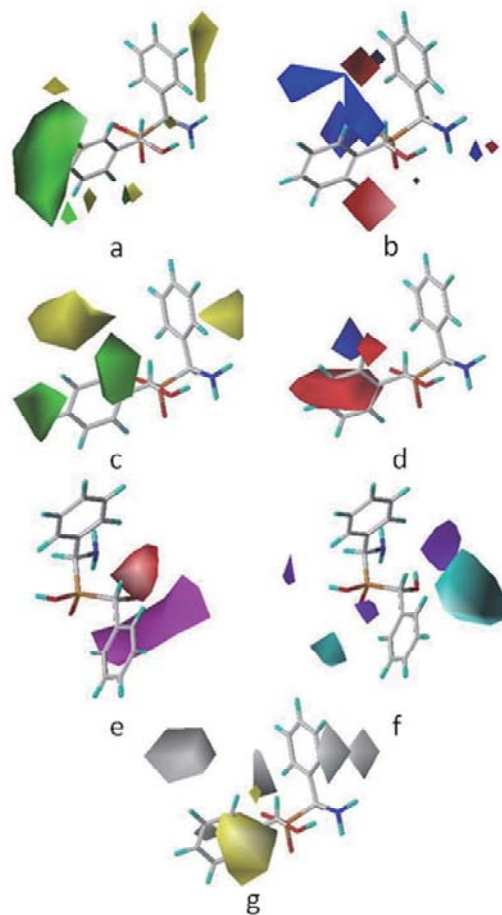


Figure 6. (a) CoMFA steric fields (color code: favored, green; disfavored, yellow); (b) CoMFA electrostatic fields (color code: increase in positive charge favored, blue; increase in negative charge favored, red); (c) CoMSIA steric fields (color code: favored, green; disfavored, yellow); (d) CoMSIA electrostatic fields (color code: increase in positive charge favored, blue; increase in negative charge favored, red); (e) CoMSIA acceptor fields (color code: favored, magenta; disfavored, red); (f) CoMSIA donor fields (color code: favored, cyan; disfavored, purple); (g) CoMSIA hydrophobic fields (color code: favored, yellow; disfavored, white). The reference molecule is **15**.

Conclusion

The present study examined a 3D-QSAR model of a set of APN inhibitors, and pharmacophore-based molecular alignment provided a QSAR model with a high level of predictability. To the extent known, this is the first time the GALAHAD module has been introduced in the process of generating CoMFA and CoMSIA models. The models derived in this study can help to elucidate the binding models of APN inhibitors and may lead to design of new acid-related phosphinates exhibiting a high level of APN inhibition.

Acknowledgements

The authors wish to thank Ms. Mei Zhou (Beijing Hongcam Software Technologies Co., Ltd.) for her helpful instruction in using the SYBYL/GALAHAD module.

References

1. Antczak C, De Meester I, Bauvois B. Ectopeptidases in pathophysiology. *BioEssays* 2001; 23:251-260.
2. Taylor A. Aminopeptidases: structure and function. *FASEB J* 1993; 7:290-298.
3. Antczak C, De Meester I, Bauvois B. Transmembrane proteases as disease markers and targets for therapy. *J Biol Regul Homeost Agents* 2001; 15:130-139.
4. Jardinaud F, Banisadr G, Noble F, Mélik-Parsadaniantz S, Chen H, Dugave C, Laplace H, Rostène W, Fournié-Zaluski MC, Roques BP, Popovici T. Ontogenic and adult whole body distribution of aminopeptidase N in rat investigated by *in vitro* autoradiography. *Biochimie* 2004; 86:105-113.
5. Delmas B, Gelfi J, L'Haridon R, Vogel LK, Sjöström H, Norén O, Laude H. Aminopeptidase N is a major receptor for the entero-pathogenic coronavirus TGEV. *Nature* 1992; 357:417-420.
6. Yeager CL, Ashmun RA, Williams RK, Cardellicchio CB, Shapiro LH, Look AT, Holmes KV. Human aminopeptidase N is a receptor for human coronavirus 229E. *Nature* 1992; 357:420-422.
7. Nakanishi K, Yaoi K, Nagino Y, Hara H, Kitami M, Atsumi S, Miura N, Sato R. Aminopeptidase N isoforms from the midgut of *Bombyx mori* and *Plutella xylostella*—their classification and the factors that determine their binding specificity to *Bacillus thuringiensis* Cry1A toxin. *FEBS Lett* 2002; 19:215-220.
8. Saiki I, Fujii H, Yoneda J, Abe F, Nakajima M, Tsuruo T, Azuma I. Role of aminopeptidase N (CD13) in tumor-cell invasion and extracellular matrix degradation. *Int J Cancer* 1993; 54:137-143.
9. Menrad A, Speicher D, Wacker J, Herlyn M. Biochemical and functional characterization of aminopeptidase N expressed by human melanoma cells. *Cancer Res* 1993; 53:1450-1455.
10. Fujii H, Nakajima M, Aoyagi T, Tsuruo T. Inhibition of tumor cell invasion and matrix degradation by aminopeptidase inhibitors. *Biol Pharm Bull* 1996; 19:6-10.
11. Fujisaki T, Otsuka T, Gondo H, Okamura T, Niho Y, Ohhinata A, Abe F. Bestatin selectively suppresses the growth of leukemic stem/progenitor cells with BCR/ABL mRNA transcript in patients with chronic myelogenous leukemia. *Int Immunopharmacol* 2003; 3:901-907.
12. Xu WF, Li QB. Progress in the development of aminopeptidase N (APN/CD13) inhibitors. *Curr Med Chem Anticancer Agents* 2005; 5:281-301.
13. Drag M, Grzywa R, Oleksyszyn J. Novel hydroxamic acid-related phosphinates: Inhibition of neutral aminopeptidase N (APN). *Bioorg Med Chem Lett* 2007; 17:1516-1519.
14. Cramer RD, Patterson DE, Bunce JD. Comparative molecular field analysis (CoMFA). 1. Effect of shape on binding of steroids to carrier proteins. *J Am Chem Soc* 1988; 110:5959-5967.
15. Klebe G, Abraham U, Mietzner T. Molecular similarity indices in a comparative analysis (CoMSIA) of drug molecules to correlate and predict their biological activity. *J Med Chem* 1994; 37:4130-4146.
16. Sybyl, version 7.0; Tripos Inc.: St. Louis, MO, 2004.
17. Sybyl, version 7.3; Tripos Inc.: St. Louis, MO, 2007.
18. GALAHAD, Tripos, St. Louis, MO; http://www.tripos.com/data/SYBYL/GALAHAD_9-7-05.pdf.

(Received December 13, 2007; Revised January 29, 2008; Accepted February 13, 2008)

Drug Discoveries & Therapeutics

Guide for Authors

1. Scope of Articles

Drug Discoveries & Therapeutics mainly publishes articles related to basic and clinical pharmaceutical research such as pharmaceutical and therapeutical chemistry, pharmacology, pharmacy, pharmacokinetics, industrial pharmacy, pharmaceutical manufacturing, pharmaceutical technology, drug delivery, toxicology, and traditional herb medicine. Studies on drug-related fields such as biology, biochemistry, physiology, microbiology, and immunology are also within the scope of this journal.

2. Submission Types

Original Articles should be reports new, significant, innovative, and original findings. An Article should contain the following sections: Title page, Abstract, Introduction, Materials and Methods, Results, Discussion, Acknowledgments, References, Figure legends, and Tables. There are no specific length restrictions for the overall manuscript or individual sections. However, we expect authors to present and discuss their findings concisely.

Brief Reports should be short and clear reports on new original findings and not exceed 4000 words with no more than two display items. *Drug Discoveries & Therapeutics* encourages younger researchers and doctors to report their research findings. Case reports are included in this category. A Brief Report contains the same sections as an Original Article, but Results and Discussion sections must be combined.

Reviews should include educational overviews for general researchers and doctors, and review articles for more specialized readers.

Policy Forum presents issues in science policy, including public health, the medical care system, and social science. Policy Forum essays should not exceed 2,000 words.

News articles should not exceed 500 words including one display item. These articles should function as an international news source with regard to topics in the life and social sciences and medicine. Submissions are not restricted to journal staff - anyone can submit news articles on subjects that would be of interest to *Drug Discoveries & Therapeutics*' readers.

Letters discuss material published in *Drug Discoveries & Therapeutics* in the last 6 months or issues of general interest. Letters should not exceed 800 words and 6 references.

3. Manuscript Preparation

Preparation of text. Manuscripts should be written in correct American English and submitted as a Microsoft Word (.doc) file in a single-column format. Manuscripts must be paginated and double-spaced throughout. Use Symbol font for all Greek characters. Do not import the figures into the text file but indicate their approximate locations directly on the manuscript. The manuscript file should be smaller than 5 MB in size.

Title page. The title page must include 1) the title of the paper, 2) name(s) and affiliation(s) of the author(s), 3) a statement indicating to whom correspondence and proofs should be sent along with a complete mailing address, telephone/fax numbers, and e-mail address, and 4) up to five key words or phrases.

Abstract. A one-paragraph abstract consisting of no more than 250 words must be included. It should state the purpose of the study, basic procedures used, main findings, and conclusions.

Abbreviations. All nonstandard abbreviations must be listed in alphabetical order, giving each abbreviation followed by its spelled-out version. Spell out the term upon first mention and follow it with the abbreviated form in parentheses. Thereafter, use the abbreviated form.

Introduction. The introduction should be a concise statement of the basis for the study and its scientific context.

Materials and Methods. Subsections under this heading should include sufficient instruction to replicate experiments, but well-established protocols may be simply referenced. *Drug Discoveries & Therapeutics* endorses the principles of the Declaration of Helsinki and expects that all research involving humans will have been conducted in accordance with these principles. All laboratory animal studies must be approved by the authors' Institutional Review Board(s).

Results. The results section should provide details of all of the experiments that are required to support the conclusions of the paper. If necessary, subheadings may be used for an orderly presentation. All figures, tables, and photographs must be referred in the text.

Discussion. The discussion should include conclusions derived from the study and supported by the data. Consideration should be given to the impact that these conclusions have on the body of knowledge in which context the experiments were conducted. In Brief Reports, Results and Discussion sections must be combined.

Acknowledgments. All funding sources should be credited in the Acknowledgments section. In addition, people who contributed to the work but who do not fit the criteria for authors should be listed along with their contributions.

References. References should be numbered in the order in which they appear in the text. Cite references in text using a number in parentheses. Citing of unpublished results and personal communications in the reference list is not recommended but these sources may be mentioned in the text. For all references, list all authors, but if there are more than fifteen authors, list the first three authors and add "et al." Abbreviate journal names as they appear in PubMed. Web references can be included in the reference list.

Example 1:

Hamamoto H, Kamura K, Razanajatovo IM, Murakami K, Santa T, Sekimizu K. Effects of molecular mass and hydrophobicity on transport rates through non-specific pathways of the silkworm

larva midgut. *Int J Antimicrob Agents* 2005; 26:38-42.

Example 2:

Mizuochi T. Microscale sequencing of N-linked oligosaccharides of glycoproteins using hydrazinolysis, Bio-Gel P-4, and sequential exoglycosidase digestion. In: *Methods in Molecular Biology: Vol. 14 Glycoprotein analysis in biomedicine* (Hounsell T, ed.). Humana Press, Totowa, NJ, USA, 1993; pp. 55-68.

Example 3:

Drug Discoveries & Therapeutics. Hot topics & news: China-Japan Medical Workshop on Drug Discoveries and Therapeutics 2007. <http://www.ddtjournal.com/hotnews.php> (accessed July 1, 2007).

Figure legends. Include a short title and a short explanation. Methods described in detail in the Materials and methods section should not be repeated in the legend. Symbols used in the figure must be explained. The number of data points represented in a graph must be indicated.

Tables. All tables should have a concise title and be typed double-spaced on pages separate from the text. Do not use vertical rules. Tables should be numbered with Roman numerals consecutively in accordance with their appearance in the text. Place footnotes to tables below the table body and indicate them with lowercase superscript letters.

Language editing. Manuscripts submitted by authors whose primary language is not English should have their work proofread by a native English speaker before submission. The Editing Support Organization can provide English proofreading, Japanese-English translation, and Chinese-English translation services to authors who want to publish in *Drug Discoveries & Therapeutics* and need assistance before submitting an article. Authors can contact this organization directly at <http://www.iacmhr.com/iac-eso>.

IAC-ESO was established in order to facilitate manuscript preparation by researchers whose native language is not English and to help edit work intended for

international academic journals. Quality revision, translation, and editing services are offered by our staff, who are native speakers of particular languages and who are familiar with academic writing and journal editing in English.

4. Figure Preparation

All figures should be clear and cited in numerical order in the text. Figures must fit a one- or two-column format on the journal page: 8.3 cm (3.3 in.) wide for a single column; 17.3 cm (6.8 in.) wide for a double column; maximum height: 24.0 cm (9.5 in.). Only use the following fonts in the figure: Arial and Helvetica. Provide all figures as separate files. Acceptable file formats are JPEG and TIFF. Please note that files saved in JPEG or TIFF format in PowerPoint lack sufficient resolution for publication. Each Figure file should be smaller than 10 MB in size. Do not compress files. A fee is charged for a color illustration or photograph.

5. Online Submission

Manuscripts should be submitted to *Drug Discoveries & Therapeutics* online at <http://www.ddtjournal.com>. The manuscript file should be smaller than 10 MB in size. If for any reason you are unable to submit a file online, please contact the Editorial Office by e-mail: office@ddtjournal.com.

Editorial and Head Office

Wei TANG, MD PhD
Secretary-in-General
TSUIN-IKIZAKA 410
2-17-5 Hongo, Bunkyo-ku
Tokyo 113-0033
Japan
Tel: 03-5840-9697
Fax: 03-5840-9698
E-mail: office@ddtjournal.com

Cover letter. A cover letter from the corresponding author including the following information must accompany the submission: name, address, phone and fax numbers, and e-mail address of the corresponding author. This should include a statement affirming that all authors concur with the submission and that the material submitted for publication has not been previously published and is not under consideration for publication elsewhere and a

statement regarding conflicting financial interests.

Authors may recommend up to three qualified reviewers other than members of Editorial board. Authors may also request that certain (but not more than three) reviewers not be chosen.

The cover letter should be submitted as a Microsoft Word (.doc) file (smaller than 1 MB) at the same time the work is submitted online.

6. Accepted Manuscripts

Proofs. Rough galley proofs in PDF format are supplied to the corresponding author via e-mail. Corrections must be returned within 4 working days of receipt of the proofs. Subsequent corrections will not be possible, so please ensure all desired corrections are indicated. Note that we may proceed with publication of the article if no response is received.

Transfer of copyrights. Upon acceptance of an article, authors will be asked to agree to a transfer of copyright. This transfer will ensure the widest possible dissemination of information. A letter will be sent to the corresponding author confirming receipt of the manuscript. A form facilitating transfer of copyright will be provided. If excerpts from other copyrighted works are included, the author(s) must obtain written permission from the copyright owners and credit the source(s) in the article.

Cover submissions. Authors whose manuscripts are accepted for publication in *Drug Discoveries & Therapeutics* may submit cover images. Color submission is welcome. A brief cover legend should be submitted with the image.

Revised February 2008



Drug Discoveries & Therapeutics



Editorial Office

TSUIN-IKIZAKA 410
2-17-5 Hongo, Bunkyo-ku
Tokyo 113-0033, Japan

Tel: 03-5840-9697
Fax: 03-5840-9698
E-mail: office@ddtjournal.com
URL: www.ddtjournal.com

JOURNAL PUBLISHING AGREEMENT

Ms No:

Article entitled:

Corresponding author:

To be published in Drug Discoveries & Therapeutics

Assignment of publishing rights:

I hereby assign to International Advancement Center for Medicine & Health Research Co., Ltd. (IACMHR Co., Ltd.) publishing Drug Discoveries & Therapeutics the copyright in the manuscript identified above and any supplemental tables and illustrations (the articles) in all forms and media, throughout the world, in all languages, for the full term of copyright, effective when and if the article is accepted for publication. This transfer includes the rights to provide the article in electronic and online forms and systems.

I understand that I retain or am hereby granted (without the need to obtain further permission) rights to use certain versions of the article for certain scholarly purpose and that no rights in patent, trademarks or other intellectual property rights are transferred to the journal. Rights to use the articles for personal use, internal institutional use and scholarly posting are retained.

Author warranties:

I affirm the author warranties noted below.

- 1) The article I have submitted to the journal is original and has not been published elsewhere.
- 2) The article is not currently being considered for publication by any other journal. If accepted, it will not be submitted elsewhere.
- 3) The article contains no libelous or other unlawful statements and does not contain any materials that invade individual privacy or proprietary rights or any statutory copyright.
- 4) I have obtained written permission from copyright owners for any excerpts from copyrighted works that are included and have credited the sources in my article.
- 5) I confirm that all commercial affiliations, stock or equity interests, or patent-licensing arrangements that could be considered to pose a financial conflict of interest regarding the article have been disclosed.
- 6) If the article was prepared jointly with other authors, I have informed the co-authors(s) of the terms of this publishing agreement and that I am signing on their behalf as their agents.

Your Status:

- I am the sole author of the manuscript.
 I am one author signing on behalf of all co-authors of the manuscript.

Please tick one of the above boxes (as appropriate) and then sign and date the document in black ink.

Signature:

Date:

Name printed:

Please return the completed and signed original of this form by express mail or fax, or by e-mailing a scanned copy of the signed original to:

Drug Discoveries & Therapeutics office
TSUIN-IKIZAKA 410, 2-17-5 Hongo,
Bunkyo-ku, Tokyo 113-0033, Japan
E-mail: proof-editing@ddtjournal.com
Fax: +81-3-5840-9698

